Arsenic contaminated groundwater: exploration of the role of organic carbon in mobilization processes and evaluation of mechanisms of arsenic sequestration by *in situ* treatment systems

Lara E. Pracht

A dissertation
submitted in partial fulfillment of the
requirements for the degree of

Doctor of Philosophy

University of Washington
2017

Reading Committee:
Rebecca B. Neumann, Chair
Michael Dodd
David E. Butman

Program Authorized to Offer Degree:
Civil and Environmental Engineering

University of Washington

Abstract

Arsenic contaminated groundwater: exploration of the role of organic carbon in mobilization processes and evaluation of mechanisms of arsenic sequestration by *in situ* treatment systems

Lara E. Pracht

Chair of the Supervisory Committee:

Assistant Professor Rebecca B. Neumann

Department of Civil and Environmental Engineering

Abstract text

Arsenic contamination of groundwater is a global concern, with environmental presence attributable to both geogenic and anthropogenic factors. Presence in the environment threatens both public and environmental health. In this study, we explored both the mobilization and sequestration of arsenic in subsurface environments, both in *in situ* treatment systems that sought to sequester the arsenic by intentional interference with the biochemistry and in natural systems where anthropogenic activities hold the potential to inadvertently exacerbate existing public health problems caused by arsenic contamination.

Our investigation into these arsenic stabilization mechanisms involved fieldwork and laboratory-based experiments and analysis methods to study three different groundwater systems. The fieldwork collected sediment and water samples from these different locations. Laboratory batch incubation experiments were conducted for two locations, to elucidate arsenic mobilization processes, with further laboratory characterizations of these experimental materials and those collected from the third site, including solid-phase speciation of arsenic and iron in sediment, molecular characterization of microbially-altered organic carbon, and isotopic characterization of carbon pools.

Our work conducted on *in situ* treatment systems analyzed two different treatments that utilized induced sulfate reduction (ISR) in permeable reactive barriers (PRB) as a means to form sulfide and iron minerals that incorporate or sorb arsenic, removing it from groundwater. Our

work found that PRBs that are formed using zerovalent iron (ZVI) in conjunction with the sulfate and carbon materials are more effective at arsenic removal, likely due to the formation of more stable minerals. Our data suggest that arsenic stabilization in non-ZVI PRBs are primarily controlled by arsenic-sulfide associations, while ZVI PRBs saw greater formation of iron sulfides and iron oxyhydroxides.

Our investigations into mechanisms responsible for subsurface mobilization of arsenic into groundwater were primarily driven by laboratory incubation experiments of aquifer materials collected from arsenic-contaminated locations. Materials collected from an aquifer in Bangladesh were incubated and sampled over one-half year, with the goal of better understanding the labile organic carbon available to fuel reductive dissolution processes that drive arsenic mobilization. Ultrahigh resolution mass spectrometry revealed a large, heterogeneous pool of bioavailable organic carbon in the sediment porewater. Despite the substantial microbial degradation of this carbon pool, most of the compounds were those types traditionally considered recalcitrant or less energetically-favorable. Our results lend weight to an ever-growing shift in understanding of carbon bioavailability. Additionally, both this sediment porewater and the aquifer recharge waters contained many organosulfur compounds, suggesting that the presence of such compounds may potentially be useful as a fingerprint for organic matter derived from organic-rich, anaerobic subsurface environments.

The existence of this pool of organic carbon in subsurface sediments that holds the potential to fuel microbial reactions that impact groundwater quality, led to our final investigation of a process that may occur in situ and mobilize such a pool: microbial priming. Laboratory incubations of aquifer sediment from Cambodia were conducted to show the occurrence of microbial priming and its potential to release mobilize arsenic in the subsurface. The results did not show explicit evidence of priming, but did show an increase in the onset of microbial activity in treatments amended with labile organic carbon. Moreover, even in treatments amended with high concentrations of labile carbon, notable arsenic mobilization was not observed. More energetically-favorable electron acceptors, iron and manganese, were reduced and dissolved into solution, but at later timepoints in the experiment began to decrease in dissolved concentrations, indicating mineral precipitation.

Acknowledgments

First and foremost, I would like to thank my advisor, Rebecca Neumann, for her support and mentorship throughout this process. Words can't express my gratitude. You modeled focus, dedication, creative problem-solving, and patience daily. You provided me with the time and space to pursue opportunities that were beneficial to my career and my self-growth, even when they slowed down my research. Your guidance made this all possible. Thank you for everything.

Thank you to other members of my PhD dissertation committee: Michael Dodd, Darlene Zabowski, and David Butman, for all their time and input, both on my dissertation and throughout my career at UW.

Thank you to so many others who have assisted me in a variety of ways: Brett Beaulieu for initiating the collaboration on the B&L Woodwaste site work, assistance with sample analysis at the synchrotron (SSRL), processing of XANES data, and fieldwork coordination and assistance; Ben Kocar for beamline assistance at SSRL and further assistance with data processing and analysis; EMSL staff at PNNL (Rosalie Chu, Ljiljana Pasa-Tolic, Malak Tfaily) for analysis of our carbon samples on FT-ICR-MS and initial processing of those data; Matthew Polizzotto for fieldwork assistance in Bangladesh, input on research methodology, and providing me with Cambodia sediment; Ethan Linenberger, Mehedi Hasan Tarek, the people of Bashailbhog village, A. Borhan M. Badruzzaman, and M. Ashraf Ali for fieldwork coordination and assistance in Bangladesh; SSRL staff (Sam Webb, Juan Lezama-Pacheco, Ryan Davis) for beamline assistance at SSRL; Floyd|Snider staff (Kristin Anderson, Lisa Meoli, Jenny Pracht, Gretchen Heavner, Erin Murray) for fieldwork coordination, fieldwork assistance, and data processing.

Thank you to my undergraduate students for everything you did to help move my research along and help me become a better mentor and teacher: Hunter Brown (so much!), Joe Ellingson (assistance in the lab and at B&L Woodwaste fieldwork), Robert Ardissono (laboratory assistance with carbon characterization methods and data, especially FT-ICR-MS), Alex Fussell, Veronica Vong (laboratory assistance with method development), Olivia Hargrave (for laboratory assistance, most notably the tedious prepping of EA-IRMS samples).

I also received invaluable laboratory support from Jen Levye (UW), Jerry Wert (Boeing Radiation Laboratory), James Gawel (UW Tacoma), Andrew Schauer (UW Isolab), and J. Sean Yeung (UW).

Thanks to the many students and postdocs I have worked with and around in the Neumann Subsurface Hydro-Biogeochemistry Group: Javier Espeleta, Colby Moorberg, Pamela Barrett, Mickey Jarvi, Farnaz Aslkhodapasand, Neil Schaner, Nick Waldo, Yasmine Farhat, Andrea

Wong, and Brianna Hunt. I hope to see my plants alive and thriving the next time I'm in the fishbowl. And yes, I probably know what that beeping sound in the lab is… just give me a call.

Thank you to those who helped me maintain balance in my life and kept me inspired throughout my academic career: Soli Turner, Liz Turner, Elissa Shortridge, Jill Daniels, Sara Bareilles, Bethany Loveless, Sonny Hong, Julie Bergene, Ingrid Michaelson, Sandra Olson, Sean Parrent, Scott Hansen, Chris Luk, Storm, Austin Bell, Stacy Magante, Gonzalo Chocque Kuno, Kristine Kennewick.

Thank you to my family: my brother, my mom, and my dad. You have always been supportive of my academic pursuits, even when they took me thousands of miles away from you.

Thank you to my wife, Jenny, who brought so much happiness into my life when I really needed it, reinvigorating my academic motivation. The pursuit of my PhD led me to you; your love and support led to me to complete it.

Table of Contents

List of Figures

List of Tables

1. Introduction

1.1 Background

Arsenic contamination of groundwater is a global concern. Presence in the environment is attributable to both geogenic factors (notable cases include contamination in Bangladesh, India, and Cambodia (Kinniburgh & Smedley, 2001; Smedley & Kinniburgh, 2002)) and anthropogenic factors (e.g., acid mine drainage (Casiot et al., 2003; Gault, Cooke, Townsend, Charnock, & Polya, 2005; Johnson & Hallberg, 2005; Smedley & Kinniburgh, 2002), impregnation of lumber for wood preservation (Hasan et al., 2010; Hingston, Collins, Murphy, & Lester, 2001), pesticide use (Belluck, Benjamin, Baveye, Sampson, & Johnson, 2003), industrial waste disposal (Beaulieu & Ramirez, 2013; Mariner, Holzmer, Jackson, Meinardus, & Wolf, 1996), and copper smelting byproducts (Belluck et al., 2003)). The ubiquitous nature of the contamination is problematic, as arsenic poses threats to both human and environmental health. When present in the environment, arsenic threatens aquatic life (e.g., physiological, hormonal, and behavioral impacts on fish (Bears, Richards, & Schulte, 2006; Bhattacharya & Bhattacharya, 2007; Nichols et al., 1984)) and plant life (e.g., negative impacts on yield when rice crops are irrigated with contaminated water or grown on contaminated soil (Abedin, Cotter-Howells, & Meharg, 2002; Delowar et al., 2005; Dittmar et al., 2010; Khan et al., 2009, 2010; Li, Stroud, Ma, McGrath, & Zhao, 2009; Panaullah et al., 2009)). Food crops grown in contaminated environments can also retain arsenic, providing another mechanism for human and animal consumption (Meharg & Rahman, 2003). If arsenic is consumed by humans, via drinking water or in food sources, individuals can develop arsenicosis which exhibits as skin lesions, cancers, and increased mortality (Argos et al., 2010). Malnutrition may exacerbate the

deleterious effects of arsenic exposure in humans (Hsueh et al., 1995, 1997; Smith & Smith, 2004), heightening the impact on individuals in poverty-stricken regions.

The global threat posed by arsenic makes it critical that we gain a better understanding of arsenic mobilization and immobilization processes. Despite geogenic arsenic concentrations in soil and sediments that are often relatively low (crustal average is 1.8 mg/kg (Greenwood & Earnshaw, 1984)), some groundwater systems contain very high levels of arsenic, that was mobilized from that sediment. The mechanisms that drive this release need to be better understood. Arsenic is mobilized off sediment via microbially-mediated reductive dissolution process, where organic carbon is used as the energy source (electron donor). Through oxidation of organic carbon, microbes reduce arsenic and/or arsenic-associated iron minerals, releasing arsenic into the aqueous phase. However, previous work has indicated that carbon degradation does not always stimulate arsenic mobilization (Neumann, Pracht, Polizzotto, Badruzzaman, & Ali, 2014; Polizzotto et al., 2006; Polizzotto, Harvey, Sutton, & Fendorf, 2005; Radloff et al., 2007) in natural sediments. Additionally, mobilization effects are not always predictable based simply on organic carbon concentrations, as priming effects may increase the amount of bioavailable carbon in groundwater systems. Priming refers to an increase in microbial utilization of soil organic matter (i.e., carbon mineralization), driven by an influx of bioavailable organic carbon to that soil and sediment (Blagodatskaya & Kuzyakov, 2008; Kuzyakov, Friedel, & Stahr, 2000). These fluxes are not likely to be captured by concentration measurements alone. Due to these potential priming effects, it is important to further explore possible human perturbations, such as pumping activities, installation of wells, and chemical waste disposal that may lead to increased mobilization.

Beyond better elucidating the mechanisms of arsenic mobilization into groundwater, it is important that we continue to explore treatment systems to remove arsenic from groundwater. Industrial contamination often leads to much more acutely severe contamination problems and thus pointed treatment systems for these contaminated locations are key. Innovative approaches to treating large amounts of water efficiently have emerged in the form of in situ permeable reactive barriers, a relatively low-cost, passive treatment option. The effectiveness of these systems at arsenic removal from groundwater must be evaluated, but it is also critical to understand the specific mechanisms that are responsible for the removal of the contaminant. Without this clearer understanding, the long-term success of treatment is put into jeopardy.

1.2 Dissertation Overview

This study utilized both fieldwork and laboratory techniques to investigate these identified gaps in knowledge. The first chapter, Chapter 2, focuses on work conducted on *in situ* treatment systems installed near Tacoma, WA, to treat a groundwater system contaminated by industrial waste. We collected sediment samples from within the two different systems, and utilized solid-phase analysis (x-ray absorption spectroscopy, x-ray fluorescence, and sequential chemical extractions) to determine mechanisms of arsenic stabilization, comparing these mechanisms to years of groundwater arsenic data as a means of evaluating the two systems and the most effective mechanisms of arsenic removal from the aqueous phase.

The next chapter, follows up on an incubation study conducted on materials collected from an arsenic-contaminated aquifer in Bangladesh (Neumann et al., 2014). That incubation study identified a previously undocumented pool of bioavailable sedimentary organic carbon. This chapter molecularly characterizes that pool, before and during microbial degradation in

these incubations, using Fourier Transform Ion Cyclotron Resonance Mass Spectrometry (FT-ICR-MS), elucidating carbon compounds key in microbial reactions.

The final chapter, Chapter 4, expands on the work in Chapter 3, presenting the results of an incubation study conducted on Cambodian aquifer sediment; sediment from an aquifer low in arsenic, but vulnerable to contamination. This work sought to demonstrate the capacity for an influx of labile organic carbon to destabilize bioavailable organic matter from the sediment, as happened in the Bangladesh study, and fuel microbial reduction reactions that released arsenic into the water. The mass of carbon as it transferred between pools, along with the isotopic composition of that carbon was tracked over time to highlight the potential for future contamination of currently clean aquifers.

1.3 References

Abedin, M. J., Cotter-Howells, J., & Meharg, A. A. (2002). Arsenic uptake and accumulation in rice (Oryza sativa L.) irrigated with contaminated water. *Plant and Soil*, *240*(2), 311–319. https://doi.org/10.1023/A:1015792723288

Argos, M., Kalra, T., Rathouz, P. J., Chen, Y., Pierce, B., Parvez, F., … Ahsan, H. (2010). Arsenic exposure from drinking water, and all-cause and chronic-disease mortalities in Bangladesh (HEALS): a prospective cohort study. *The Lancet*, *376*(9737), 252–258. https://doi.org/10.1016/S0140-6736(10)60481-3

Bears, H., Richards, J. G., & Schulte, P. M. (2006). Arsenic exposure alters hepatic arsenic species composition and stress-mediated gene expression in the common killifish (Fundulus heteroclitus). *Aquatic Toxicology*, *77*(3), 257–266. https://doi.org/10.1016/j.aquatox.2005.12.008

Beaulieu, B., & Ramirez, R. E. (2013). Arsenic Remediation Field Study Using a Sulfate Reduction and Zero-Valent Iron PRB. *Groundwater Monitoring & Remediation*, *33*(2), 85–94. https://doi.org/10.1111/gwmr.12007

Belluck, D. A., Benjamin, S. L., Baveye, P., Sampson, J., & Johnson, B. (2003). Widespread Arsenic Contamination of Soils in Residential Areas and Public Spaces: An Emerging Regulatory or Medical Crisis? *International Journal of Toxicology*, *22*(2), 109–128. https://doi.org/10.1080/10915810305087

Bhattacharya, A., & Bhattacharya, S. (2007). Induction of oxidative stress by arsenic in Clarias batrachus: Involvement of peroxisomes. *Ecotoxicology and Environmental Safety*, *66*(2), 178–187. https://doi.org/10.1016/j.ecoenv.2005.11.002

Blagodatskaya, E., & Kuzyakov, Y. (2008). Mechanisms of real and apparent priming effects and their dependence on soil microbial biomass and community structure: critical review. *Biology and Fertility of Soils*, *45*(2), 115–131. https://doi.org/10.1007/s00374-008-0334-y

Casiot, C., Morin, G., Juillot, F., Bruneel, O., Personné, J.-C., Leblanc, M., … Elbaz-Poulichet, F. (2003). Bacterial immobilization and oxidation of arsenic in acid mine drainage (Carnoulès creek, France). *Water Research*, *37*(12), 2929–2936. https://doi.org/10.1016/S0043-1354(03)00080-0

Delowar, H., Yoshida, I., Harada, M., Sarkar, A., Miah, M., Razzaque, A., … Delowar, H. (2005). Growth and uptake of arsenic by rice irrigated with As-contaminated water. *Journal of Food Agriculture and Environment*, *3*(2), 287–291.

Dittmar, J., Voegelin, A., Maurer, F., Roberts, L. C., Hug, S. J., Saha, G. C., … Kretzschmar, R. (2010). Arsenic in Soil and Irrigation Water Affects Arsenic Uptake by Rice: Complementary Insights from Field and Pot Studies. *Environmental Science & Technology*, *44*(23), 8842–8848. https://doi.org/10.1021/es101962d

Gault, A. G., Cooke, D. R., Townsend, A. T., Charnock, J. M., & Polya, D. A. (2005). Mechanisms of arsenic attenuation in acid mine drainage from Mount Bischoff, western Tasmania. *Science of The Total Environment*, *345*(1–3), 219–228. https://doi.org/10.1016/j.scitotenv.2004.10.030

Greenwood, N. N., & Earnshaw, A. (1984). *Chemistry of the elements*. Oxford [Oxfordshire]; New York: Pergamon Press.

Hasan, A. R., Hu, L., Solo-Gabriele, H. M., Fieber, L., Cai, Y., & Townsend, T. G. (2010). Field-scale leaching of arsenic, chromium and copper from weathered treated wood.

Environmental Pollution, *158*(5), 1479–1486. https://doi.org/10.1016/j.envpol.2009.12.027

Hingston, J. A., Collins, C. D., Murphy, R. J., & Lester, J. N. (2001). Leaching of chromated copper arsenate wood preservatives: a review. *Environmental Pollution*, *111*(1), 53–66. https://doi.org/10.1016/S0269-7491(00)00030-0

Hsueh, Y. M., Cheng, G. S., Wu, M. M., Yu, H. S., Kuo, T. L., & Chen, C. J. (1995). Multiple risk factors associated with arsenic-induced skin cancer: effects of chronic liver disease and malnutritional status. *British Journal of Cancer*, *71*(1), 109–114.

Hsueh, Y. M., Chiou, H. Y., Huang, Y. L., Wu, W. L., Huang, C. C., Yang, M. H., … Chen, C. J. (1997). Serum beta-carotene level, arsenic methylation capability, and incidence of skin cancer. *Cancer Epidemiology, Biomarkers & Prevention: A Publication of the American Association for Cancer Research, Cosponsored by the American Society of Preventive Oncology*, *6*(8), 589–596.

Johnson, D. B., & Hallberg, K. B. (2005). Acid mine drainage remediation options: a review. *Science of The Total Environment*, *338*(1–2), 3–14. https://doi.org/10.1016/j.scitotenv.2004.09.002

Khan, M. A., Islam, M. R., Panaullah, G. M., Duxbury, J. M., Jahiruddin, M., & Loeppert, R. H. (2009). Fate of irrigation-water arsenic in rice soils of Bangladesh. *Plant and Soil*, *322*(1–2), 263–277. https://doi.org/10.1007/s11104-009-9914-3

Khan, M. A., Islam, M. R., Panaullah, G. M., Duxbury, J. M., Jahiruddin, M., & Loeppert, R. H. (2010). Accumulation of arsenic in soil and rice under wetland condition in Bangladesh. *Plant and Soil*, *333*(1–2), 263–274. https://doi.org/10.1007/s11104-010-0340-3

Kinniburgh, D. G., & Smedley, P. L. (2001). *Arsenic contamination of groundwater in Bangladesh*. Keyworth: British Geological Survey.

Kuzyakov, Y., Friedel, J. K., & Stahr, K. (2000). Review of mechanisms and quantification of priming effects. *Soil Biology and Biochemistry*, *32*(11–12), 1485–1498. https://doi.org/10.1016/S0038-0717(00)00084-5

Li, R. Y., Stroud, J. L., Ma, J. F., McGrath, S. P., & Zhao, F. J. (2009). Mitigation of Arsenic Accumulation in Rice with Water Management and Silicon Fertilization. *Environmental Science & Technology*, *43*(10), 3778–3783. https://doi.org/10.1021/es803643v

Mariner, P. E., Holzmer, F. J., Jackson, R. E., Meinardus, H. W., & Wolf, F. G. (1996). Effects of High pH on Arsenic Mobility in a Shallow Sandy Aquifer and on Aquifer Permeability along the Adjacent Shoreline, Commencement Bay Superfund Site, Tacoma, Washington. *Environmental Science & Technology*, *30*(5), 1645–1651. https://doi.org/10.1021/es9506420

Meharg, A. A., & Rahman, M. M. (2003). Arsenic Contamination of Bangladesh Paddy Field Soils: Implications for Rice Contribution to Arsenic Consumption. *Environmental Science & Technology*, *37*(2), 229–234. https://doi.org/10.1021/es0259842

Neumann, R. B., Pracht, L. E., Polizzotto, M. L., Badruzzaman, A. B. M., & Ali, M. A. (2014). Biodegradable Organic Carbon in Sediments of an Arsenic-Contaminated Aquifer in Bangladesh. *Environmental Science & Technology Letters*, *1*(4), 221–225. https://doi.org/10.1021/ez5000644

Nichols, J. W., Wedemeyer, G. A., Mayer, F. L., Dickhoff, W. W., Gregory, S. V., Yasutake, W. T., & Smith, S. D. (1984). Effects of freshwater exposure to arsenic trioxide on the parr-

smolt transformation of coho salmon (Oncorhynchus kisutch. *Environmental Toxicology and Chemistry*, *3*(1), 143–149. https://doi.org/10.1002/etc.5620030116

Panaullah, G. M., Alam, T., Hossain, M. B., Loeppert, R. H., Lauren, J. G., Meisner, C. A., … Duxbury, J. M. (2009). Arsenic toxicity to rice (Oryza sativa L.) in Bangladesh. *Plant and Soil*, *317*(1–2), 31–39. https://doi.org/10.1007/s11104-008-9786-y

Polizzotto, M. L., Harvey, C. F., Li, G., Badruzzman, B., Ali, A., Newville, M., … Fendorf, S. (2006). Solid-phases and desorption processes of arsenic within Bangladesh sediments. *Chemical Geology*, *228*(1–3), 97–111. https://doi.org/10.1016/j.chemgeo.2005.11.026

Polizzotto, M. L., Harvey, C. F., Sutton, S. R., & Fendorf, S. (2005). Processes conducive to the release and transport of arsenic into aquifers of Bangladesh. *Proceedings of the National Academy of Sciences of the United States of America*, *102*(52), 18819–18823. https://doi.org/10.1073/pnas.0509539103

Radloff, K. A., Cheng, Z., Rahman, M. W., Ahmed, K. M., Mailloux, B. J., Juhl, A. R., … Van Geen, A. (2007). Mobilization of arsenic during one-year incubations of grey aquifer sands from Araihazar, Bangladesh. *Environmental Science & Technology*, *41*(10), 3639–3645.

Smedley, P. L., & Kinniburgh, D. G. (2002). A review of the source, behaviour and distribution of arsenic in natural waters. *Applied Geochemistry*, *17*(5), 517–568. https://doi.org/10.1016/S0883-2927(02)00018-5

Smith, A. H., & Smith, M. M. H. (2004). Arsenic drinking water regulations in developing countries with extensive exposure. *Toxicology*, *198*(1–3), 39–44. https://doi.org/10.1016/j.tox.2004.02.024

2. Evaluation of the mechanisms of arsenic sequestration in *in-situ* groundwater treatment systems implementing induced sulfate reduction via permeable reactive barriers with and without utilization of zero-valent iron

2.1 Introduction

Arsenic contamination of groundwater is a global concern. Arsenic presence in the environment is attributable to both geogenic factors (notable cases include contamination in Bangladesh, India, and Cambodia (Kinniburgh & Smedley, 2001; Smedley & Kinniburgh, 2002)) and anthropogenic factors (e.g., acid mine drainage (Casiot et al., 2003; Gault, Cooke, Townsend, Charnock, & Polya, 2005; Johnson & Hallberg, 2005; Smedley & Kinniburgh, 2002), impregnation of lumber for wood preservation (Hasan et al., 2010; Hingston, Collins, Murphy, & Lester, 2001), pesticide use (Belluck, Benjamin, Baveye, Sampson, & Johnson, 2003), industrial waste disposal (Beaulieu & Ramirez, 2013; Mariner, Holzmer, Jackson, Meinardus, & Wolf, 1996), and copper smelting byproducts (Belluck et al., 2003)). The ubiquitous nature of the contamination is problematic, as arsenic poses threats to both human and environmental health. Human health risks include cancer and increased mortality (Argos et al., 2010). When present in the environment, arsenic threatens aquatic life (e.g., physiological, hormonal, and behavioral impacts on fish (Bears, Richards, & Schulte, 2006; Bhattacharya & Bhattacharya, 2007; Nichols et al., 1984) and plant life (e.g., negative impacts on yield when rice crops are irrigated with contaminated water or grown on contaminated soil) (Abedin, Cotter-Howells, & Meharg, 2002; Delowar et al., 2005; Dittmar et al., 2010; Khan et al., 2009, 2010; Li, Stroud, Ma, McGrath, & Zhao, 2009; Panaullah et al., 2009).

In light of the global threat of arsenic contamination in groundwater, evaluation of treatment systems is a pressing need. Determination of a system's short- and long-term effectiveness, widespread applicability, and susceptibility to failure is needed to move towards effective solutions. One promising *in-situ* remediation strategy is the creation of localized

biogeochemical conditions favorable to arsenic sequestration by manually inducing microbial sulfate reduction. The goal of induced sulfate reduction (ISR) is to precipitate sulfide minerals that provide sorption sites for arsenic or incorporate arsenic into their crystal matrix. One method to induce these conditions is to install permeable reactive barriers (PRBs). PRBs are a low cost, passive treatment system that are installed in regions that intercept the groundwater flow pathway. PRBs contain reactive materials (material selection varies depending on identified contaminant) that facilitate biogeochemical reactions, transforming contaminants to less mobile or less toxic forms. They can either be installed by excavation of soil and sediment in the pathway of groundwater flow and backfilling the area with reactive media or by injecting reactive materials directly into the groundwater and/or sediment. PRBs have been used to successfully remove chlorinated hydrocarbons (Gillham & O'Hannesin, 1994; Richards, 2008; Su et al., 2012; Vogan, Focht, Clark, & Graham, 1999; Wilkin, Puls, & Sewell, 2003), hexavalent chromium (Wilkin et al., 2003), uranium (Morrison, Metzler, & Carpenter, 2001), arsenic (Beak & Wilkin, 2009; Beaulieu & Ramirez, 2013), and other contaminants from groundwater.

Many applications of PRB approaches that focus on arsenic removal utilize zero-valent iron (ZVI), providing a potential for more minerals to form that facilitate arsenic immobilization. An application of induced sulfate reduction (ISR) with only organic carbon and sulfate materials (i.e., without ZVI) is likely to form arsenic-sulfide minerals, such as realgar and orpiment (O'Day, 2006; O'Day, Vlassopoulos, Root, Rivera, & Turekian, 2004) and amorphous iron-sulfide minerals, such as mackinawite, that may over time develop into pyrite (Morse & Cornwell, 1987). Iron (hydr)oxides are unlikely to form. Conversely, a PRB installation for ISR that includes ZVI application leads to the creation of Fe(II) and H_2 gas, additional reductants that

improve arsenic removal (Wilkin, Acree, Ross, Beak, & Lee, 2009; Zheng, Apps, Zhang, Xu, & Birkholzer, 2009) and the system is likely to form FeS minerals, such as mackinawite (Furukawa, Kim, Watkins, & Wilkin, 2002; Roh, Lee, & Elless, 2000). Moreover, many additional iron minerals, such as iron (oxy)hydroxides (Manning, Hunt, Amrhein, & Yarmoff, 2002; Melitas, Wang, Conklin, O'Day, & Farrell, 2002; Phillips et al., 2000) may form during the oxidation of the ZVI, leading to additional sorption sites and opportunities for coprecipitation of arsenic species.

Despite the increased reductants provided by ZVI, a system without ZVI may be preferred for many reasons, including cost, ease of installation (Floyd|Snider & AMEC, 2013), or prevention of long-term permeability issues (Henderson & Demond, 2013). In our study, the ZVI treatment contained insoluble ZVI and thus had to be injected with a direct-push drill rig. Additionally, its propriety nature led to it being more expensive than a custom solution. The custom solution also carried the ability to be deposited into the aquifer via existing groundwater monitoring wells.

PRBs for remediation of arsenic in groundwater have had limited implementation, largely due to sparse field-level studies exhibiting their effectiveness and long-term stability. Only a few field-based studies have been conducted on ISR systems without zero-valent iron added (O'Day et al., 2004), or on applications of these systems as PRBs utilizing ZVI to treat arsenic (Wilkin et al., 2009). In lieu of field-based applications, a wide-array of laboratory-based studies have been conducted to assess methods of ISR (Henderson & Demond, 2013), ability of ISR to remove As (Keimowitz et al., 2007; Onstott, Chan, Polizzotto, Lanzon, & DeFlaun, 2011), and ability of ZVI to remove arsenic from water, both as part of an ISR system and as a standalone product (Gibert, de Pablo, Cortina, & Ayora, 2010; Lackovic, Nikolaidis, & Dobbs, 2000).

The goals of this study were to determine the *in situ* performance difference between a PRB application with ZVI and an application without ZVI, as well as identify the specific sequestration mechanisms responsible for removal of arsenic from groundwater in these systems. We sought to fill gaps in the current literature regarding specific mineral formations that occur in field-based application of these systems, how ZVI impacts these specific minerals, and what minerals arsenic associates with and in what capacity (i.e. sorbed or coprecipitated) during its removal from water. To achieve these ends, we combined groundwater monitoring data from two field-based applications of ISR at an industrial-contamination site with solid-phase speciation analyses of arsenic and iron in sediment obtained from the PRBs. Speciation analysis provides insight into the sequestration mechanisms responsible for arsenic immobilization, by indicating possible minerals formed. Solid-phase speciation analysis was conducted via microscale x-ray absorption (μXAS), x-ray fluorescence (XRF) mapping, as well as functionally defined fractionation of arsenic and iron species via sequential chemical extraction methods. Determining the specific mechanisms occurring in the sediment will allow us to draw conclusions about the long-term stability of arsenic in ISR PRBs and to predict system behavior over time and with changing biogeochemical conditions in the aquifer. The results of this work will ultimately help inform strategies for arsenic cleanup in both geogenic and anthropogenic contamination sites, in particular the field site where this work was conducted.

2.2 Methods

For this study, data was collected via field sampling, synchrotron analysis (XAS and XRF measurements), and sequential extractions. Our work focused on a field site located near

Tacoma, WA. For many years, from the mid 1970's until the early 1980's, it was the recipient of slag-contaminated wastes from log sort yards in Commencement Bay that were contaminated from the Asarco smelter in North Tacoma/ Ruston, WA. In the early 1990's, the Washington State Department of Ecology issued an Enforcement Order for all responsible parties to take steps to remediate the arsenic, as they found arsenic in the bottom of the landfill to be in contact with the water table during parts of the year, and arsenic levels in a nearby wetland to be above cleanup levels(WSDE, 2007). The contaminated groundwater endangers Hylebos Creek, a nearby waterway that feeds into Commencement Bay and ultimately to Puget Sound, and thus is considered a threat to ecological and human health. Concentrations in the contaminated wetland reach 4000 ug/L (WSDE, 2007), nearly 1000-times higher than background levels for the site of 5 ug/L (WSDE, 2007, 2013).

2.2.1 Experimental Setup

At our field site, two different treatment systems were tested for their ability to remove arsenic from contaminated groundwater. Both approaches implement PRBs as a vehicle for chemically inducing microbial sulfate reduction. The location of the two systems within the field site are indicated on Figure 2.1 ("Z PRB" and "NZ PRB"). The systems vary in the slurry materials used (notably ZVI), arsenic concentrations entering the system, size, and performance to this point. Table properties are summarized in Table 1.

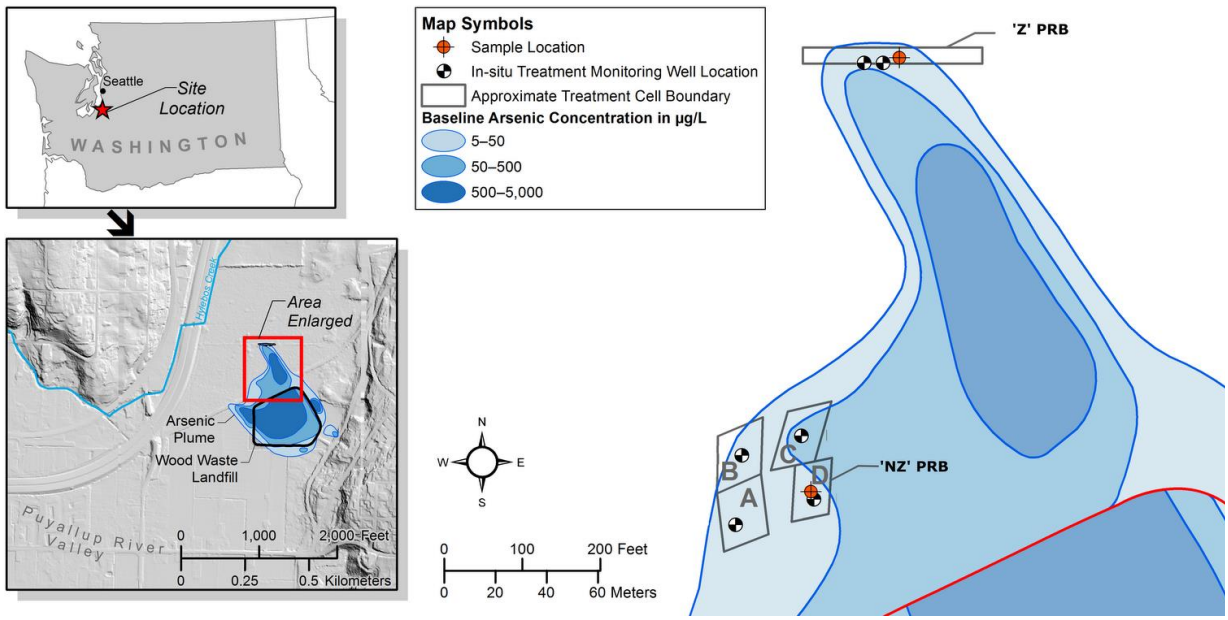

Figure 2.1: Location of experimental field site and ISR PRBs. All installed PRBs are shown, with the PRBs where sediment was collected for solid-phase analysis indicated by 'Z' (ZVI system) and 'NZ' (non-ZVI system). Sediment sample locations are shown as orange symbols. PRBs labeled A-D are pilot-scale studies, with two containing ZVI (A,B) and two not containing ZVI (C,D).

The first system, installed on 12/16/2009, utilized a proprietary injection slurry, EHC-M (Adventus Americas Inc., Freeport, Illinois), that contains a hydrophilic organic carbon source (ground plant fibers), sulfate salts (Mg- and K-), and ZVI. This system will henceforth be referred to as the ZVI system (or Z in Figures and Tables). This system is located in a higher-concentration area of the arsenic plume. The system covers an area of 220 feet by 20 feet, and is 10-22 feet deep. Details of the system installation have been previously described in publication (Beaulieu & Ramirez, 2013).

In the second system, a non-proprietary mixture containing a carbon source (food-grade high fructose corn syrup), a pH buffer (sodium bicarbonate), and sulfate salts ($NaSO_4$ and K_2SO_4) was injected into the groundwater via injection wells. This second system contains no ZVI, and will henceforth be referred to as the non-ZVI system (or NZ). This system was installed

at the site on 10/7/2011. It is located in an area of lower arsenic concentration than the ZVI system (~35 ppb (Floyd|Snider & AMEC, 2013)), but still has higher arsenic concentrations than the regulatory limit of 5 μg/L (WSDE, 2007, 2013). The system is a smaller size than the ZVI system, measuring 50 feet by 85 feet, and extending from 5 feet below ground surface to 15 feet bgs.

Table 2.1: PRB Properties. Summary of the known and expected properties of each ISR system that was analyzed for solid-phase speciation and mineral associations.

	Zerovalent Iron PRB (Z)	Non-zerovalent Iron PRB (NZ)
Proprietary?	Proprietary (EHC-M®, Adventus Americas, Inc., Freeport, IL)	Non-proprietary
Slurry Materials	Carbon (hydrophilic, ground plant fibers) S (Mg, K·SO_4 salts) ZVI	Carbon (food-grade, high-fructose corn syrup) S (Na, K·SO_4 salts) NaHCO3 (pH buffer)
Minerals Expected to Form	Iron monosulfide minerals Iron (oxy)hydroxides	Iron monosulfide minerals Other monosulfides
Example Minerals	Disordered mackinawite (FeS) Realgar (AsS) Green rusts (Mixed valence iron (oxy)hydroxides·SO_4)	Disordered mackinawite (FeS) Realgar (AsS)
PRB Size	220 ft X 20 ft, 10-22 ft bgs	85 ft X 50 ft, 5-15 ft bgs

2.2.2 Material/ Sample Collection

Groundwater was periodically sampled from monitoring wells (as shown in Figure 2.1) throughout the study. Sampling methods have been previously described (Beaulieu & Ramirez, 2013). During sampling, pH, temperature, ORP, DO, and conductivity were measured. Aquifer sediment samples were collected from the B&L Woodwaste site prior to installation of the PRBs in September 2006, using a direct-push drill rig. Samples were collected from a depth of 6-7'. After installation of the two PRB systems, additional sediment samples were collected on September 11, 2012, with similar methods, at locations in Treatment Cell D (Pilot Study treatment – non-ZVI PRB) and the 12th Street East Treatment Zone (ZVI PRB) at depths of 13.5 to 16.5 feet and 17 to 20 feet, respectively (see Figure 1). Collection of samples and all subsequent sample processing was conducted under anaerobic conditions. Initial samples,

collected prior to PRB installation, were processed inside of an anaerobic glovebag maintained with a nitrogen atmosphere in the field. This sediment was divided into glass jars and placed in a cooler with dry ice. After transport back to the lab, sediment was stored in the freezer. All post-PRB samples were collected in plastic core liners and capped. Cores were then put into gas-impermeable bags (ESCAL, Mitsubishi Gas Company), heat sealed with oxygen-scavenging sachets with oxygen-indicators (GasPak, BD Diagnostic Systems) inside, and placed in a cooler with dry ice. After transport back to the lab, samples were stored in the freezer. Samples were closely monitored for infiltration of oxygen and oxygen-scavenging packets were promptly replaced as needed. Handling of the samples was always done inside an H_2/N_2 atmosphere in an anaerobic chamber. Oxygen levels in the chamber were monitored by an anaerobic meter (Coy Lab Products).

2.2.3 Synchrotron Analyses

2.2.3.1 Preparation of Synthetic Minerals

For the synchrotron analyses, two synthetic minerals were created in the lab. Minerals chosen are representative of those present in the aquifer sediment material at B&L Woodwaste: mackinawite (an iron sulfide) and ferrihydrite (an iron (oxy)hydroxide). These minerals were spiked with sufficient arsenite solution to achieve adsorption onto the precipitates, while avoiding incorporation into the mineral matrix. A total concentration of 5 X 10-5 M (6.15 mg/L) was selected for mackinawite based on literature (Farquhar, Charnock, Livens, & Vaughan, 2002; Gallegos, Hyun, & Hayes, 2007; Han, Demond, & Hayes, 2013) and applied to the ferrihydrite standard for consistency.

The ferrihydrite sample was created by dissolving $Fe(NO_3)_2$ salt in 0.5 L of ultrapure water to achieve 0.2M, and adjusting pH to 5.5 with HCl. Next, NaOH was titrated into the solution until pH 8.0 was reached. The solution was stirred vigorously for 2 hours and adjusted to 1L (Zhao, Jia, Xu, & Zhao, 2011). After letting the solution age for 24 hours at 20°C, it was spiked with arsenite, tumbled for 48 hours, and vacuum filtered through a 22 μm filter (cellulose) and then a 0.2um membrane (polyethersulfone) filter. The solids collected on the filter were air-dried, knocked off the filter, and ground with an agate mortar and pestle. This powder was spread out with a silicone spatula as a thin layer on Kapton tape, then covered with another piece of Kapton tape. This sample was stored inside of a gas impermeable bag (ESCAL) for transport. Note that this sample was created in an ambient atmosphere.

The mackinawite (FeS) sample was created by adding 0.5 L of 0.30 M Na_2S to 0.5 L of 0.228 M $FeCl_2$ (Butler & Hayes, 1998). After letting the solution age for 29 hours, the pH was adjusted to 6.5 and kept stable for 26 hours. It was then spiked with arsenite, tumbled for 48 hours, and vacuum-filtered through a 22 μm filter (cellulose) and then a 0.2 μm membrane filter (polyethersulfone). The solids collected on the filter were air-dried inside of a glovebox (N_2/H_2 atmosphere). Unlike the ferrihydrite synthetic mineral however, this only achieved the consistency of a paste. This paste was spread out in a thin layer on a piece of Kapton tape, then covered with another piece of tape. This sample was then stored inside of an ESCAL bag, along with an oxygen-scavenging packet to maintain anoxic conditions for transport. Note that this sample was created in entirety inside of the anaerobic glovebox.

2.2.3.2 Preparation of Natural Samples

The pre-PRB installation sample was prepared at the synchrotron facility in a N_2/H_2 atmosphere glovebox. The sample was thawed inside the chamber, lightly ground into a paste

using an acid-washed agate mortar and pestle, loaded into a 1 mm Teflon sample holder using an acid-washed silicone spatula, and sealed with Kapton tape.

Post-PRB installation samples were prepared at the University of Washington, with final steps conducted at the synchrotron facility. One three foot core of each aquifer sample (ZVI and non-ZVI PRB) was thawed inside of the anaerobic chamber. Each core was then dried inside the glove box and homogenized with an acid-washed plastic spoon in an acid-washed and furnaced (550 ℃ for 4 hours) glass bowl. Dried samples were sieved with a plastic #200 sieve (Model SV-165#200, Gilson Company, Inc., Lewis Center, OH) to isolate the fine fraction: this was done to concentrate the arsenic and achieve stronger XAS results.

For bulk-scale analysis, these fines, from both the ZVI and non-ZVI PRBs, were transported to the beamline in anaerobic conditions, heat-sealed in gas-impermeable bags containing oxygen-scavenging sachets and oxygen indicators. and then loaded onto a 1mm titanium mount inside of an anaerobic glovebox and sealed on both sides with Kapton tape to maintain the anoxic atmosphere. For microscale analyses of the post-installation natural sediment samples, isolated fines fraction were spread out onto a piece of Kapton tape and sealed with additional Kapton tape inside of the anaerobic chamber at the University of Washington. These samples were then sealed into an ESCAL bag with an oxygen-scavenging sachet for transport to the synchrotron.

2.2.3.3 Synchrotron Methods

Bulk x-ray absorption spectroscopy (XAS)

Bulk-scale analysis of anaerobically prepared aquifer sediment samples was performed to gain a better understanding of the "average" associations of arsenic. Samples were analyzed on beamline 11-2 at the Stanford Synchrotron Radiation Lightsource (SSRL), SLAC National Accelerator Laboratory in Menlo Park, CA., with XAS crystal Si220 at phi = 90. X-ray absorption spectroscopy (XAS) scans were collected for As and Fe.

Within an anaerobic chamber at SSRL, samples were mounted on titanium sample mounts, oval-shaped, 6 mm x 2.5 mm and 1 mm thick. Once outside of the anaerobic chamber, the samples were mounted onto a cryostat and mounted in the beamline hutch. The sample was surrounded by an empty chamber box, approximately 6" x 6" x 6". A vacuum was then placed on the chamber and maintained throughout analysis. Freezing temperatures were achieved by pouring liquid nitrogen into the cryostat. The vacuum surrounding the sample helped maintain anoxic conditions, as well as keeping uniform freezing temperatures and preventing the development of frost on and around the sample.

Due to the dilute concentrations of arsenic, only XANES (X-ray absorption near edge structure) scans were taken, from an energy of approximately 11640 to 12210 eV. For each sample, 18-20 scans were taken for As, and later averaged. Data was collected in fluorescence mode with a 100-node Ge detector. The instrument was calibrated to the correct edge position by simultaneous analysis of an Au standard foil, in transmission mode, calibrated to 11919 eV. To achieve the strongest arsenic detection, without interference from the high concentrations of iron, 8 layers of aluminum foil were used to decrease fluorescence detection of that element.

Iron speciation in the samples was analyzed via fluorescence, in the same manner as arsenic. Energies used for the XAS scans varied between samples, but both samples collected data at a minimum for the range 6880-7169 eV. For each sample, 6-9 scans were taken, then later averaged. Data was collected in fluorescence mode with a 100-node Ge detector, with the instrument calibrated with an iron foil (Fe^0), which was collected for each sample simultaneously, in transmission mode and calibrated to an edge of 7112 eV. To reduce the effect of other elements with edge position energies close to iron, a Mn filter (Q = 3) was installed in front of the detector, along with solar slits.

Analysis of subsequent XAS scans showed no signs of beamline alteration of the samples, for arsenic or iron. All data were analyzed using the SIXPack software. Analysis for both arsenic and iron was done with a slit width of 4mm and height of 1.5 mm.

Micro x-ray fluorescence (μXRF) and absorption spectroscopy (μXAS)

Microscale analyses of samples in Kapton tape were conducted on beamline 2-3 at SSRL. Using this beamline, micro-x-ray absorption spectroscopy (μXAS) spectra were collected, along with micro x-ray fluorescence (μXRF) element maps to elucidate the solid-phase local coordination environment of As. Micro x-ray absorption spectroscopy (μXAS) scans were collected for As and Fe, while μXRF element maps were collected for the following elements: As, Fe, S, Si, P, Cl, K, Ca, Ti, Cr, Mn, Ni, Cu, and Zn.

Micro-x-ray fluorescence was first used to create spatial maps of element locations and relative concentrations. The mapped domain was a square with sides between 50 and 150 μm along the edge. The maps were composed of pixels (step size) sized 1 μm^2. Dwell time was

30ms. All data were analyzed using the Microprobe Analysis Toolkit software (Samuel Webb, SSRL).

The spatial element maps generated by μXRF were used to determine ideal locations for μXAS analysis. The low concentrations of As in the soil (low relative to the instrument's detection ability), required that μXAS data be collected from "hotspots" of As. Once these locations were determined, between 6-7 scans were generated for As and 1-6 scans were generated for iron. Arsenic scans were collected from an energy of 11640 to 11900 eV, sufficiently surrounding the As K-edge (11867 eV). Fe scans were collected from an energy of 7090 to 7160 eV, surrounding the Fe K-edge (7111 eV). All data were calibrated by shifting energies by a constant value, determined by the adjustment of iron and arsenate foil standards scans to their proper, known k-edge. All data were analyzed using the SIXPack software (Samuel Webb, SSRL).

2.2.4 Sequential Chemical Extractions

To provide information about the nature of physicochemical associations between arsenic, iron, and other compounds in the sediment minerals, sequential chemical extractions were performed on the same homogenized sediment samples collected and prepared for analysis on the synchrotron. Sequential extractions were performed in a modified protocol of that presented by Keon et al. 2001(Keon, Swartz, Brabander, Harvey, & Hemond, 2001). Operational fractions targeted by our extractions were: (1) strongly adsorbed [extracted with 1M NaH_2PO_4], (2) coprecipitated with acid-volatile sulfides (AVS), carbonate, manganese, very amorphous iron oxides, [extracted with 1 N HCl] (3) coprecipitated with amorphous iron oxyhydroxides

[extracted with 0.2 M ammonium oxalate/oxalic acid], (4) coprecipitated with crystalline iron oxyhydroxides [extracted with 0.05 M Ti(III)-citrate-EDTA-bicarbonate], (5) coprecipitated with pyrite and amorphous arsenic sulfides (As_2S_3) [extracted with 16 N HNO_3], (5) recalcitrant [extracted with 16 N HNO_3 and 30% H_2O_2 using microwave digestion]. These extractions were performed on both the bulk sediment and the fines fraction, to ensure meaningful correlation of data between these analyses and the synchrotron analyses. All chemicals used in extractions were of reagent grade purity or higher. The following modifications were made to the Keon 2001 protocol:

1. Samples were centrifuged for 1 hour at 4150 rpm (~3860g) before decanting and filtering, instead of 25 min at 11000 g.
2. 2.5 g (wet mass) sediment was added to 30 mL extractant, instead of 0.4 g (dry mass) to 40 mL extractant. This change was made to ensure high enough arsenic concentrations in final solution to accurately measure.
3. After centrifuging, samples were syringe-filtered by 0.2um nylon filters, instead of directly decanting after centrifuging.

Total digestions were conducted in a microwave digester, with 5-8 mL nitric acid and 5-8 mL hydrogen peroxide in a 1:1 ratio, according to the protocol of EPA Method 3050B (USEPA, 1996). All the extraction samples were analyzed on either a GFAAS (Shimadzu AA-6800) using paladium as a matrix modifier and platform-style graphite tubes or an ICP-MS (PerkinElmer SCIEX ELAN-DRCe). To reduce matrix effects, samples analyzed on the ICP-MS were analyzed as duplicates, with the second duplicate spiked with a known concentration of standard

solution. The difference in readings between the unspiked and spiked samples were used to calculate concentrations, instead of a calibration curve.

Some of the resultant extraction solution from the TiCl extractions precipitated out as white or clear crystal-like material. Despite further digestion attempts of these crystals, insufficient dissolution and increased analysis associated with these additional dilutions rendered this fraction to too uncertain to use.

2.3 Results

2.3.1 Groundwater Sampling

The results from the groundwater sampling campaigns show a notable difference in the performance of the different types of ISR applications (Figure 2.2). Note that while we focused on two PRBs for our solid-phase analyses, there are more applications of these two types of ISR at the field site and groundwater data for all the PRBs are included here. The locations of all of these monitoring wells are noted on Figure 2.1. In the PRBs where ZVI was utilized in conjunction with carbon and sulfate, aqueous-phase arsenic concentrations significantly decreased. This is seen in the two pilot studies ("Pilot A" and "Pilot B"), as well as the large-scale PRB ("Well 1 'Z'" and "Well 2 'Z'") where sediment samples were collected for the solid-phase studies. Arsenic concentrations in Pilot A dropped from ~85 ppb As to ~15 ppb As, while Pilot B dropped from ~25 ppb As to ~5 ppb As. The ZVI PRB (Wells 1 and 2) was effective in reducing arsenic concentrations from ~60 ppb down to ~5 ppb, capturing approximately 97% of the mass entering the PRB over the first 16 months (Beaulieu & Ramirez, 2013). In contrast, arsenic concentrations in the non-ZVI applications of ISR actually increased after PRB

installation. In both Pilot C and Pilot D ("NZ"), initial concentrations of ~160 and ~35 ppb As, respectively, more than doubled, increasing to ~325 and ~75 ppb.

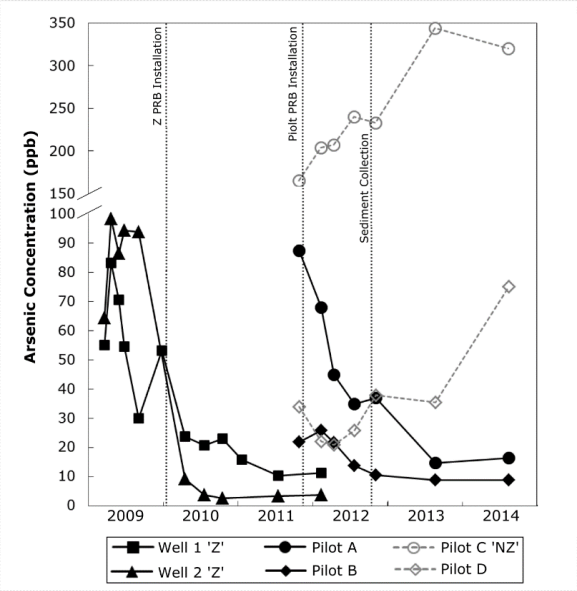

Figure 2.2: Observed groundwater arsenic concentrations in all installed PRB applications of ISR at the field site. Open, grey data points correspond to applications without ZVI, whereas black, filled data points correspond to applications with ZVI. Those PRBs corresponding to our solid-phase analyses are denoted by 'Z' and 'NZ'. Note that the 'Z' PRB contained multiple monitoring wells; the two shown are representative of the overall behavior of the PRB. All monitoring wells are noted on Figure 2.1 A portion of these data have previously been published *(Beaulieu & Ramirez, 2013).*

2.3.2 Synchrotron Analysis

XANES spectroscopy results are shown in Figure 2.3 and Figure 2.4. Normalized first-derivative absorbance is shown for multiple locations on the sample from the Z PRB, NZ PRB, and standard, known minerals. Pre-PRB installation samples, denoted as Z0, indicate that prior to installation of PRBs at the site, arsenic present in the solid phase was present as a mixture of arsenate and arsenite species. This arsenic could have been either sorbed species or incorporated into minerals. However, due to the presence of both species, As(V) and As(III), in particular after treatment, it is likely that arsenate is present in a mineral phase and arsenite is a sorbed species on that mineral. Once the Z PRB was installed, uXANES data (Z1a-A, Z3a1) indicate that arsenic shifted to lower valence species, namely arsenite and possibly arsenopyrite or other arsenic-sulfur

species, such as realgar or orpiment. Due to the micro-scale nature of the analysis, there is some inevitable variability between absorbance readings collected from the same sample, microns apart. This is part of the rationale for additional analysis of the sediment, conducted on the bulk-scale sediment, noted as “Z Bulk”, etc. The bulk sample agrees with Z3a1, more so than the most reduced sample (Z1a-A). In the NZ PRB, the uXANES samples are again a mixture of valences, with all three (NZ2a, NZ4a, NZ4c) exhibiting some level of peak increase at the location of arsenate peaks. However, two of the three (NZ2a, NZ4a) more strongly indicate formation of arsenic-sulfur species. NZ Bulk is most indicative of the presence of arsenite. In the bulk samples, there appears to be little difference between the Z and NZ PRB.

Iron XANES are shown in Figure 2.4. These data show less clear patterns than the arsenic XANES. The two bulk samples, NZ Bulk and Z Bulk, both show slight peaks at energies that indicate presence of magnetite (location d), a mixed-valence iron oxide. However, NZ Bulk also has a peak at location b, indicating FeS, an Fe(II)-sulfide. In contrast, Z Bulk has peak at location e, indicating HFO, a ferric iron mineral. Both of these samples show additional peaks that are not as easily classifiable. Similarly, the microscale scans show general trends, but specific peaks are hard to identify. The NZ uXANES (NZ4a, NZ4b, and NZ4c) have peaks that overlap locations b, c, and d, ferrous iron and mixed-valence iron minerals. NZ4a also has additional peaks suggesting presence of more oxidized iron minerals. The Z uXANES scans (Z1a-A, Z1a-B, Z2a-A, Z2a-B, and Z3a1) also have peaks present at lower energies, suggesting more reduced and mixed-valence iron minerals. However, Z1a-A and Z3a1 also have higher energy peaks, mimicking the shape, and thus composition, of Z Bulk.

For better understanding of the iron speciation of iron minerals present, we noted the location of the pre-edge peak, k-edge, and white line, all key features of iron XANES scans, and

compared them to known reference standards (Figure 2.5). For all three features, the bulk sample scans show a clear separation from the micro-scale data.

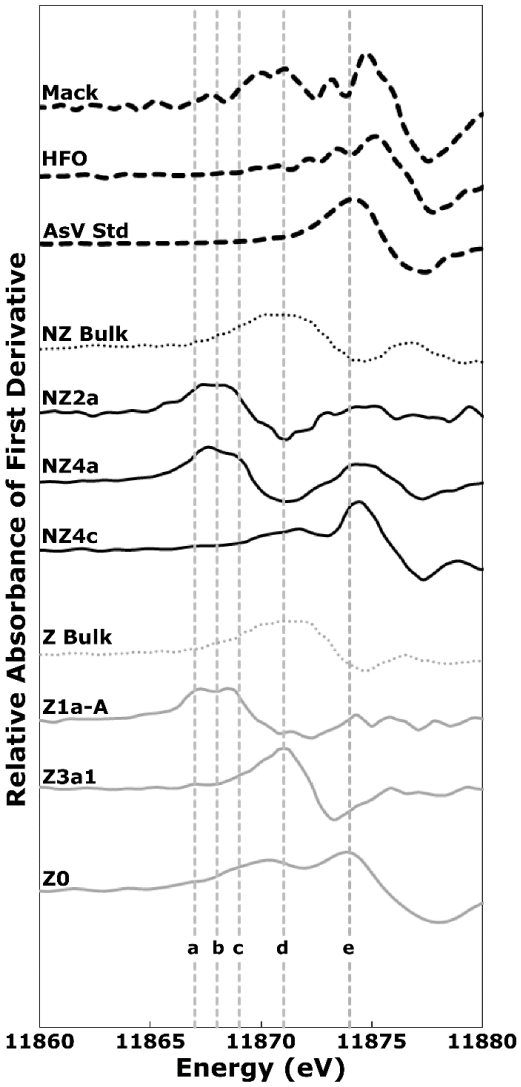

Figure 2.3: First-derivative arsenic XANES spectra. Black-colored scans are samples from the non-ZVI PRB and grey-colored are those from the ZVI PRB. Labeled sample names correspond to the XRF scans, shown in Figure 2.6. Dotted lines shown are k-edge values for arsenic in different minerals, according to standards in the literature. Standards: (a) Arsenopyrite, As(0) *(Beak & Wilkin, 2009; Onstott et al., 2011)* ***(b) Realgar*** *(Onstott et al., 2011)* ***(c) Orpiment As(III)*** *(Beak & Wilkin, 2009; Kocar, Borch, & Fendorf, 2010; Onstott et al., 2011)* ***(d) Arsenite As(III)*** *(Kocar et al., 2010; Onstott et al., 2011)* ***(e) Arsenate As(V)*** *(Beak & Wilkin, 2009; Kocar et al., 2010; Onstott et al., 2011).*

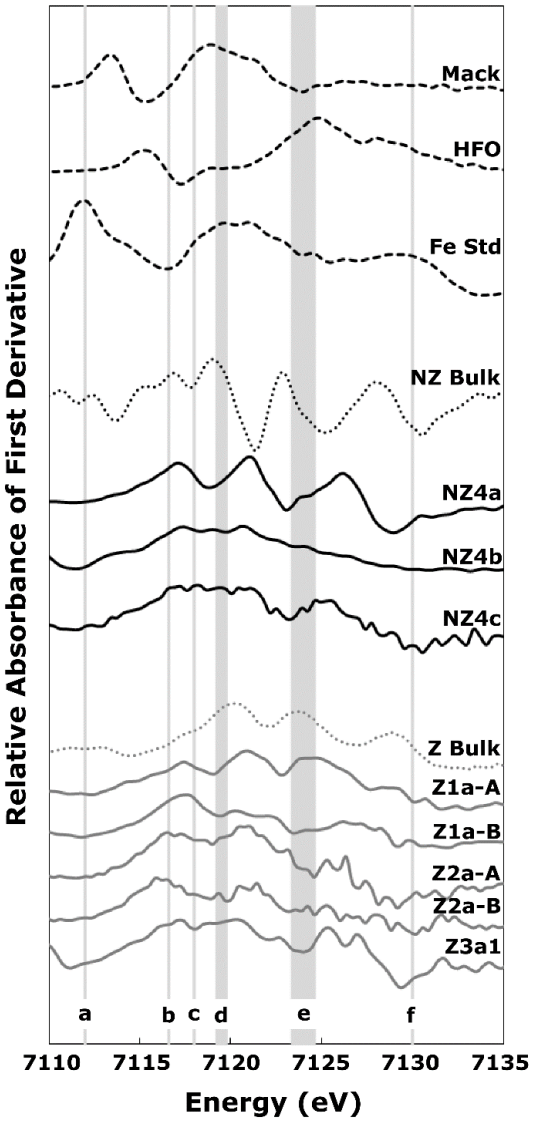

Figure 2.4: Normalized first derivative of iron XANES. Shaded bars shown are k-edge values for iron in different minerals, according to standards in the literature. Standards: (a) Iron Foil Fe(0) (b) FeS, Iron (II) sulfide *(Prietzel, Thieme, Eusterhues, & Eichert, 2007)* ***(c) Pyrite*** *(Prietzel et al., 2007)****, green rust*** *(Benner, Hansel, Wielinga, Barber, & Fendorf, 2002)****, biotite*** *(La Force & Fendorf, 2000)* ***(d) Magnetite*** *(Benner et al., 2002; La Force & Fendorf, 2000)* ***(e) HFO*** *(Benner et al., 2002; La Force & Fendorf, 2000; Prietzel et al., 2007)* ***(f) Schwertmannite*** *(Prietzel et al., 2007).*

Key features for the bulk scans of ZVI PRB are present at higher energies than for NZ PRB, indicating iron present at higher oxidation states in Z. Locations of the white line (panel a) compared to standard spectra are ambiguous for determination of iron valence state of our minerals. It appears likely that the majority of the microscale samples consisted of ferrous iron. NZ Bulk was most likely composed of mixed valence state iron minerals and Z Bulk of ferric iron minerals. Using the inflection point location (panel b) for determination of iron valence state, all the micro-scale scans showed the presence of iron(II) minerals. The bulk-scale scans indicated the NZ PRB was composed of iron (II) minerals, while the Z PRB was composed of iron(III) minerals. The pre-edge peak centroid location (panel c) for our micro-scale scans is far below those of standard materials, thus no conclusions can be drawn from those particular data. The locations of the pre-edge peak for the bulk-scale scans indicate that the Z PRB is composed of iron minerals primarily containing Fe(III), whereas the NZ PRB mostly consists of Fe(II). Overall, taking these three key features together, these data suggest that the locations of uXANES, where arsenic and iron were most concentrated, iron was present at more reduced states, compared to the bulk samples. Additionally, these data suggest that at the bulk level, the NZ PRB contained more reduced forms of iron, Fe(II), than the Z PRB, which contained more Fe(III) and Fe(II)/Fe(III) minerals, counter to what would be expected in each of these treatments.

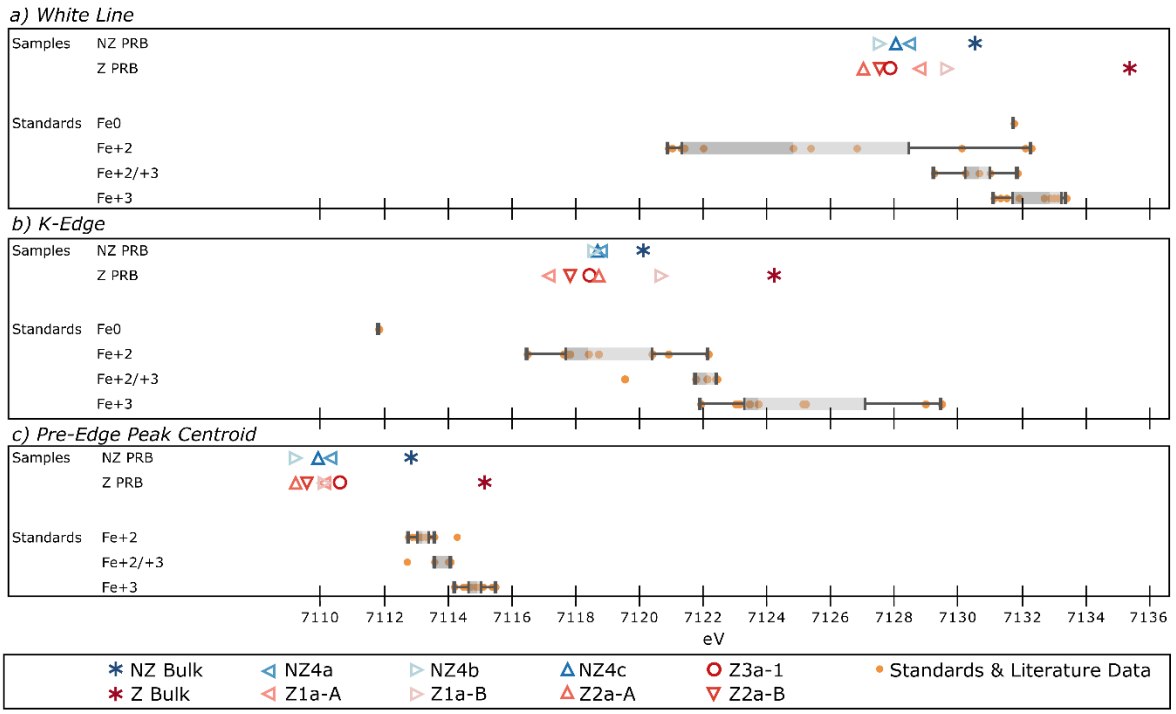

Figure 2.5: Energy locations of key features of iron XANES scans of our samples, compared to known reference minerals. Red symbols are the samples taken from Z PRB, blue symbols are samples taken from NZ PRB. Standard spectra data are from the literature *(Kocar et al., 2010; Prietzel et al., 2007)****. Spectra for Fe(0) were collected from elemental iron foil. For the box and whiskers plots, the extents of the boxes represent the first and third quartiles of the dataset and the whiskers represent a distance of 1.5x the inter-quartile range.***

Locations of XANES scans were chosen based on µXRF scans done on sections of the sediment. To achieve scans with the strongest signal strength possible, spatial hotspots were selected for the XAS scans. A select number of those XRF scans are shown below in Figure 2.6. These scans are useful in providing guidance for optimal locations for µXANES analysis, but also for providing spatial information about element associations within the sediment. Correlation plots are included in that figure, indicating in which samples arsenic and iron, arsenic and sulfur, and iron and sulfur are most correlated. Results for the XRF analysis of the samples at a micro-scale indicate heterogeneity in the sample matrix, a confirmation of the results we observed in the XANES scans. In some of the sample locations, strong correlations existed

between arsenic and iron; however this was not universally true (as in panel a, panel c, panel f). In the ZVI samples, it should be noted that while there was not always a strong correlation between arsenic hotspots and iron hotspots, there was a correlation between arsenic hotspots and iron. This strange relationship is true for most of the NZ samples as well, with the exception of panel f of Figure 2.6 (sample NZ4c), where arsenic appears not to be associated with iron at all. What was universally true for all samples though, was the strong correlation between iron and sulfur.

Arsenic spatial correlations with other elements were also determined. The coefficient of determination values (R^2) of the correlation plots were determined and are shown in 2.7. It is clear from these data that arsenic is not well correlated with many elements in the Z samples. In the NZ samples, the elements all seem to have been relatively well associated with arsenic, with the exception of Ca in NZ4a, Cu in NZ4b, and all elements other than Ca in NZ4c.

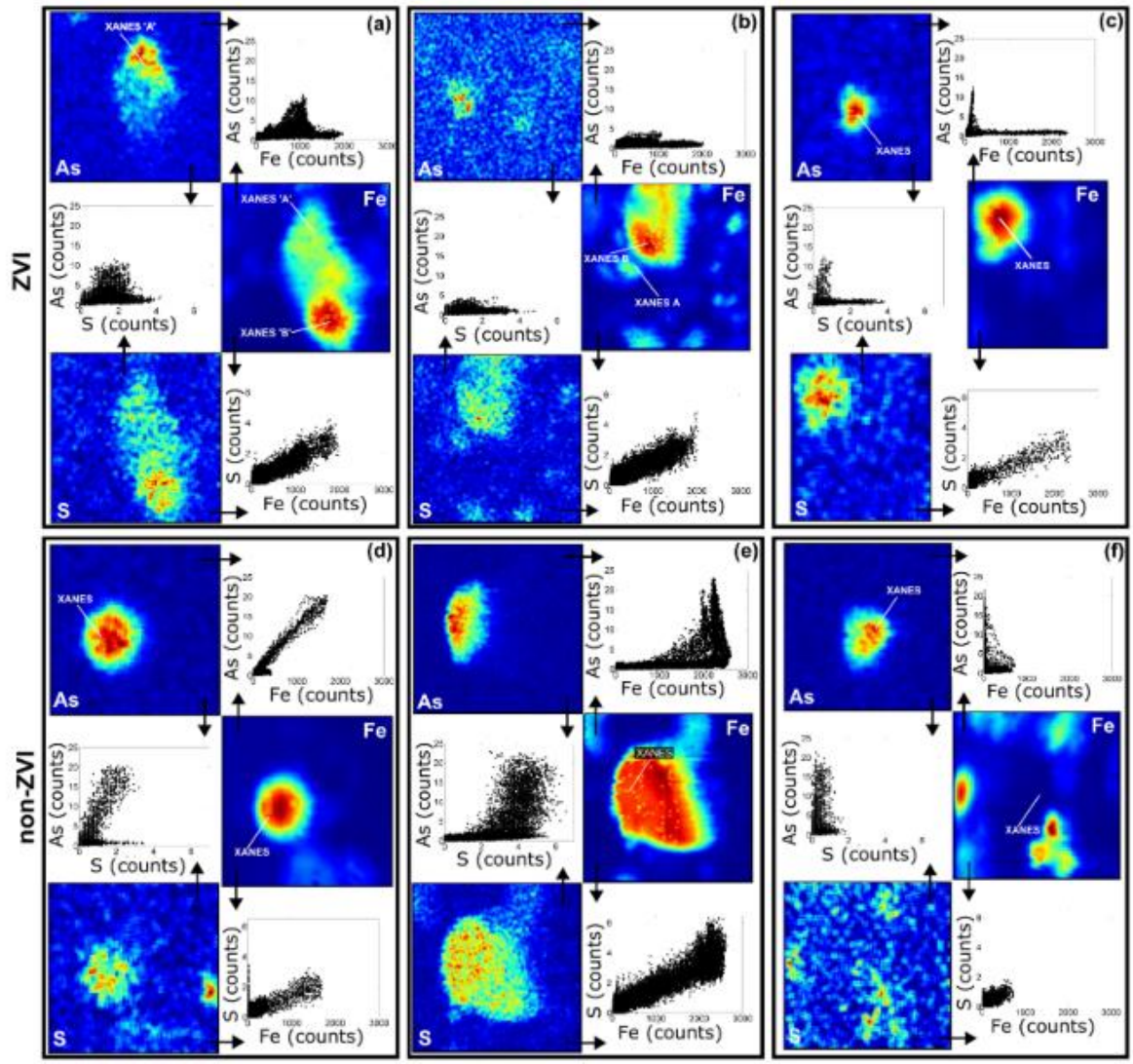

Figure 2.6: XRF scans of 3 discrete locations on sediment from the Z PRB and 3 from the NZ PRB. Correlation plots between As & Fe, As & S, and Fe & S are shown in between the relevant scans and are indicated by arrows. These locations are selectively shown here as representative of associations seen in the different sediments. Locations where XANES scans were taken are indicated. NZ2a not shown (As XANES). (a) Z1a (100µm x 100µm) (b) Z2a (150µm x 150µm) (c) Z3a1 (50µm x 60µm) (d) NZ4a (70µm x 70µm) (e) NZ4b (150µm x 150µm) (f) NZ4c (80µm x 80µm).

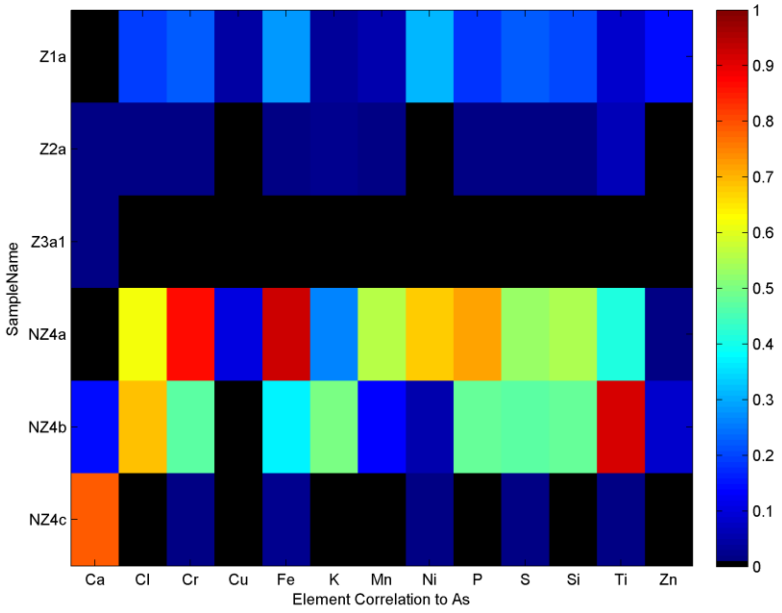

Figure 2.7: Correlation relationship strength between As and other minerals. Coloring for each rectangle (z-axis) indicates the coefficient of determination (R^2) of the correlation plot between arsenic and the element listed in the x-axis.

2.3.3 Sequential Extractions

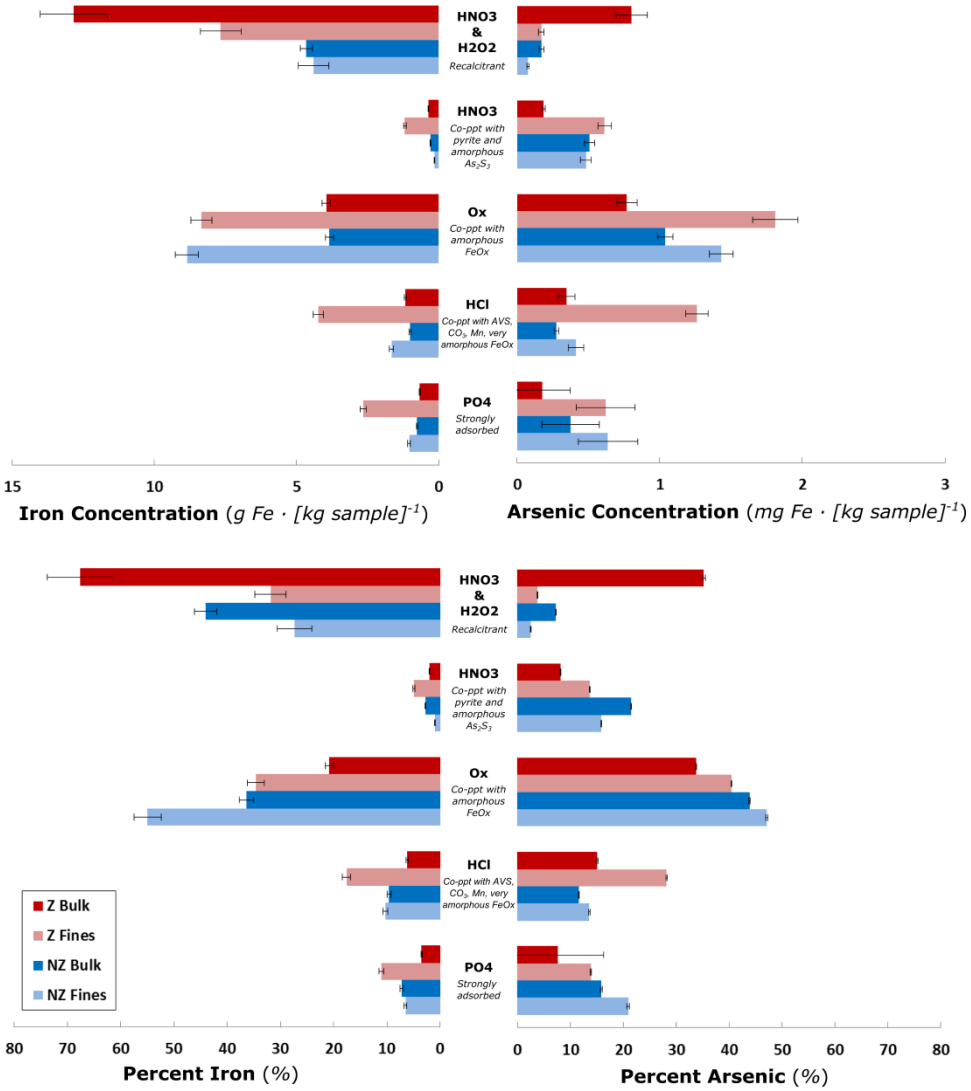

Figure 2.8: Results of sequential chemical extractions. Error bars depict propagated standard deviation of instrumental readings for all samples within an operational fraction and the subtracted extractant blank. Percentages given are percent mass of a given fraction, relative to the total mass extracted in all extractions shown.

Sequential extraction results indicate that in the fines of the samples, a very small percentage of arsenic present on the sediment from the two ISR systems was HNO_3 & $H2O_2$-extractable. In

both systems, similar amounts of the total arsenic present on the fines fractions were in the following forms: (1) HNO_3 - extractable (2) HNO_3 & $H2O_2$-extractable. In contrast, the key differences were in the following forms: (1) PO_4 – extractable (2) HCl - extractable, and (3) oxalate – extractable. For both systems, the arsenic was present at a greater percentage as oxalate - extractable, than in any other form.

The extractions conducted on the fines samples indicate that approximately 30% of the iron in the sediment was HNO_3 & $H2O_2$-extractable. The ZVI system contained more iron present as (1) HNO_3 - extractable, (2) HCl - extractable, and (3) PO_4 – extractable, while the non-ZVI system contained more oxalate – extractable iron. As with arsenic, iron was present at a greater percentage as coprecipitated with amorphous iron oxides, than in any other form, with the exception of the recalcitrant forms.

However, the extractions conducted on the bulk fractions of the sediment samples collected from both systems do not entirely agree with the findings of the fines fractions analyses. The ZVI bulk sediment sample contained nearly 40% HNO_3 & $H2O_2$-extractable forms of arsenic, in great contrast to both the non-ZVI bulk sample (~8%) and the fines fractions for both systems (both less than 5%). The remaining extractions on the bulk samples did reveal similar patterns between the two ISR systems: arsenic present at a greater percentage for the ZVI system as HCl - extractable, while a greater percentage of arsenic in the other forms for the non-ZVI system.

2.4 Discussion

The goals of this study were to assess two different field implementations of ISR using PRBs as in-situ arsenic treatment systems, determining their effectiveness at removing arsenic, and elucidating the removal mechanisms responsible for their success and/ or failure. We hypothesized that these two systems, one utilizing ZVI and one using only carbon and sulfur materials, would form different minerals and thus remove arsenic via different mechanisms and with varying efficacy.

Groundwater data from the site indicated that arsenic removal in the two different types of PRB implementations was vastly different. In systems which added ZVI, removal of the arsenic contamination from groundwater occurred, whereas the arsenic was not removed, and in fact increased in concentration, in the systems which did not include ZVI addition. We can begin to explain these different behaviors via the results from the solid-phase analyses.

For the NZ PRB, we anticipated arsenic-sulfides and amorphous iron-sulfides to form, and our results support this. XRF data showed strong arsenic-sulfur correlations, and XAS data supports this. XAS data for arsenic indicated a shift in arsenic speciation after implementation of ISR. On a fine scale, at the micro-level, arsenic-sulfides appear to have formed, and iron XANES indicate the presence of arsenic-iron-sulfide minerals and/or iron-sulfide minerals. Peaks remain at the location of As(V), indicating that conditions did not become altered enough to remove mineral phases with incorporated arsenate. The sequential extractions indicated that most of the arsenic on the NZ fines was extractable by solutions that target arsenic coprecipitated with amorphous iron oxides. The XRF data also show some correlation between arsenic and iron, and strong correlations between sulfur and iron, which likely indicates sorption of arsenic (likely

arsenite) onto the surface of iron or iron-sulfide minerals. Sequential extraction results also indicate that some of the arsenic present in the samples (both the fines and the bulk sample) were adsorbed to the sediment surface (15-20% was PO_4 - extractable). Arsenic in sample NZ4b, which only associated with a portion of the iron shown in the scan (see Figure, panel e), might have simply sorbed onto a particular form of iron present at that location (i.e., preferential sorption onto a specific species or form).

For the Z PRB, we anticipated formation of FeS minerals, as well as iron (oxy)hydroxides. Again, our results support this original hypothesis; XRF data showed strong correlations between Fe and S, iron XANES data indicate that Z Bulk formed magnetite and HFO. Sequential extractions suggest that the majority of arsenic present in the Z PRB was coprecipitated with amorphous iron oxides and coprecipitated with AVS, carbonate, manganese, and very amorphous iron oxides. These extraction results also showed that around 15% of the arsenic present in the sediment was adsorbed.

In some of the XRF scans of the Z PRB sediment, arsenic was associated with iron, but not with the iron hotspots. This may indicate the preferential association of arsenic with particular types of iron (that are formed at lower concentrations) than others (which formed the hotspots). In panel c, closer inspection of the location of the arsenic hotspot reveals iron presence at the same location. Likewise, panel a shows arsenic associated with a lower concentration area of iron presence. XANES scans for arsenic indicate that the arsenic present in panel a and panel c were reduced species, arsenopyrite/realgar/orpiment and arsenite, respectively. These data may indicate that the arsenic present in panel c (Z3a1) was arsenic sorbed to a mineral phase, whereas the other samples may either indicate arsenic sorption or incorporation into arsenic-sulfur and arsenic-sulfur-iron species.

In addition to the iron and arsenic speciation and association, the association between arsenic and other elements may provide insight into arsenic sequestration mechanisms in these systems. The correlation relationships between arsenic and other elements for the NZ PRB are all relatively high, except for in sample NZ4c, in large contrast to the Z PRB, which indicates arsenic is not well-associated with any other elements. However, this may be reflective of the tendency of arsenic in these systems to partially associate with iron and sulfur, thus skewing the r-squared values. It may also indicate the formation of multiple forms of iron in the subsurface, with arsenic only associating with some of those forms, as is seen in the XRF data. Notably, the correlation between arsenic and Ca in NZ4c was the only semi-strong relationship within that sample location. This may indicate the formation of a calcium-arsenate mineral (Zhu, Zhang, Xie, Wang, & Cheng, 2006). This contrasts with the other two NZ samples (NZ4a and NZ4b), which had strong correlations with most elements, other than Ca.

The results of our study provide some insight into the potential differences in performance between the two ISR applications. First, XANES data suggest that the NZ PRB sediment formed more reduced minerals than the Z PRB, with the NZ PRB forming more mixed-valence arsenic and iron minerals, as well as Fe(II) and As(III) species. In contrast, the Z PRB primarily formed Fe(III) and As(V) species, with some formation of mixed-valence minerals. This is counter to what would be expected in each of these systems. Most likely, the iron concentrations in the ZVI PRB were much higher than in the NZ PRB, thus even if more reduced species were formed, the majority of the iron may have remained as more oxidized forms, masking the presence of those reduced forms in our measurements.

Despite many iron minerals that were not associated with arsenic, based on the XRF data, arsenic in the Z PRB only appeared where iron was present. In the NZ PRB, As and S

correlations were much stronger, as we predicted. The key difference in the sequential extraction data is the higher amount of co-precipitation with AVS, carbonate, manganese, and very amorphous iron oxides in the Z PRB. These results all suggest that the As-S stabilization mechanisms responsible for arsenic removal in the NZ PRB are not as effective as As-Fe or As-Fe-S mechanisms, like the ones formed in the Z PRB.

2.5 References

Abedin, M. J., Cotter-Howells, J., & Meharg, A. A. (2002). Arsenic uptake and accumulation in rice (Oryza sativa L.) irrigated with contaminated water. *Plant and Soil*, *240*(2), 311–319. https://doi.org/10.1023/A:1015792723288

Argos, M., Kalra, T., Rathouz, P. J., Chen, Y., Pierce, B., Parvez, F., … Ahsan, H. (2010). Arsenic exposure from drinking water, and all-cause and chronic-disease mortalities in Bangladesh (HEALS): a prospective cohort study. *The Lancet*, *376*(9737), 252–258. https://doi.org/10.1016/S0140-6736(10)60481-3

Beak, D. G., & Wilkin, R. T. (2009). Performance of a zerovalent iron reactive barrier for the treatment of arsenic in groundwater: Part 2. Geochemical modeling and solid phase studies. *Journal of Contaminant Hydrology*, *106*(1–2), 15–28. https://doi.org/10.1016/j.jconhyd.2008.12.003

Bears, H., Richards, J. G., & Schulte, P. M. (2006). Arsenic exposure alters hepatic arsenic species composition and stress-mediated gene expression in the common killifish (Fundulus heteroclitus). *Aquatic Toxicology*, *77*(3), 257–266. https://doi.org/10.1016/j.aquatox.2005.12.008

Beaulieu, B., & Ramirez, R. E. (2013). Arsenic Remediation Field Study Using a Sulfate Reduction and Zero-Valent Iron PRB. *Groundwater Monitoring & Remediation*, *33*(2), 85–94. https://doi.org/10.1111/gwmr.12007

Belluck, D. A., Benjamin, S. L., Baveye, P., Sampson, J., & Johnson, B. (2003). Widespread Arsenic Contamination of Soils in Residential Areas and Public Spaces: An Emerging Regulatory or Medical Crisis? *International Journal of Toxicology*, *22*(2), 109–128. https://doi.org/10.1080/10915810305087

Benner, S. G., Hansel, C. M., Wielinga, B. W., Barber, T. M., & Fendorf, S. (2002). Reductive Dissolution and Biomineralization of Iron Hydroxide under Dynamic Flow Conditions. *Environmental Science & Technology*, *36*(8), 1705–1711. https://doi.org/10.1021/es0156441

Bhattacharya, A., & Bhattacharya, S. (2007). Induction of oxidative stress by arsenic in Clarias batrachus: Involvement of peroxisomes. *Ecotoxicology and Environmental Safety*, *66*(2), 178–187. https://doi.org/10.1016/j.ecoenv.2005.11.002

Butler, E. C., & Hayes, K. F. (1998). Effects of Solution Composition and pH on the Reductive Dechlorination of Hexachloroethane by Iron Sulfide. *Environmental Science & Technology*, *32*(9), 1276–1284. https://doi.org/10.1021/es9706864

Casiot, C., Morin, G., Juillot, F., Bruneel, O., Personné, J.-C., Leblanc, M., … Elbaz-Poulichet, F. (2003). Bacterial immobilization and oxidation of arsenic in acid mine drainage (Carnoulès creek, France). *Water Research*, *37*(12), 2929–2936. https://doi.org/10.1016/S0043-1354(03)00080-0

Delowar, H., Yoshida, I., Harada, M., Sarkar, A., Miah, M., Razzaque, A., … Delowar, H. (2005). Growth and uptake of arsenic by rice irrigated with As-contaminated water. *Journal of Food Agriculture and Environment*, *3*(2), 287–291.

Dittmar, J., Voegelin, A., Maurer, F., Roberts, L. C., Hug, S. J., Saha, G. C., … Kretzschmar, R. (2010). Arsenic in Soil and Irrigation Water Affects Arsenic Uptake by Rice: Complementary Insights from Field and Pot Studies. *Environmental Science & Technology*, *44*(23), 8842–8848. https://doi.org/10.1021/es101962d

Farquhar, M. L., Charnock, J. M., Livens, F. R., & Vaughan, D. J. (2002). Mechanisms of Arsenic Uptake from Aqueous Solution by Interaction with Goethite, Lepidocrocite,

Mackinawite, and Pyrite: An X-ray Absorption Spectroscopy Study. *Environmental Science & Technology*, *36*(8), 1757–1762. https://doi.org/10.1021/es010216g

Floyd|Snider & AMEC. (2013). *Phase 2 In-situ Pilot Study Monitoring Report for B&L Woodwaste Site, Pierce County Washington, prepared for B&L Custodial Trust*. Seattle, WA.

Furukawa, Y., Kim, J., Watkins, J., & Wilkin, R. T. (2002). Formation of Ferrihydrite and Associated Iron Corrosion Products in Permeable Reactive Barriers of Zero-Valent Iron. *Environmental Science & Technology*, *36*(24), 5469–5475. https://doi.org/10.1021/es025533h

Gallegos, T. J., Hyun, S. P., & Hayes, K. F. (2007). Spectroscopic Investigation of the Uptake of Arsenite from Solution by Synthetic Mackinawite. *Environmental Science & Technology*, *41*(22), 7781–7786. https://doi.org/10.1021/es070613c

Gault, A. G., Cooke, D. R., Townsend, A. T., Charnock, J. M., & Polya, D. A. (2005). Mechanisms of arsenic attenuation in acid mine drainage from Mount Bischoff, western Tasmania. *Science of The Total Environment*, *345*(1–3), 219–228. https://doi.org/10.1016/j.scitotenv.2004.10.030

Gibert, O., de Pablo, J., Cortina, J. –., & Ayora, C. (2010). In situ removal of arsenic from groundwater by using permeable reactive barriers of organic matter/limestone/zero-valent iron mixtures. *Environmental Geochemistry and Health*, *32*(4), 373–8. https://doi.org/http://dx.doi.org/10.1007/s10653-010-9290-1

Gillham, R. W., & O'Hannesin, S. F. (1994). Enhanced Degradation of Halogenated Aliphatics by Zero-Valent Iron. *Ground Water*, *32*(6), 958–967.

Han, Y.-S., Demond, A. H., & Hayes, K. F. (2013). Impact of dissolved silica on arsenite removal by nano-particulate FeS and FeS-coated sand. *Chemosphere*, *92*(4), 477–481. https://doi.org/10.1016/j.chemosphere.2013.02.033

Hasan, A. R., Hu, L., Solo-Gabriele, H. M., Fieber, L., Cai, Y., & Townsend, T. G. (2010). Field-scale leaching of arsenic, chromium and copper from weathered treated wood. *Environmental Pollution*, *158*(5), 1479–1486. https://doi.org/10.1016/j.envpol.2009.12.027

Henderson, A. D., & Demond, A. H. (2013). Permeability of iron sulfide (FeS)-based materials for groundwater remediation. *Water Research*, *47*(3), 1267–1276. https://doi.org/10.1016/j.watres.2012.11.044

Hingston, J. A., Collins, C. D., Murphy, R. J., & Lester, J. N. (2001). Leaching of chromated copper arsenate wood preservatives: a review. *Environmental Pollution*, *111*(1), 53–66. https://doi.org/10.1016/S0269-7491(00)00030-0

Johnson, D. B., & Hallberg, K. B. (2005). Acid mine drainage remediation options: a review. *Science of The Total Environment*, *338*(1–2), 3–14. https://doi.org/10.1016/j.scitotenv.2004.09.002

Keimowitz, A. R., Mailloux, B. J., Cole, P., Stute, M., Simpson, H. J., & Chillrud, S. N. (2007). Laboratory Investigations of Enhanced Sulfate Reduction as a Groundwater Arsenic Remediation Strategy. *Environmental Science & Technology*, *41*(19), 6718–6724. https://doi.org/10.1021/es061957q

Keon, N. E., Swartz, C. H., Brabander, D. J., Harvey, C., & Hemond, H. F. (2001). Validation of an Arsenic Sequential Extraction Method for Evaluating Mobility in Sediments.

Environmental Science & Technology, *35*(13), 2778–2784. https://doi.org/10.1021/es001511o

Khan, M. A., Islam, M. R., Panaullah, G. M., Duxbury, J. M., Jahiruddin, M., & Loeppert, R. H. (2009). Fate of irrigation-water arsenic in rice soils of Bangladesh. *Plant and Soil*, *322*(1–2), 263–277. https://doi.org/10.1007/s11104-009-9914-3

Khan, M. A., Islam, M. R., Panaullah, G. M., Duxbury, J. M., Jahiruddin, M., & Loeppert, R. H. (2010). Accumulation of arsenic in soil and rice under wetland condition in Bangladesh. *Plant and Soil*, *333*(1–2), 263–274. https://doi.org/10.1007/s11104-010-0340-3

Kinniburgh, D. G., & Smedley, P. L. (2001). *Arsenic contamination of groundwater in Bangladesh*. Keyworth: British Geological Survey.

Kocar, B. D., Borch, T., & Fendorf, S. (2010). Arsenic repartitioning during biogenic sulfidization and transformation of ferrihydrite. *Geochimica et Cosmochimica Acta*, *74*(3), 980–994. https://doi.org/10.1016/j.gca.2009.10.023

La Force, M. J., & Fendorf, S. (2000). Solid-Phase Iron Characterization During Common Selective Sequential Extractions. *Soil Science Society of America Journal*, *64*(5). https://doi.org/10.2136/sssaj2000.6451608x

Lackovic, J. A., Nikolaidis, N. P., & Dobbs, G. M. (2000). Inorganic Arsenic Removal by Zero-Valent Iron. *Environmental Engineering Science*, *17*(1), 29–39. https://doi.org/10.1089/ees.2000.17.29

Li, R. Y., Stroud, J. L., Ma, J. F., McGrath, S. P., & Zhao, F. J. (2009). Mitigation of Arsenic Accumulation in Rice with Water Management and Silicon Fertilization. *Environmental Science & Technology*, *43*(10), 3778–3783. https://doi.org/10.1021/es803643v

Manning, B. A., Hunt, M. L., Amrhein, C., & Yarmoff, J. A. (2002). Arsenic(III) and Arsenic(V) Reactions with Zerovalent Iron Corrosion Products. *Environmental Science & Technology*, *36*(24), 5455–5461. https://doi.org/10.1021/es0206846

Mariner, P. E., Holzmer, F. J., Jackson, R. E., Meinardus, H. W., & Wolf, F. G. (1996). Effects of High pH on Arsenic Mobility in a Shallow Sandy Aquifer and on Aquifer Permeability along the Adjacent Shoreline, Commencement Bay Superfund Site, Tacoma, Washington. *Environmental Science & Technology*, *30*(5), 1645–1651. https://doi.org/10.1021/es9506420

Melitas, N., Wang, J., Conklin, M., O'Day, P., & Farrell, J. (2002). Understanding Soluble Arsenate Removal Kinetics by Zerovalent Iron Media. *Environmental Science & Technology*, *36*(9), 2074–2081. https://doi.org/10.1021/es011250y

Morrison, S. J., Metzler, D. R., & Carpenter, C. E. (2001). Uranium Precipitation in a Permeable Reactive Barrier by Progressive Irreversible Dissolution of Zerovalent Iron. *Environmental Science & Technology*, *35*(2), 385–390. https://doi.org/10.1021/es001204i

Morse, J. W., & Cornwell, J. C. (1987). Analysis and distribution of iron sulfide minerals in recent anoxic marine sediments. *Marine Chemistry*, *22*(1), 55–69. https://doi.org/10.1016/0304-4203(87)90048-X

Nichols, J. W., Wedemeyer, G. A., Mayer, F. L., Dickhoff, W. W., Gregory, S. V., Yasutake, W. T., & Smith, S. D. (1984). Effects of freshwater exposure to arsenic trioxide on the parr-smolt transformation of coho salmon (Oncorhynchus kisutch. *Environmental Toxicology and Chemistry*, *3*(1), 143–149. https://doi.org/10.1002/etc.5620030116

O'Day, P. A. (2006). Chemistry and Mineralogy of Arsenic. *Elements*, *2*(2), 77–83. https://doi.org/10.2113/gselements.2.2.77

O'Day, P. A., Vlassopoulos, D., Root, R., Rivera, N., & Turekian, K. K. (2004). The Influence of Sulfur and Iron on Dissolved Arsenic Concentrations in the Shallow Subsurface under Changing Redox Conditions. *Proceedings of the National Academy of Sciences of the United States of America*, *101*(38), 13703–13708.

Onstott, T. C., Chan, E., Polizzotto, M. L., Lanzon, J., & DeFlaun, M. F. (2011). Precipitation of arsenic under sulfate reducing conditions and subsequent leaching under aerobic conditions. *Applied Geochemistry*, *26*(3), 269–285. https://doi.org/10.1016/j.apgeochem.2010.11.027

Panaullah, G. M., Alam, T., Hossain, M. B., Loeppert, R. H., Lauren, J. G., Meisner, C. A., … Duxbury, J. M. (2009). Arsenic toxicity to rice (Oryza sativa L.) in Bangladesh. *Plant and Soil*, *317*(1–2), 31–39. https://doi.org/10.1007/s11104-008-9786-y

Phillips, D. H., Gu, B., Watson, D. B., Roh, Y., Liang, L., & Lee, S. Y. (2000). Performance Evaluation of a Zerovalent Iron Reactive Barrier: Mineralogical Characteristics. *Environmental Science & Technology*, *34*(19), 4169–4176. https://doi.org/10.1021/es001005z

Prietzel, J., Thieme, J., Eusterhues, K., & Eichert, D. (2007). Iron speciation in soils and soil aggregates by synchrotron-based X-ray microspectroscopy (XANES,μ-XANES). *European Journal of Soil Science*, *58*(5), 1027–1041. https://doi.org/10.1111/j.1365-2389.2006.00882.x

Richards, P. (2008). Seven-year performance evaluation of a permeable reactive barrier. *Remediation Journal*, *18*(3), 63–78. https://doi.org/10.1002/rem.20172

Roh, Y., Lee, S. Y., & Elless, M. P. (2000). Characterization of corrosion products in the permeable reactive barriers. *Environmental Geology*, *40*(1–2), 184–194. https://doi.org/10.1007/s002540000178

Smedley, P. L., & Kinniburgh, D. G. (2002). A review of the source, behaviour and distribution of arsenic in natural waters. *Applied Geochemistry*, *17*(5), 517–568. https://doi.org/10.1016/S0883-2927(02)00018-5

Su, C., Puls, R. W., Krug, T. A., Watling, M. T., O'Hara, S. K., Quinn, J. W., & Ruiz, N. E. (2012). A two and half-year-performance evaluation of a field test on treatment of source zone tetrachloroethene and its chlorinated daughter products using emulsified zero valent iron nanoparticles. *Water Research*, *46*(16), 5071–5084. https://doi.org/10.1016/j.watres.2012.06.051

USEPA. (1996). Method 3050B - Acid Digestion of Sediments, Sludges, and Soils.

Vogan, J. L., Focht, R. M., Clark, D. K., & Graham, S. L. (1999). Performance evaluation of a permeable reactive barrier for remediation of dissolved chlorinated solvents in groundwater. *Journal of Hazardous Materials*, *68*(1–2), 97–108. https://doi.org/10.1016/S0304-3894(99)00033-3

Wilkin, R. T., Acree, S. D., Ross, R. R., Beak, D. G., & Lee, T. R. (2009). Performance of a zerovalent iron reactive barrier for the treatment of arsenic in groundwater: Part 1. Hydrogeochemical studies. *Journal of Contaminant Hydrology*, *106*(1–2), 1–14. https://doi.org/10.1016/j.jconhyd.2008.12.002

Wilkin, R. T., Puls, R. W., & Sewell, G. W. (2003). Long-term performance of permeable reactive barriers using zero-valent iron: Geochemical and microbiological effects. *Ground Water*, *41*(4), 493–493.

WSDE. (2007). Cleanup Action Plan: B&L Woodwaste Site. WSDE.

WSDE. (2013). Model Toxics Control Act Regulation and Statute.

Zhao, Z., Jia, Y., Xu, L., & Zhao, S. (2011). Adsorption and heterogeneous oxidation of As(III) on ferrihydrite. *Water Research*, *45*(19), 6496–6504. https://doi.org/10.1016/j.watres.2011.09.051

Zheng, L., Apps, J. A., Zhang, Y., Xu, T., & Birkholzer, J. T. (2009). On mobilization of lead and arsenic in groundwater in response to CO2 leakage from deep geological storage. *Chemical Geology*, *268*(3–4), 281–297. https://doi.org/10.1016/j.chemgeo.2009.09.007

Zhu, Y. N., Zhang, X. H., Xie, Q. L., Wang, D. Q., & Cheng, G. W. (2006). Solubility and Stability of Calcium Arsenates at 25∘C. *Water, Air, and Soil Pollution*, *169*(1–4), 221–238. https://doi.org/10.1007/s11270-006-2099-y

3. Molecular characterization of dissolved organic matter mobilized from Bangladeshi aquifer sediment: tracking carbon compositional change during microbial utilization

3.1 Abstract

Bioavailable organic carbon (OC) in aquifer-recharge waters and sediments can fuel microbial reactions with implications for groundwater quality. OC in recharge water is typically considered more bioavailable than that in sediment. However, an incubation experiment using two different recharge waters and sediment collected from a site in Bangladesh demonstrated that OC mobilized off sediment during collection and during incubation due to pH changes was fermented into methane. We used high resolution mass spectrometry to characterize this mobilized OC, to compare its composition to that of recharge waters, and to track compositional changes during incubation. OC in the two recharge waters was molecularly similar and less chemically diverse than sedimentary OC, but all samples were rich with compounds containing nitrogen, phosphorous and, in particular, sulfur. We propose organosulfur compounds could act as a marker for carbon originating from anaerobic subsurface environments. Indices of chemical liability did not predict bioavailability; sedimentary OC contained thousands of chemically labile compounds that had persisted in the aquifer, and during incubation, microbes operated on chemically recalcitrant compounds. Microbes fully degraded recalcitrant compounds that lacked sulfur and phosphorous, and increased the heteroatom content of those that contained sulfur and phosphorous, potentially generating molecules needed for methanogenesis.

3.2 Introduction

Organic carbon (OC) in aquifer sediments can impact groundwater quality, both positively and negatively, by fueling microbial reactions that remove and contribute dissolved contaminants to groundwater (e.g., natural attenuation of nitrate (Korom, 1992), mobilization of geogenic arsenic (Postma et al., 2007), methane production (Parkin & Simpkins, 1995)).

Ultimately, the reactivity and bioavailability of sedimentary OC (SOC) will dictate the extent to which it can fuel subsurface reactions. In sedimentary aquifers, OC is often considered to have a low reactivity relative to that found in soils and marine sediments (Christensen et al., 2000; Hartog, van Bergen, de Leeuw, & Griffioen, 2004; Jakobsen & Postma, 1994), with increasing age frequently corresponding with increased chemical recalcitrance (Chapelle et al., 2009; Jakobsen & Postma, 1994; Postma et al., 2012). Over time, more chemically labile OC is thought to be preferentially degraded, leaving more chemically recalcitrant forms behind.

However, OC reactivity is controlled by more than its chemical nature. Studies in soils and sediments demonstrate that ambient conditions, such as pH, temperature and nutrient concentrations can control rates at which microbes process OC (Arndt et al., 2013; McDowell et al., 2006; van Bergen, Nott, Bull, Poulton, & Evershed, 1998); physical protection mechanisms, such as OC sorption to mineral surfaces, can limit microbial access to carbon (Baldock & Skjemstad, 2000; Petridis et al., 2014); and energetic constraints and metabolic capacity of microbial communities can control the ability of microbes to process different chemical forms of OC (Fontaine et al., 2007; Trulleyová & Rulík, 2004). It is these factors that help explain the presence of old (i.e., thousands of years old) but chemically reactive OC in soils and sediments (Fontaine et al., 2007; Gurwick et al., 2008; Parkin & Simpkins, 1995).

Neumann et al. (Neumann, Pracht, Polizzotto, Badruzzaman, & Ali, 2014a) previously conducted an incubation experiment using sediment and waters from Munshiganj, Bangladesh, that was designed to evaluate the ability of OC in aquifer-recharge waters and aquifer sediment to fuel microbial reduction reactions and arsenic mobilization. The study uncovered a pool of bioavailable OC in the aquifer sediments, equating to 0.33 ± 0.06 mg OC g^{-1} sediment, or $8.8 \pm 0.7\%$ of the total SOC (See Chapter 4, Section 1), likely destabilized during sampling and

collection. By the end of the experiment, the native microbial community fermented the mobilized SOC into methane. The tested sediment was a fine-grained sand and lacked peat (Chapelle, 2000), silt, and clay components (Aravena & Wassenaar, 1993; Chapelle et al., 2009; Desbarats, Koenig, Pal, Mukherjee, & Beckie, 2014; McMahon & Chapelle, 1991) often implicated as sources of SOC fueling subsurface reactions.(Aravena & Wassenaar, 1993; Chapelle et al., 2009; Desbarats et al., 2014; McMahon & Chapelle, 1991) The experiment demonstrated that old (~5000 years old), sandy aquifer sediments can contain a notably large amount of microbially-available OC. While SOC in the experiment was destabilized, and thus made accessible to microbial degradation, during sampling, homogenizing, and/or handling of the sediment, there is potential for *in situ* release of SOC. At the field site where incubation materials were collected, dissolved organic carbon (DOC) concentrations in groundwater remained constant with depth, but DOC age increased (Harvey et al., 2002); a situation that is only possible if SOC was released along the groundwater flow path as younger DOC was mineralized or sequester into sediment (Neumann et al., 2010). Previous work in an anthropogenically disturbed system in Vietnam (van Geen et al., 2013) similarly supports the potential for *in situ* destabilization of SOC. At this site, which is impacted by urban groundwater pumping, an influx of riverine DOC into a Pleistocene-aged aquifer led to the release of SOC. Along the recharge pathway, DOC concentrations peaked where microbial reduction and arsenic mobilization were occurring, and the river could not have supplied enough carbon for the reduction reactions.

Given the potential importance of SOC for fueling subsurface reactions, we sought to identify the carbon compounds mobilized off aquifer sediment in the Neumann et al. (Neumann et al., 2014a) experiment, to compare this carbon composition to that of aquifer-recharge waters,

and to track changes in chemical composition as mobilized SOC was fermented into methane. This effort characterizes a previously undocumented pool of bioavailable OC in sandy aquifer sediments and advances understanding of how OC chemical composition relates to bioavailability.

To characterize OC, we utilized Fourier transform ion cyclotron resonance mass spectrometry (FT-ICR-MS), coupled with electrospray ionization (ESI) in negative ion-mode. FT-ICR-MS is currently the only analytical technique capable of characterizing the thousands of different compounds contained in OC. The technique is not quantitative, as the ionization efficiency of compounds vary, making some compounds more difficult or impossible to identify (Sleighter & Hatcher, 2007). FT-ICR-MS resolves carbon compounds of unique mass-to-charge ratios (m/z), which are used to determine the elemental composition of compounds present, with a focus on C, H, O, N, S, and P atoms. This technique has been applied to natural organic matter in a variety of environments (D'Andrilli et al., 2010; Longnecker & Kujawinski, 2011; Spencer et al., 2014; Tfaily et al., 2013), but no studies have assessed the chemical composition of OC associated with aquifer sediment. Further, most studies have focused on characterizing OC; only a handful have directly tracked changes in elemental composition as OC was processed by microbes and protozoa (Chipman et al., 2010; Kim, Kaplan, & Hatcher, 2006; Kujawinski, Del Vecchio, Blough, Klein, & Marshall, 2004; Longnecker & Kujawinski, 2011; Lu et al., 2015; Osborne et al., 2013).

3.3 Materials and Methods

Incubation. Material collection details and setup of the incubation experiment were previously described (Neumann et al., 2014a). Briefly, water and sediment for the experiments

were collected from a field site in Munshiganj, Bangladesh. Aquifer sediment was collected from a depth of 9.1 m, where conditions were anoxic and groundwater arsenic concentrations were <10 $\mu g \cdot L^{-1}$ (Swartz et al., 2004). Sediment was homogenized and half of it was dried and sterilized. Sediment that was not sterilized prior to incubation was used in the "biotic" treatments, providing the native microbial populations, whereas sterilized sediment was used in the "abiotic" sediment. Prior to incubation, aliquots of homogenized aquifer sediment were vacuum-filtered through 0.2 μm polyethersulfone (PES) filters to collect sediment porewater. Aquifer-recharge waters were collected from underneath a rice field and from sediments of a 200-year-old pond; rice fields and ponds represent the two main aquifer-recharge sources at this site (Harvey et al., 2006). Recharge waters collected from these locations were previously characterized by other researchers at our field site by biologically degradable OC (BDOC) experiments (Neumann et al., 2010). Aquifer sediment (8.2 g, dry weight) was combined with recharge water (10 mL) and, over the course of the experiment, bottles were destructively sampled. The experiment was maintained until DOC concentrations decreased and then stabilized. Samples were kept anoxic during all collection and processing steps.

FT-ICR-MS. Aliquots of vacuum-filtered water samples from the incubation experiment were immediately frozen and later packed in dry ice and shipped to the Environmental Molecular Sciences Laboratory at Pacific Northwest National Laboratory in Richland, WA, where they were analyzed using a 12 Tesla Bruker SolariX Fourier transform ion cyclotron resonance (FT-ICR) mass spectrometer. Analysis details and instrument parameters are included in the SI (*Section 3.2*).

To improve robustness of sample characterization, experimental replicates were combined during data processing. Peaks present in any replicate were considered present for the

combined sample. Further, since low DOC concentrations can reduce ionization effectiveness, incubation samples collected in close temporal proximity to each other, and with similar DOC concentrations, were treated as replicates; samples collected between 17-20 days and between 80-91 days after experiment initiation were combined. Due to variation in ionization efficiency of different compounds, peak presence was used rather than peak intensity. Elemental formulas in combined samples were used to divide OC into 8 distinct heteroatom groups (CHO, CHON, CHOP, CHONP, CHOS, CHONS, CHOSP, and CHONSP) and to calculate an aromaticity index (AI) (Koch & Dittmar, 2006, 2016),

$$AI= [1 + C - 0.5*O – S - 0.5*(N+P+H)] / (C - 0.5*O – S – N – P), \quad (1)$$

which identifies samples as alkanes (AI=0), olefinics ($0<AI\leq0.5$), aromatics ($AI>0.5$), or condensed aromatics ($AI\geq0.67$) (Koch & Dittmar, 2006; Willoughby, Wozniak, & Hatcher, 2014).

Plots of the ratio of oxygen-to-carbon vs. hydrogen-to-carbon within identified organic compounds (i.e., van Krevelen plots) (Kim, Kramer, & Hatcher, 2003; van Krevelen, 1950) were generated to gain insight into the chemical nature of OC; major chemical classes (e.g., lipids, proteins, amino sugars, cellulose, lignins, tannins, condensed hydrocarbons) occupy known H-to-C and O-to-C regions (see Figure 3.1) (Hedges, 1990; Kim et al., 2003; Pedler Sherwood et al., 2015). In particular, compounds with H-to-C ratios greater than 1.5 (i.e., higher degree of hydrogen saturation) are considered more bioavailable (D'Andrilli, Cooper, Foreman, & Marshall, 2015).

3.4 Results and Discussion

DOC Composition in Aquifer-Recharge Waters. Pond and rice field recharge waters collected for the incubation experiment had similar numbers (same order of magnitude) of assigned formulas from FT-ICR-MS: 835 (pond) and 627 (rice field). Both waters contained a mixture of OC that included compounds with varied heteroatom groups, H-to-C and O-to-C ratios, masses, and aromaticity (Figures 3.1a, 3.1b, Appendix.1). The overall chemical composition of DOC in the two waters was similar. In particular, Figures 3.1a and 3.1b show that compounds in the two waters with equivalent heteroatom groups and comparable masses occupied analogous areas of the van Krevelen diagram. This correspondence indicates that not only did DOC in the two waters have similar classes of compounds, but that these compound classes were composed of similarly-sized molecules containing comparable heteroatom groups.

Despite the correspondence, DOC in the two waters did slightly differ from each other, and these differences indicated that DOC in pond recharge water was more chemically labile than that in rice field recharge water. Based on aromaticity index, DOC in pond recharge water had a higher percentage of olefinic compounds (45% vs. 37% in rice field recharge) and lower percentage of condensed aromatic compounds (19% vs. 30% in rice field recharge) (Figure Appendix.1). Figures 3.1a and 3.1b similarly shows that in pond recharge water, 38% of organic molecules had H-to-C ratios >1.5, compared to 33% in rice field recharge water. More chemically labile compounds are associated with H-to-C ratios >1.5 (D'Andrilli et al., 2015). However, as discussed in *Chemical Indices and Bioavailability,* H-to-C ratios provide insight into chemical lability, but they do not necessarily indicate if compounds will be biologically degraded. Microbial utilization of compounds in the incubation experiment was not always biased toward those with high H-to-C ratios (see *Carbon Transformations: Day 18 to 85*).

The relatively small compositional differences between the two waters align with a previously conducted biological degradable organic carbon (BDOC) assay, by other researchers at our site, that showed pond recharge water contained ~7mg/L more BDOC than rice field recharge water (Neumann et al., 2010). The assay used waters from the same pond and rice field and tracked loss of DOC in aerobic conditions by microbes contained within the sampled recharge water.

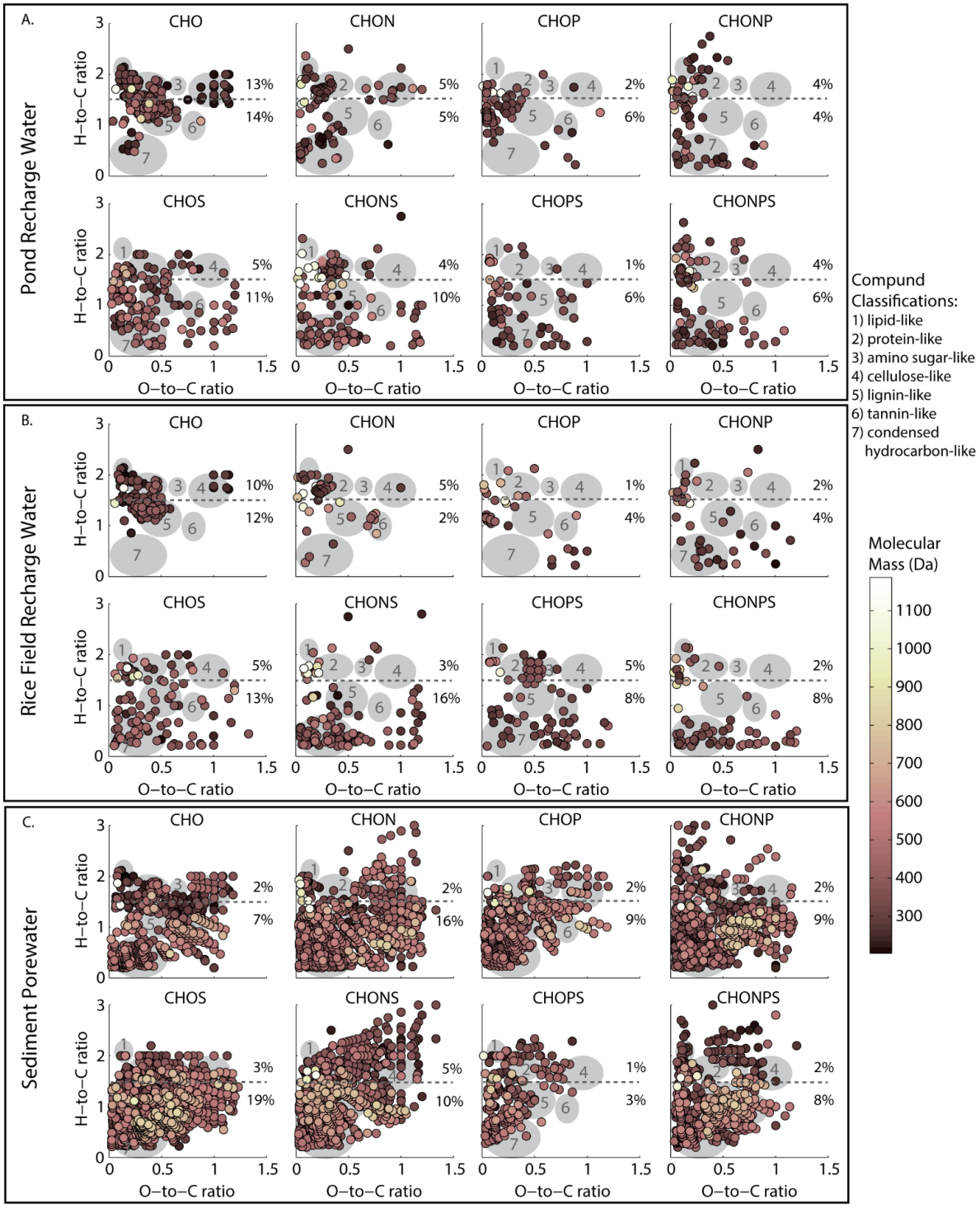

Figure 3.1: van Krevelen diagrams for each heteroatom group in the native incubation materials: (a) pond recharge water, (b) rice field recharge water, and (c) sediment porewater. Data point color reflects molecular mass of the organic compound according to the color bar. Grey shaded areas mark the H-to-C and O-to-C ratio of model chemical classes, as indicated in the legend. The percent of compounds present in each heteroatom group with H-to-C ratios above and below 1.5 is noted on each diagram above the below the dashed line, respectively.

If waters used in the two assessments (i.e., BDOC and FT-ICR-MS) were directly comparable, results imply that small (i.e., 5%) differences in OC composition can have measurable impacts on overall bioavailability. However, the waters may not be directly comparable because they were collected in different years. In addition, FT-ICR-MS does not evenly ionize every OC compound and compositional analyses cannot account for microbial community composition and selective preference for carbon types. Recharge waters were collected from anaerobic environments and were kept anaerobic for molecular characterization, but the BDOC experiments that were conducted previously by other researchers were conducted aerobically. Aerobic exposure could have altered microbial viability or DOC composition.

DOC Composition in Sediment Porewater. Concentration and character of OC mobilized off aquifer sediment into sediment porewater differed from that in the aquifer-recharge waters. The sediment porewater, which was previously shown to have a higher DOC concentration than the recharge waters (1059 ± 186 mg/L (Neumann et al., 2014a) vs. 17 ± 7 mg/L (rice field) and 30 ± 3 mg/L (pond)), also had a higher total number of assigned formulas (5263 vs. 835 (pond) and 627 (rice field)). Similar to DOC in recharge waters, DOC in sediment porewater ranged in size from 200 to 1100 Da, and was relatively well distributed among the eight different heteroatom groups (Figure 3.3c). DOC in sediment porewater had a heavier mass distribution than that in the recharge waters, particularly for compounds with H-to-C ratios below 1.5 (Figure Appendix.2).

Comparing the overlap of identified compounds with known compound classes in the van Krevelen diagram (Figure 3.1c) indicates that ~25% of DOC in sediment porewater had H-to-C and O-to-C ratios matching that of terrestrially derived organic matter (i.e., cellulose, lignin and tannin-like compounds), ~15% had ratios matching that of microbially-derived organic matter

(i.e., lipid-, protein-, amino-sugar-like compounds), and ~30% had ratios matching that of highly condensed organic matter (i.e., coal-, soot-, charcoal- and black-carbon-like compounds). The remaining 30% had ratios that did not overlap with a known class. Compound overlap for recharge waters (Figures 3.1a and 3.1b) indicates that proportionately less DOC in pond and rice field recharge had H-to-C and O-to-C ratios matching that of terrestrially derived organic matter (~20% versus ~25% in sediment porewater) and highly condensed organic matter (~20% versus ~30% in sediment porewater), and proportionately more had ratios matching that of microbially-derived organic matter (~30% versus ~15% in sediment porewater). Similar to sediment porewater, 30% of DOC in the recharge waters had ratios that did not overlap with a known class. These overlaps imply that all water types were composed of differentially sourced organic matter, but that recharge waters likely contained proportionately more microbially-derived organic matter than the aquifer sediment.

In all waters, roughly half of all identified molecules had sulfur heteroatoms (47% in pond recharge, 60% in rice field recharge, and 51% in sediment porewater) (Figure 3.3). Other FT-ICR-MS studies focused on groundwater systems have similarly found that DOC in groundwater is rich with sulfur heteroatoms (Evert, 2015; Longnecker & Kujawinski, 2011). Organosulfur compounds form in organic, sulfate-reducing environments where reduced sulfide species can react with various forms of organic matter (Heitmann & Blodau, 2006; Perlinger, Kalluri, Venkatapathy, & Angst, 2002; Schouten, van Driel, Sinninghe Damsté, & de Leeuw, 1993). As such, organosulfur compounds have been detected in various anaerobic environments (Brown, 1986; Urban, Ernst, & Bernasconi, 1999). In an aquifer system in Rifle, CO, sulfur heteroatom abundance increased as DOC was sampled from more chemically reduced zones (Evert, 2015). Sediment and water samples obtained for our incubation study similarly came

from chemically reduced environments. Sulfurization of organic matter is an abiotic process that occurs early in sediment diagenesis at ambient temperatures and pressures (Kohnen, Sinninghe Damste, & De Leeuw, 1991; Schouten et al., 1993). However, biologically-mediated reactions can also form organosulfur compounds, for example, methionine and cysteine are sulfur-containing amino acids (Brosnan & Brosnan, 2006). In the incubations, large numbers of organosulfur species were lost, formed and modified by both biotic and abiotic reactions (see sections titled *Carbon Transformations*).

Based on aromaticity index, DOC in sediment porewater had a similar percentage of alkanes, a smaller percentage of olefinics, and a larger percentage of aromatics compared to DOC in recharge waters (Figure Appendix.1). The percentage of condensed aromatics in sediment porewater DOC was larger than that in pond recharge, but matched that in rice field recharge. These AI differences imply that DOC in sediment porewater consisted of proportionately more refractory carbon compounds than DOC in recharge waters. Similarly, Figure 3.1 shows that the percentage of organic compounds with H-to-C ratios above 1.5 in sediment porewater was roughly half of that in aquifer-recharge waters (19% versus 38% (pond) and 33% (rice)). Collectively, these results align with classical understanding that young surface-derived OC is more chemically reactive than older sedimentary-derived OC (Schmidt et al., 2011). However, given sediment porewater contained ~35-times more DOC than the recharge waters, the pool of chemically reactive OC was actually larger in sediment porewater than in recharge water. Existence of thousands of chemically labile organic molecules within aquifer sediment that is thousands of years old implies that these organic molecules were inaccessible to *in situ* microbes, otherwise they would have been metabolized. Possible explanations for existence of these carbon compounds within the sandy aquifer sediment could include those put

forward to explain the presence of old, chemically labile organic matter in soils: physical, energetic and/or nutritional limitations (Schmidt et al., 2011).

Carbon Transformations: Day 1.5 to 18. At the onset of the incubation experiment, 1.5 days after recharge waters were mixed with aquifer sediment, DOC concentrations and composition were dominated by sediment porewater. DOC concentrations were approximately 150-250 mg/L (Figures 3.2a-d), which could be explained by dilution of DOC in sediment porewater with recharge water (Neumann et al., 2014a). At this early time point, the number of compounds identified in each incubation treatment was 3051 for pond recharge water mixed with sterilized sediment (i.e., pond abiotic incubation), 3162 for pond recharge water mixed with native sediment (i.e., pond biotic incubation), 4089 for rice field recharge water mixed with sterilized sediment (i.e., rice field abiotic incubation), and 4120 for rice field recharge water mixed with native sediment (i.e., rice field biotic incubation) (Figures 3.2e-h). Characterization of DOC showed that these initial incubation samples were more similar to sediment porewater than to aquifer-recharge waters (compare Figure 3.1 to Figures Appendix.3a and Appendix.4a).

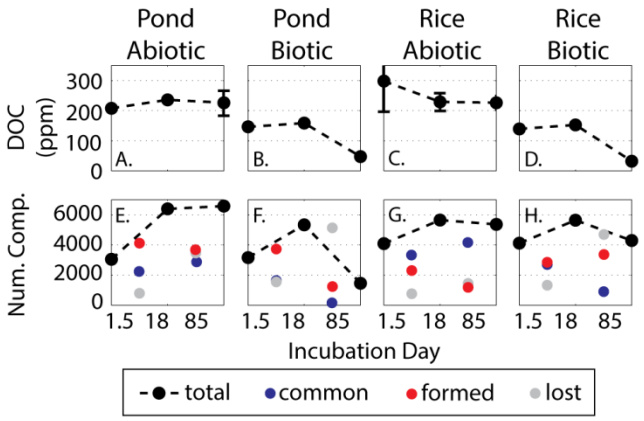

Figure 3.2: Concentrations of DOC (panels a-d) and number of organic compounds (panels e-h) 1.5, 18 and 85 days after initiation of the incubation experiments. In panels e-h, black symbols indicate the total number of compounds present at a given time point. Symbols plotted between the time points indicate (blue) the number of compounds common to both time points, (red) the number of new compounds formed between the two time points, and (grey) the number of compounds lost between the two timepoints.

Between day 1.5 and day 18, DOC concentrations did not noticeably change in incubations conducted with rice field recharge water (i.e., a change of -69±104 mg/L and +13±16 mg/L in abiotic and biotic rice field incubations, respectively) and concentrations increased in incubations conducted with pond recharge water (i.e., a change of +28±16 mg/L and +13±5 mg/L in abiotic and biotic rice field incubations, respectively) (Figures 3.2 a-d). During this time period, the number of identified compounds increased in all treatments relative to the beginning of the incubation, with abiotic and biotic pond incubations both receiving ~4000 new compounds and abiotic and biotic rice field incubations both receiving ~2000 new compounds (Figures 3.2 e-h). These new compounds were distributed across all heteroatom groups, with S- and P-containing groups (i.e., CHOS, CHONS and CHONPS) receiving the largest number of new compounds (Figure 3.3b). Fewer compounds were lost during this time period than were formed, and the type of recharge water used in incubation had no impact on the number of lost compounds. Instead, use of sterilized versus native sediment controlled compound loss. Both incubation sets with native sediment (i.e., pond and rice field biotic incubations) lost ~1500

compounds while both incubation sets with sterilized sediment (i.e., pond and rice field abiotic incubations) lost ~800 compounds (Figures 3.2e-h). The fact that a similar number of new compounds were formed in both abiotic and biotic treatments for a given recharge water, and that a greater formation than loss of compounds occurred (i.e., new single compounds did not simply evolve from a single lost compound) implies that OC was mobilized off the aquifer sediment in the early stages of incubation, with pond recharge water facilitating greater mobilization of OC than rice field recharge water. Further, OC mobilized off sediment prior to incubation (i.e., DOC in sediment porewater) was rich in compounds containing S and P heteroatom groups (Figure 3.1c), aligning with the greater formation of CHOS, CHONS and CHONPS compounds during incubation (Figure 3.3b). If this interpretation is correct, mobilization in pond recharge incubations was large enough to measurably increase DOC concentrations, while mobilization in rice field recharge incubations was not.

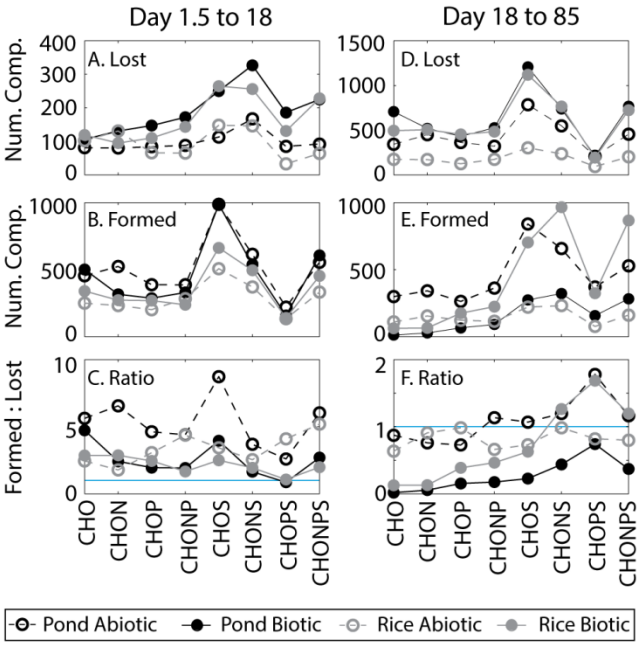

Figure 3.3: The number of compounds lost (panels a, d), the number of compounds formed (panels b, e), and the ratio of formed to lost compound (panels c, f) in the incubation experiments for each heteroatom group between days 1.5 and 18 (panels a-c) and between days 18 and 85 (panels d-f). The blue line in panels c and F mark the 1:1 ratio of formed to lost compounds.

In agreement with this interpretation, multiple ways of visualizing FT-ICR-MS data reveal that newly formed compounds at day 18 of incubation were chemically similar to those present at day 1.5. The red and black lines labeled A in Figure 3.4, as well as in Figures Appendix.5-Appendix.7, plot the total number of compounds present at day 18 of incubation (red lines) and the number of compounds present at day 18 that were also present at day 1.5 (black lines) against the H-to-C, O-to-C, N-to-C, P-to-C and S-to-C ratios for each heteroatom group. These plots demonstrate that newly formed compounds had similar heteroatom ratios as existing compounds, and that compound growth was focused in areas with the largest initial compound occurrence. Finally, the mass distribution of compounds detected at day 18 of incubation mimicked that of compounds detected at day 1.5 of incubation (Figures Appendix.8, Appendix.9). The relative proportion of compounds within a given mass range was similar at the two time points, but the total number of compounds in each mass range was greater at day 18 than at day 1.5.

Greater mobilization of carbon off aquifer sediment in incubations conducted with pond recharge water could be related to the higher initial pH of these incubations. At day 1.5, average pH for incubations conducted with pond recharge water (abiotic and biotic treatments) was 7.94 ± 0.04 while those conducted with rice field recharge water (abiotic and biotic treatments) was 7.59 ± 0.20. Multiple soil-focused studies have demonstrated that an increase in solution pH promotes desorption of natural organic matter (Gu, Schmitt, Chen, Liang, & McCarthy, 1994; Jardine, McCarthy, & Weber, 1989; Kaiser & Zech, 1999).

Greater loss of compounds in incubation sets conducted with native sediment relative to those conducted with sterilized sediment indicate that microbial transformation of OC occurred during the first 18 days of the experiment, even though such transformations were not notably

decreasing DOC concentrations (Figure 3.2). Figure 3.3a indicates that these microbial transformations were focused on compounds containing S and P, but that the greatest loss occurred for compounds that contained S but lacked P (i.e., CHOS and CHONS).

Overall, there was a similar pattern of compound loss across heteroatom groups for both biotic and abiotic incubations, indicating that these initial microbial transformations were likely enhancing those occurring abiotically. Figure 3.4, as well as Figures Appendix.5–Appendix.7, show that lost compounds in all incubations had low H-to-C, N-to-C, P-to-C and S-to-C ratios and more evenly distributed O-to-C ratios (see grey lines labeled A). Fate of the lost compounds is unclear and largely masked by the large formation of new compounds.

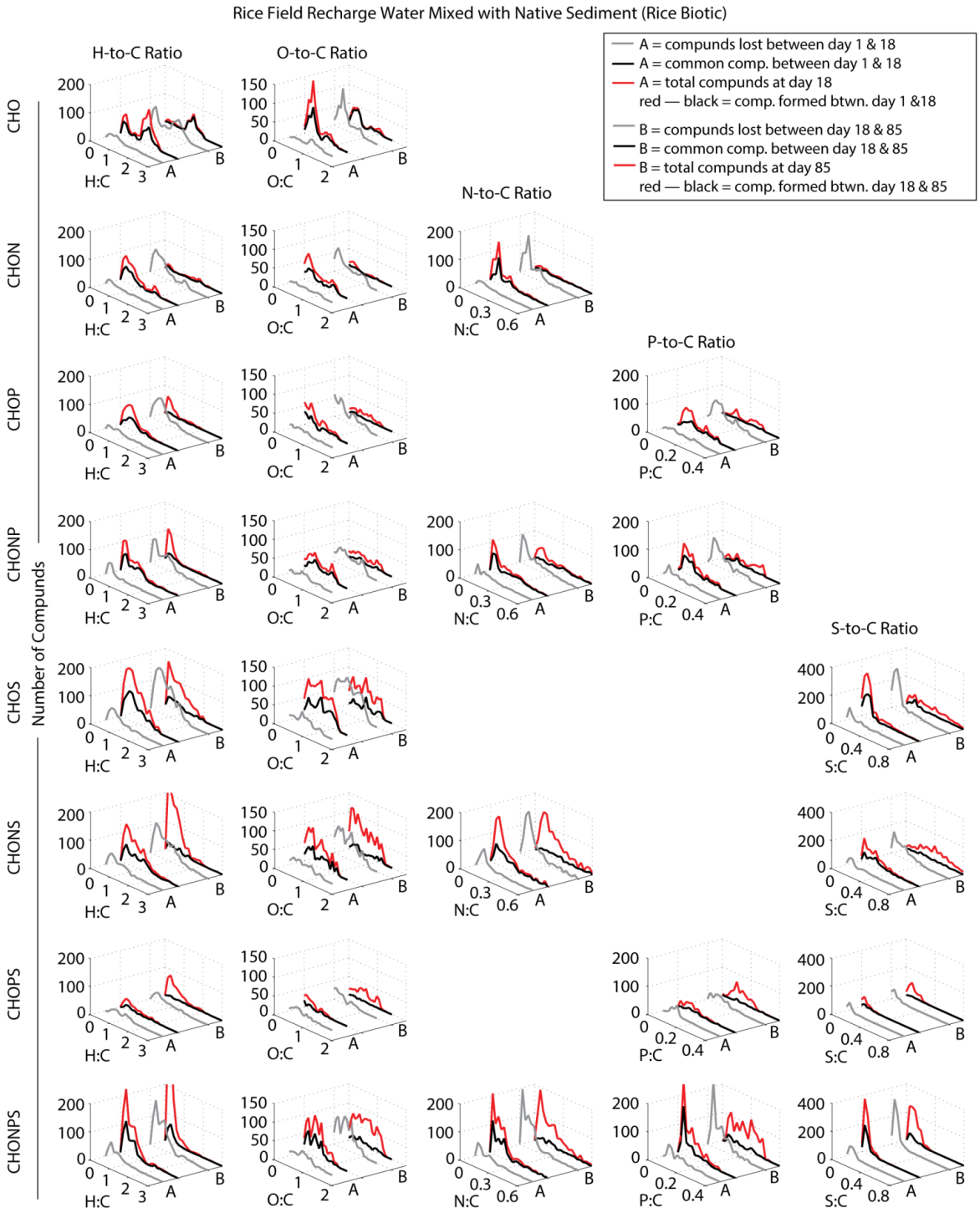

Figure 3.4: Evolution of H-to-C, O-to-C, N-to-C, P-to-C and S-to-C ratios over time in the biotic rice field incubations for each heteroatom group. Grey lines reflect the number of compounds lost between days 1.5 and 18 (labeled A) and between days 18 and 85 (labeled B), black lines reflect the number of compounds common to the noted timepoints, and red lines reflect the total number of compounds present at the latest of the noted timepoints (i.e., day 18 for line A and day 85 for line B).

Carbon Transformations: Day 18 to Day 85. Between day 18 and 85, DOC was lost from incubations conducted with native sediment, but not from those conducted with sterilized sediment (Figures 3.2a-d). Carbon mass balance calculations indicated that DOC lost in biotic incubations was fermented into methane (Neumann et al., 2014a). Accordingly, the number of identified compounds by FT-ICR-MS decreased in both biotic incubations but did not change in abiotic incubations (Figures 3.2e-h). However, there was not a direct relationship between DOC concentration and number of compounds; both biotic incubations lost similar amounts of DOC by day 85 (i.e., -111 ± 12 and -120 ± 16 mg/L in pond and rice field incubations, respectively), but compound decrease was larger for those conducted with pond recharge water than for those conducted with rice field recharge water (Figure 3.2).

In abiotic incubations, the ratio of formed-to-lost compounds in all heteroatom groups hovered near one (Figure 3f) with the exception of CHOPS in the abiotic pond incubation where the ratio was notably larger than one. The pattern of formation and loss across heteroatom groups during this later time period (i.e., 18 to 85 days) was similar to that during the early time period (i.e., 1.5 to 18 days), with S- and P- containing groups experiencing the greatest loss and gain of new compounds (Figures 3.3a,b,d,e). There are a few possible interpretations for these abiotic patterns. The first is that in this later time period, organic matter continued to be mobilized off aquifer sediment, as was assumed to have occurred in the earlier time period, but rates of mobilization (i.e., formation of new compounds) were slower such that they matched rates of abiotic conversion (i.e., loss of compounds). Additionally, S- and P- containing compounds could have simply exchanged with each other on the sediment. Exchange of OC is known to occur in soils, driven by differences in hydrophobicity (Kaiser & Zech, 1998). Another possibility is that no further organic matter was mobilized off aquifer sediment and newly

formed compounds largely evolved from lost compounds. In this situation, the larger loss and gain of compounds with S and P could reflect that fact that these compounds types were more chemically reactive than those lacking S and P. As was the case in the earlier time period, abiotic reactions in this later period did not notably change the character of OC. Figures Appendix.5 and Appendix.7 illustrate that lost and formed compounds had similar heteroatom ratios and Figure Appendix.10 demonstrates they had almost identical molecular mass distributions.

In biotic incubations, patterns of compound formation and loss across different heteroatom groups was similar to that in abiotic incubations, with S- and P- containing groups experiencing the largest loss and gain of compounds (Figures 3.3d-e). However, in biotic incubations, there was a greater overall loss of compounds in all heteroatom groups, except CHOPS where compound loss was similar between biotic and abiotic incubations (Figure 3.3d). In the biotic pond incubation, the ratio of formed to lost compounds was below one for all heteroatom groups (Figure 3.3f), indicating there was more compound loss than formation in this incubation. In the biotic rice field incubation, the ratio of formed to lost compounds was below one for all but the CHONS, CHOPS and CHONPS heteroatom groups (Figure 3.3f). In both pond and rice field biotic incubations, there was a general increasing trend in the formed-to-lost ratio as P and S heteroatoms were added to molecules.

Some formation and loss of S- and P-containing compounds in biotic incubations could reflect abiotic processes. However, in biotic incubations, unlike in abiotic incubations, loss and formation of compounds changed the overall chemical character of OC. Even in the biotic rice field incubation, where the ratio of formed-to-lost compounds for S- and P-containing heteroatom groups exceeded one (Figure 3.3f), there was a net loss of certain compound types. The fully lost types included P-containing compounds (i.e., CHOP and CHONP) with H-to-C

ratios greater than 0.8 and S-containing compounds (i.e., CHOS, CHONS, CHOSP, CHONSP) with H-to-C ratios greater than 1.5 (Figures Appendix.3, Appendix.4). Interestingly, compounds not fitting these general patterns were those with larger molecular mass (i.e., greater than 900 to 1000 Da); larger compounds with high H-to-C ratios existed at both time periods.

With regards to formation of S- and P-containing compounds, in biotic incubations, these compound types had higher O-to-C, P-to-C, and S-to-C ratios at day 85 than at day 18 (compare grey and red lines labeled B in Figure 3.4 and Appendix.6). The H-to-C and N-to-C ratios did not notably change. This shift in heteroatom ratios did not occur in abiotic incubations (Figures Appendix.5 and Appendix.7), indicating microbes either added O, P, and S to existing molecules or decreased the size of existing molecules with O, P, and S. The relative mass distributions of compounds present at day 18 and 85 remained the same (Figure Appendix.11), and thus we interpret the change as microbially-driven heteroatom enrichment. The O, P, and S enrichment of compounds that remained after most OC was fermented into methane could reflect microbial metabolites, enzymes or other microbially-produced compounds needed for methanogenesis. Sulfur and phosphorous are both required nutrients for methanogenesis (Hand & Honek, 2005; Medvedeff, Inglett, & Inglett, 2014), and some required organic compounds could have high heteroatom ratios. One example is thiol 2-mercaptoethanesulfonate, or coenzyme M, which is required for methanogenesis, and has an S-to-C ratio of one (Hand & Honek, 2005). Other studies have directly connected presence of organosulfur species (D'Andrilli, Foreman, Marshall, & McKnight, 2013; Gonsior et al., 2011) and generation of oxygen-rich functional groups (Meng, Huang, Li, & Li, 2012) with microbial activity.

In contrast to heteroatom groups containing S and P, the two groups lacking S and P (i.e., CHO and CHON) both lost compounds between days 18 and 85 in the biotic incubation and

gained few compounds during this period (Figures 3.3d-e). Compound loss in both groups defied what is expected based on indices of chemical lability. In the CHO group, compounds with lower H-to-C ratios were lost and not regenerated, while those that remained unmodified by microbial activity had higher H-to-C ratios (i.e., H-to-C >1.25; Figures 3.4, Appendix.3, Appendix.4, Appendix.6). In the CHON group, almost all compounds were fully utilized and not regenerated by native microbes, including those typically considered chemically recalcitrant (Figures 3.4, Appendix.3, Appendix.4, Appendix.6). Microbes may have targeted CHON compounds to gain access to nitrogen; however, other nitrogen containing compounds were not targeted in the same manner. Alternatively, microbes may have degraded CHON compounds in order to create CHONP, CHONS and CHONPS compounds.

Overall, the chemical character of OC remaining at day 85 was highly heterogeneous and unique from that found initially in the recharge waters and sediment porewater (compare Figures 3.1a and 3.1b to Figures Appendix.3a and Appendix.4a). Dissolved organic concentrations were similar to those in recharge waters (Figures 3.2b,d), but DOC in the incubation was more chemically diverse and contained notably more organosulfur compounds with low H-to-C ratios than DOC in recharge waters.

Chemical Indices and Bioavailability. The direct link between microbial use of OC and chemical character of OC afforded by this study demonstrates that indices of chemical lability (e.g., H-to-C ratios) are helpful for understanding microbial processing of organic matter, but they cannot predict bioavailability. During incubation, microbes operated on compounds considered chemically recalcitrant. For the CHO and CHON heteroatom groups, these recalcitrant compounds were fully utilized and not regenerated (Figures 3.4, Appendix.6). For S- and P-containing heteroatom groups, microbes increased the S-to-C and P-to-C ratio of

chemically recalcitrant compounds (Figures 4, Appendix.6), potentially converting them into forms needed for methanogenesis. This conversion of chemically recalcitrant compounds implies that while these compound types are not mineralized by microbes, they might, nonetheless, be important for facilitating mineralization of other OC forms. Thus, chemically recalcitrant compounds should not necessarily be interpreted as inert terminal end products (Large, 1983; Weston & Joye, 2005). These examples align with those evolving from the soil science literature (Schmidt et al., 2011) demonstrating that chemical lability is one of many factors controlling fate of OC.

Broader Perspective for Destabilization of SOC. In this experiment, OC was initially mobilized off Bangladeshi aquifer sediment due to sampling, homogenizing, and/or handling of the sediment. The incubation demonstrated the carbon was microbially-available; most of it was fermented into methane (Neumann et al., 2014a). As previously discussed, if this pool of OC were destabilized *in situ*, it could fuel microbially-mediated subsurface reactions with consequences for groundwater quality. Groundwater in Bangladesh contains high concentrations of dissolved methane, and this methane gets directly emitted to the atmosphere when groundwater is pumped up for rice irrigation (Neumann, Pracht, Polizzotto, Badruzzaman, & Ali, 2014b). Increases in DOC concentrations early in incubation, as well as increases in the number of compounds identified by FT-ICR-MS during this period with both native and sterilized sediment (Figure 3.2) imply that OC was abiotically released from aquifer sediment. Release presumably reflected re-equilibration of OC between dissolved and sorbed phases, driven by a change in pH, and indicates a mechanism for *in situ* destabilization of SOC. Changes in groundwater chemistry (e.g., an increase in groundwater pH), driven, for example, by pumping induced rearrangement of groundwater flow paths, could facilitate mobilization of SOC.

Incubation data indicated that pond recharge water had a higher pH than rice field recharge water, and thus pond recharge water facilitated greater SOC mobilization (Figure 3.2). If this behavior is applicable to the field setting where incubation materials were obtained, then SOC could be mobilized when sediment that has been in contact with groundwater that evolved from rice field recharge is suddenly exposed to higher pH groundwater that evolved from pond recharge.

FT-ICR-MS showed that the mobilized SOC was highly diverse. It was composed of a large number of compounds containing a variety of heteroatom groups and likely originating from both terrestrial and microbial sources. Many of these compounds contained sulfur. Given that other FT-ICR-MS studies focused on subsurface systems have similarly seen a large presence of organosulfur compounds (Evert, 2015; Longnecker & Kujawinski, 2011; Sleighter et al., 2014), S-containing compounds could act as a marker for carbon evolving from organic-rich, anaerobic subsurface environments. During incubation, organosulfur compounds were actively transformed in both abiotic and biotic treatments; but after most of the DOC was fermented into methane ~80% of the remaining OC contained S (Figures Appendix.3b and Appendix.4b).

3.5 Acknowledgments

We thank Rosalie K. Chu for analytical assistance with FT-ICR-MS. A portion of the research was performed using EMSL, a DOE Office of Science User Facility sponsored by the Office of Biological and Environmental Research (BER) and located at Pacific Northwest National Laboratory.

3.6 References

Aravena, R., & Wassenaar, L. I. (1993). Dissolved organic carbon and methane in a regional confined aquifer, southern Ontario, Canada: Carbon isotope evidence for associated subsurface sources. *Applied Geochemistry*, *8*(5), 483–493. https://doi.org/10.1016/0883-2927(93)90077-T

Arndt, S., Jørgensen, B. B., LaRowe, D. E., Middelburg, J. J., Pancost, R. D., & Regnier, P. (2013). Quantifying the degradation of organic matter in marine sediments: A review and synthesis. *Earth-Science Reviews*, *123*, 53–86. https://doi.org/10.1016/j.earscirev.2013.02.008

Baldock, J. A., & Skjemstad, J. O. (2000). Role of the soil matrix and minerals in protecting natural organic materials against biological attack. *Organic Geochemistry*, *31*(7–8), 697–710. https://doi.org/10.1016/S0146-6380(00)00049-8

Brosnan, J. T., & Brosnan, M. E. (2006). The sulfur-containing amino acids: an overview. *The Journal of Nutrition*, *136*(6 Suppl), 1636S–1640S.

Brown, K. A. (1986). Formation of organic sulphur in anaerobic peat. *Soil Biology and Biochemistry*, *18*(2), 131–140. https://doi.org/10.1016/0038-0717(86)90017-9

Chapelle, F. H. (2000). The significance of microbial processes in hydrogeology and geochemistry. *Hydrogeology Journal*, *8*(1), 41–46. https://doi.org/10.1007/PL00010973

Chapelle, F. H., Bradley, P. M., Goode, D. J., Tiedeman, C., Lacombe, P. J., Kaiser, K., & Benner, R. (2009). Biochemical Indicators for the Bioavailability of Organic Carbon in Ground Water. *Ground Water*, *47*(1), 108–121. https://doi.org/10.1111/j.1745-6584.2008.00493.x

Chipman, L., Podgorski, D., Green, S., Kostka, J., Cooper, W., & Huettel, M. (2010). Decomposition of plankton-derived dissolved organic matter in permeable coastal sediments. *Limnology and Oceanography*, *55*(2), 857–871. https://doi.org/10.4319/lo.2010.55.2.0857

Christensen, T. H., Bjerg, P. L., Banwart, S. A., Jakobsen, R., Heron, G., & Albrechtsen, H.-J. (2000). Characterization of redox conditions in groundwater contaminant plumes. *Journal of Contaminant Hydrology*, *45*(3–4), 165–241. https://doi.org/10.1016/S0169-7722(00)00109-1

D'Andrilli, J., Cooper, W. T., Foreman, C. M., & Marshall, A. G. (2015). An ultrahigh-resolution mass spectrometry index to estimate natural organic matter lability. *Rapid Communications in Mass Spectrometry*, *29*(24), 2385–2401. https://doi.org/10.1002/rcm.7400

D'Andrilli, J., Dittmar, T., Koch, B. P., Purcell, J. M., Marshall, A. G., & Cooper, W. T. (2010). Comprehensive characterization of marine dissolved organic matter by Fourier transform ion cyclotron resonance mass spectrometry with electrospray and atmospheric pressure photoionization. *Rapid Communications in Mass Spectrometry*, *24*(5), 643–650. https://doi.org/10.1002/rcm.4421

D'Andrilli, J., Foreman, C. M., Marshall, A. G., & McKnight, D. M. (2013). Characterization of IHSS Pony Lake fulvic acid dissolved organic matter by electrospray ionization Fourier transform ion cyclotron resonance mass spectrometry and fluorescence spectroscopy. *Organic Geochemistry*, *65*, 19–28. https://doi.org/10.1016/j.orggeochem.2013.09.013

Desbarats, A. J., Koenig, C. E. M., Pal, T., Mukherjee, P. K., & Beckie, R. D. (2014). Groundwater flow dynamics and arsenic source characterization in an aquifer system of

West Bengal, India. *Water Resources Research*, *50*(6), 4974–5002. https://doi.org/10.1002/2013WR014034

Evert, M. H. (2015). *Influence of NOM Molecular Characteristic on Uranium Cycling in a Catchment*. The Ohio State University. Retrieved from https://etd.ohiolink.edu/pg_10?0::NO:10:P10_ETD_SUBID:103657

Fontaine, S., Barot, S., Barré, P., Bdioui, N., Mary, B., & Rumpel, C. (2007). Stability of organic carbon in deep soil layers controlled by fresh carbon supply. *Nature*, *450*(7167), 277–80. https://doi.org/http://dx.doi.org.offcampus.lib.washington.edu/10.1038/nature06275

Gonsior, M., Peake, B. M., Cooper, W. T., Podgorski, D. C., D'Andrilli, J., Dittmar, T., & Cooper, W. J. (2011). Characterization of dissolved organic matter across the Subtropical Convergence off the South Island, New Zealand. *Marine Chemistry*, *123*(1–4), 99–110. https://doi.org/10.1016/j.marchem.2010.10.004

Gu, B., Schmitt, J., Chen, Z., Liang, L., & McCarthy, J. F. (1994). Adsorption and desorption of natural organic matter on iron oxide: mechanisms and models. *Environmental Science & Technology*, *28*(1), 38–46. https://doi.org/10.1021/es00050a007

Gurwick, N. P., McCorkle, D. M., Groffman, P. M., Gold, A. J., Kellogg, D. Q., & Seitz-Rundlett, P. (2008). Mineralization of ancient carbon in the subsurface of riparian forests. *Journal of Geophysical Research: Biogeosciences*, *113*(G2), G02021. https://doi.org/10.1029/2007JG000482

Hand, C., & Honek, J. (2005). Biological Chemistry of Naturally Occurring Thiols of Microbial and Marine Origin. *Journal of Natural Products*, *68*(2), 293–308. https://doi.org/10.1021/np049685x

Hartog, N., van Bergen, P. F., de Leeuw, J. W., & Griffioen, J. (2004). Reactivity of organic matter in aquifer sediments: geological and geochemical controls. *Geochimica et Cosmochimica Acta*, *68*(6), 1281–1292. https://doi.org/10.1016/j.gca.2003.09.004

Harvey, C. F., Ashfaque, K. N., Yu, W., Badruzzaman, A. B. M., Ali, M. A., Oates, P. M., … Ahmed, M. F. (2006). Groundwater dynamics and arsenic contamination in Bangladesh. *Chemical Geology*, *228*(1–3), 112–136. https://doi.org/10.1016/j.chemgeo.2005.11.025

Harvey, C. F., Swartz, C. H., Badruzzaman, A. B. M., Keon-Blute, N., Yu, W., Ali, M. A., … Ahmed, M. F. (2002). Arsenic Mobility and Groundwater Extraction in Bangladesh. *Science*, *298*(5598), 1602–1606. https://doi.org/10.1126/science.1076978

Hedges, J. I. (1990). Compositional indicators of organic-acid sources and reactions in natural environments. In *Organic acids in aquatic ecosystems* (pp. 43–63). Wiley.

Heitmann, T., & Blodau, C. (2006). Oxidation and incorporation of hydrogen sulfide by dissolved organic matter. *Chemical Geology*, *235*(1–2), 12–20. https://doi.org/10.1016/j.chemgeo.2006.05.011

Jakobsen, R., & Postma, D. (1994). In situ rates of sulfate reduction in an aquifer (Rømø, Denmark) and implications for the reactivity of organic matter. *Geology*, *22*(12), 1101–1106. https://doi.org/10.1130/0091-7613(1994)022<1103:ISROSR>2.3.CO;2

Jardine, P. M., McCarthy, J. F., & Weber, N. L. (1989). Mechanisms of Dissolved Organic Carbon Adsorption on Soil. *Soil Science Society of America Journal*, *53*(5), 1378. https://doi.org/10.2136/sssaj1989.03615995005300050013x

Kaiser, K., & Zech, W. (1998). Rates of dissolved organic matter release and sorption in forest soils. *Soil Science*, *163*, 714–725.

Kaiser, K., & Zech, W. (1999). Release of Natural Organic Matter Sorbed to Oxides and a Subsoil. *Soil Science Society of America Journal*, *63*(5), 1157.

Kim, S., Kaplan, L. A., & Hatcher, P. G. (2006). Biodegradable dissolved organic matter in a temperate and a tropical stream determined from ultra-high resolution mass spectrometry. *Limnology and Oceanography*, *51*(2), 1054–1063. https://doi.org/10.4319/lo.2006.51.2.1054

Kim, S., Kramer, R. W., & Hatcher, P. G. (2003). Graphical Method for Analysis of Ultrahigh-Resolution Broadband Mass Spectra of Natural Organic Matter, the Van Krevelen Diagram. *Analytical Chemistry*, *75*(20), 5336–5344. https://doi.org/10.1021/ac034415p

Koch, B. P., & Dittmar, T. (2006). From mass to structure: an aromaticity index for high-resolution mass data of natural organic matter. *Rapid Communications in Mass Spectrometry*, *20*(5), 926–932. https://doi.org/10.1002/rcm.2386

Koch, B. P., & Dittmar, T. (2016). From mass to structure: an aromaticity index for high-resolution mass data of natural organic matter. *Rapid Communications in Mass Spectrometry*, *30*(1), 250–250. https://doi.org/10.1002/rcm.7433

Kohnen, M. E. L., Sinninghe Damste, J. S., & De Leeuw, J. W. (1991). Biases from natural sulphurization in palaeoenvironmental reconstruction based on hydrocarbon biomarker distributions. *Nature*, *349*(6312), 775–778. https://doi.org/10.1038/349775a0

Korom, S. F. (1992). Natural denitrification in the saturated zone: A review. *Water Resources Research*, *28*(6), 1657–1668. https://doi.org/10.1029/92WR00252

Kujawinski, E. B., Del Vecchio, R., Blough, N. V., Klein, G. C., & Marshall, A. G. (2004). Probing molecular-level transformations of dissolved organic matter: insights on photochemical degradation and protozoan modification of DOM from electrospray

ionization Fourier transform ion cyclotron resonance mass spectrometry. *Marine Chemistry*, *92*(1–4), 23–37. https://doi.org/10.1016/j.marchem.2004.06.038

Large, J. L. (1983). In J. A. Cole (Ed.), *Aspects of Microbiology* (Vol. 8, pp. 11–24). Washington DC: AMS Publications.

Longnecker, K., & Kujawinski, E. B. (2011). Composition of dissolved organic matter in groundwater. *Geochimica et Cosmochimica Acta*, *75*(10), 2752–2761. https://doi.org/10.1016/j.gca.2011.02.020

Lu, Y., Li, X., Mesfioui, R., Bauer, J. E., Chambers, R. M., Canuel, E. A., & Hatcher, P. G. (2015). Use of ESI-FTICR-MS to Characterize Dissolved Organic Matter in Headwater Streams Draining Forest-Dominated and Pasture-Dominated Watersheds. *PLOS ONE*, *10*(12), e0145639. https://doi.org/10.1371/journal.pone.0145639

McDowell, W. H., Zsolnay, A., Aitkenhead-Peterson, J. A., Gregorich, E. G., Jones, D. L., Jödemann, D., … Schwesig, D. (2006). A comparison of methods to determine the biodegradable dissolved organic carbon from different terrestrial sources. *Soil Biology and Biochemistry*, *38*(7), 1933–1942. https://doi.org/10.1016/j.soilbio.2005.12.018

McMahon, P. B., & Chapelle, F. H. (1991). Microbial production of organic acids in aquitard sediments and its role in aquifer geochemistry. *Nature*, *349*(6306), 233–235. https://doi.org/10.1038/349233a0

Medvedeff, C. A., Inglett, K. S., & Inglett, P. W. (2014). Evaluation of direct and indirect phosphorus limitation of methanogenic pathways in a calcareous subtropical wetland soil. *Soil Biology and Biochemistry*, *69*, 343–345. https://doi.org/10.1016/j.soilbio.2013.11.018

Meng, F., Huang, G., Li, Z., & Li, S. (2012). Microbial Transformation of Structural and Functional Makeup of Human-Impacted Riverine Dissolved Organic Matter. *Industrial & Engineering Chemistry Research*, *51*(17), 6212–6218. https://doi.org/10.1021/ie300504d

Neumann, R. B., Ashfaque, K. N., Badruzzaman, A. B. M., Ashraf Ali, M., Shoemaker, J. K., & Harvey, C. F. (2010). Anthropogenic influences on groundwater arsenic concentrations in Bangladesh. *Nature Geoscience*, *3*(1), 46–52. https://doi.org/10.1038/ngeo685

Neumann, R. B., Pracht, L. E., Polizzotto, M. L., Badruzzaman, A. B. M., & Ali, M. A. (2014a). Biodegradable Organic Carbon in Sediments of an Arsenic-Contaminated Aquifer in Bangladesh. *Environmental Science & Technology Letters*, *1*(4), 221–225. https://doi.org/10.1021/ez5000644

Neumann, R. B., Pracht, L. E., Polizzotto, M. L., Badruzzaman, A. B. M., & Ali, M. A. (2014b). Sealing rice field boundaries in Bangladesh: a pilot study demonstrating reductions in water use, arsenic loading to field soils, and methane emissions from irrigation water. *Environmental Science & Technology*, *48*(16), 9632–9640. https://doi.org/10.1021/es500338u

Osborne, D. M., Podgorski, D. C., Bronk, D. A., Roberts, Q., Sipler, R. E., Austin, D., … Cooper, W. T. (2013). Molecular-level characterization of reactive and refractory dissolved natural organic nitrogen compounds by atmospheric pressure photoionization coupled to Fourier transform ion cyclotron resonance mass spectrometry. *Rapid Communications in Mass Spectrometry: RCM*, *27*(8), 851–858. https://doi.org/10.1002/rcm.6521

Parkin, T. B., & Simpkins, W. W. (1995). Contemporary Groundwater Methane Production from Pleistocene Carbon. *Journal of Environment Quality*, *24*(2), 367. https://doi.org/10.2134/jeq1995.00472425002400020021x

Pedler Sherwood, B., Shaffer, E. A., Reyes, K., Longnecker, K., Aluwihare, L. I., & Azam, F. (2015). Metabolic characterization of a model heterotrophic bacterium capable of significant chemical alteration of marine dissolved organic matter. *Marine Chemistry*, *177*, *Part 2*, 357–365. https://doi.org/10.1016/j.marchem.2015.06.027

Perlinger, J. A., Kalluri, V. M., Venkatapathy, R., & Angst, W. (2002). Addition of Hydrogen Sulfide to Juglone. *Environmental Science & Technology*, *36*(12), 2663–2669. https://doi.org/10.1021/es015602c

Petridis, L., Ambaye, H., Jagadamma, S., Kilbey, S. M., Lokitz, B. S., Lauter, V., & Mayes, M. A. (2014). Spatial Arrangement of Organic Compounds on a Model Mineral Surface: Implications for Soil Organic Matter Stabilization. *Environmental Science & Technology*, *48*(1), 79–84. https://doi.org/10.1021/es403430k

Postma, D., Larsen, F., Minh Hue, N. T., Duc, M. T., Viet, P. H., Nhan, P. Q., & Jessen, S. (2007). Arsenic in groundwater of the Red River floodplain, Vietnam: Controlling geochemical processes and reactive transport modeling. *Geochimica et Cosmochimica Acta*, *71*(21), 5054–5071. https://doi.org/10.1016/j.gca.2007.08.020

Postma, D., Larsen, F., Thai, N. T., Trang, P. T. K., Jakobsen, R., Nhan, P. Q., … Murray, A. S. (2012). Groundwater arsenic concentrations in Vietnam controlled by sediment age. *Nature Geoscience*, *5*(9), 656–661. https://doi.org/10.1038/ngeo1540

Schmidt, M. W. I., Torn, M. S., Abiven, S., Dittmar, T., Guggenberger, G., Janssens, I. A., … Trumbore, S. E. (2011). Persistence of soil organic matter as an ecosystem property. *Nature*, *478*(7367), 49–56. https://doi.org/10.1038/nature10386

Schouten, S., van Driel, G. B., Sinninghe Damsté, J. S., & de Leeuw, J. W. (1993). Natural sulphurization of ketones and aldehydes: A key reaction in the formation of organic sulphur compounds. *Geochimica et Cosmochimica Acta*, *57*(23), 5111–5116. https://doi.org/10.1016/0016-7037(93)90613-2

Sleighter, R. L., Chin, Y.-P., Arnold, W. A., Hatcher, P. G., McCabe, A. J., McAdams, B. C., & Wallace, G. C. (2014). Evidence of Incorporation of Abiotic S and N into Prairie Wetland Dissolved Organic Matter. *Environmental Science & Technology Letters*, *1*(9), 345–350. https://doi.org/10.1021/ez500229b

Sleighter, R. L., & Hatcher, P. G. (2007). The application of electrospray ionization coupled to ultrahigh resolution mass spectrometry for the molecular characterization of natural organic matter. *Journal of Mass Spectrometry*, *42*(5), 559–574. https://doi.org/10.1002/jms.1221

Spencer, R. G. M., Guo, W., Raymond, P. A., Dittmar, T., Hood, E., Fellman, J., & Stubbins, A. (2014). Source and biolability of ancient dissolved organic matter in glacier and lake ecosystems on the Tibetan Plateau. *Geochimica et Cosmochimica Acta*, *142*, 64–74. https://doi.org/10.1016/j.gca.2014.08.006

Swartz, C. H., Blute, N. K., Badruzzman, B., Ali, A., Brabander, D., Jay, J., … Harvey, C. F. (2004). Mobility of arsenic in a Bangladesh aquifer: Inferences from geochemical profiles, leaching data, and mineralogical characterization. *Geochimica et Cosmochimica Acta*, *68*(22), 4539–4557. https://doi.org/10.1016/j.gca.2004.04.020

Tfaily, M. M., Hamdan, R., Corbett, J. E., Chanton, J. P., Glaser, P. H., & Cooper, W. T. (2013). Investigating dissolved organic matter decomposition in northern peatlands using complimentary analytical techniques. *Geochimica et Cosmochimica Acta*, *112*, 116–129. https://doi.org/10.1016/j.gca.2013.03.002

Trulleyová, Š., & Rulík, M. (2004). Determination of biodegradable dissolved organic carbon in waters: comparison of batch methods. *Science of The Total Environment*, *332*(1–3), 253–260. https://doi.org/10.1016/j.scitotenv.2004.04.018

Urban, N. R., Ernst, K., & Bernasconi, S. (1999). Addition of sulfur to organic matter during early diagenesis of lake sediments. *Geochimica et Cosmochimica Acta*, *63*(6), 837–853. https://doi.org/10.1016/S0016-7037(98)00306-8

van Bergen, P. F., Nott, C. J., Bull, I. D., Poulton, P. R., & Evershed, R. P. (1998). Organic geochemical studies of soils from the Rothamsted Classical Experiments—IV. Preliminary results from a study of the effect of soil pH on organic matter decay. *Organic Geochemistry*, *29*(5–7), 1779–1795. https://doi.org/10.1016/S0146-6380(98)00188-0

van Geen, A., Bostick, B. C., Thi Kim Trang, P., Lan, V. M., Mai, N.-N., Manh, P. D., … Berg, M. (2013). Retardation of arsenic transport through a Pleistocene aquifer. *Nature*, *501*(7466), 204–207. https://doi.org/10.1038/nature12444

van Krevelen, D. W. (1950). Graphical-statistical method for the study of structure and reaction processes of coal. *Fuel*, *29*, 269–284.

Weston, N. B., & Joye, S. B. (2005). Temperature-driven decoupling of key phases of organic matter degradation in marine sediments. *Proceedings of the National Academy of Sciences of the United States of America*, *102*(47), 17036–17040. https://doi.org/10.1073/pnas.0508798102

Willoughby, A. S., Wozniak, A. S., & Hatcher, P. G. (2014). A molecular-level approach for characterizing water-insoluble components of ambient organic aerosol particulates using ultrahigh-resolution mass spectrometry. *Atmos. Chem. Phys.*, *14*(18), 10299–10314. https://doi.org/10.5194/acp-14-10299-2014

4. Microbially-Mediated Destabilization of Sedimentary Organic Carbon: Isotopic Tracking of Carbon Movement in Laboratory Incubations of Glucose-Amended Aquifer Sediment to Determine Priming Effects

4.1 Introduction

Arsenic-contaminated groundwater is a worldwide concern; the result of both geogenic and anthropogenic sources. In naturally-contaminated systems, organic carbon fueling reductive dissolution of iron hydroxides is considered to be the primary mechanism of mobilization of arsenic off sediment into groundwater. Previous laboratory incubations (Neumann, Pracht, Polizzotto, Badruzzaman, & Ali, 2014) of aquifer sediment and groundwater collected from a contaminated subsurface system in Bangladesh revealed a pool of biologically available organic carbon mobilized from the sandy sediment. Results indicated that sediments can contain chemically labile organic carbon that is physically protected or otherwise inaccessible to microbial communities. Destabilization of this pool of sedimentary organic carbon could fuel microbial reactions that mobilize contaminants such as arsenic.

One potential way that this carbon pool could be destabilized is through the priming effect, an effect where an input of labile organic matter (OM) impacts the utilization of older, more refractory OM. Priming can have a negative or positive effect on the utilization rate of this more recalcitrant OM. Priming is hypothesized to occur via two mechanisms: 1) labile organic carbon activates a larger variety of microbial communities, working in succession or in conjunction with each other to mineralize OM that would otherwise not be utilized (Derrien et al., 2014; Fontaine, Mariotti, & Abbadie, 2003; Y Kuzyakov, Friedel, & Stahr, 2000; Yakov Kuzyakov, 2010); 2) labile organic carbon fuels microbial-driven reductive dissolution reactions, destabilizing mineral-associated, reactive organic matter (Eusterhues, Rumpel, Kleber, & Kögel-Knabner, 2003; Mikutta, Kleber, Torn, & Jahn, 2006).

Most studies done on the priming effect have focused on soils, which contain much higher concentrations of organic matter than aquifer sediments. Few studies have looked at sediments, and those that have focused on sediments from lakes and oceans (Gontikaki, Thornton, Huvenne, & Witte, 2013; Hannides & Aller, 2016; van Nugteren et al., 2009) or oil sands tailing ponds (Ahad & Pakdel, 2013). However, there is evidence that these effects could occur in groundwater aquifer sediments. In aquifers, inputs of fresh, labile organic carbon from the surface may be introduced into a system via alterations to groundwater flow patterns, e.g., caused by changes in groundwater pumping schemes, as in a study conducted in Vietnam that saw arsenic mobilization reactions increase after significant groundwater pumping alterations (van Geen et al., 2013). In that study, increased pumping of groundwater to a large city mobilized arsenic in greater concentration than could be accounted for with amount of DOC present in the source water that was being pumped through the aquifer, and higher DOC concentrations were measured in the aquifer than in the source water.

In our current study, we tested the ability of an input of highly bioavailable organic carbon (glucose) into batch incubations of Cambodian aquifer sediment to destabilize sedimentary organic carbon (SOC) and fuel further microbial reactions, including reactions that mobilize arsenic, iron, and manganese off the sediment. Here we measured both concentrations and natural abundance stable carbon isotopes ($\delta^{13}C$) of inorganic and organic carbon pools within the solid and aqueous phase, in microcosm experiments to track the movement and transformation of carbon over time. We hypothesized that the addition of a labile source of organic carbon would destabilize bioavailable organic carbon from the sediments, which would fuel further microbial reactions responsible for metal mobilization.

4.2 Materials and Methods

4.2.1 Incubation Experimental Setup

In a 10mL amber glass serum vial, 10 mL of 0.1 M de-oxygenated NaCl solution was mixed with 4.3 g (dry mass) of aquifer sediment, collected in November 2011 in Cambodia; the sediment and sediment collection have previously been described (Gillispie, Andujar, & Polizzotto, 2016). The NaCl was added to the incubation solution to adjust ionic strength to a typical value for groundwater near the collected sediment, in order to prevent non environmentally-relevant sorption behavior. The field site is southeast of Phnom Penh. Sediment was collected from a Pleistocene aquifer that contains low concentrations of dissolved arsenic (As concentrations are below 10 μg/L (UNICEF, 2009)). Sediment was collected from three locations, at different depths (6 m, 18 m, and 21 m). Sample collection was conducted anaerobically, and temperatures maintained at 4 °C. Due to limited sample mass, sediment was homogenized in an anaerobic chamber at the University of Washington.

Vials were stoppered and filled using syringes and needles, to eliminate the entire headspace, removing the necessity to conduct any analyses of gas-phase carbon throughout the experiment. In half of the bottles, sterilized (subjected to 25 kGy gamma irradiation) sediment was used. NaCl solution was made with three different concentrations of glucose, amounting to 0 mg/L C (“Low”), 50 mg/L C (“Medium”), and 100 mg/L C (“High”). Incubation bottles were set up to sample at 6 different timepoints, with three replicates each of low, medium, and high glucose concentrations for each timepoint (108 total incubation vials). Over time, incubation samples were destructively sampled. Water and sediment were subsampled and analyzed as described in the following sections.

4.2.2 Electrochemical Parameters

During sampling, electrochemical parameters were measured on unfiltered water, including conductivity, pH, oxidation-reduction potential (ORP), and temperature. Conductivity and temperature was measured on a Mettler Toledo InLab 751-4mm glass conductivity probe, while pH and ORP were measured on a Fisher Scientific accumet pH/ORP combination titration glass electrode.

4.2.3 Dissolved Inorganic Carbon Concentration and Isotopic Signature

Dissolved inorganic carbon (DIC) concentration and $\delta^{13}C$ signature were measure on a GasBench II system interfaced to a Delta V Plus IRMS (Thermo Scientific, Bremen, Germany) at the Stable Isotope Facility (SIF) at University of California, Davis. During incubation sampling, 2 mL of sample was syringe filtered through a 0.2 μm polyethersulfone (PES) filter into an evacuated (flushed with N_2 gas, evacuated with a vacuum pump and 20G syringe needle, repeated 6 times) 12 mL Exetainer vial (Labco Ltd, High Wycombe, UK), containing 1 mL of concentrated phosphoric acid (Atekwana & Krishnamurthy, 1998; Li et al., 2007).

4.2.4 Dissolved Organic Carbon Concentration and Isotopic Signature

During incubation sampling, an aliquot of water was vacuum-filtered through a 0.2 μm PES filter; 175 μL were added to an ashed 200 μL glass insert, inside a 2 mL HPLC vial, while a second subsample was added into a 40 mL I-Chem 200 series glass vial and diluted with ultrapure deionized water (Milli-Q) to achieve necessary volume and concentration. The aliquot in the HPLC vial was used to determine dissolved organic carbon (DOC) concentrations. DOC was measured on a GE Analytical Instruments Sievers 900 TOC analyzer (model TOC 900

Portable) in line with a Dionex UltiMate 3000 high-performance liquid chromatography system (HPLC) system that functioned as an autosampler. The subsample in the I-Chem vial was sent to the SIF at UC Davis, for analysis of isotopic composition of $\delta^{13}C$ in DOC. These were measured on an O.I. Analytical Model 1030 TOC analyzer Analyzer (Xylem Analytics, College Station, TX) interfaced to a PDZ Europa 20-20 isotope ratio mass spectrometer (Sercon Ltd., Cheshire, UK) utilizing a GD-100 Gas Trap Interface (Graden Instruments), according to the laboratory-suggested method (St-Jean, 2003).

4.2.5 Solid-phase Carbon Concentration and Isotopic Signature

During sampling, an aliquot of sediment was placed in an acid-washed serum vial and later dried at 60 °C. The aliquot was further divided into 6 subsamples of ~20mg, weighed into silver 5 x 9 mm capsules (Costech, #41067). Three subsamples were fumigated in a desiccator with a beaker of concentrated HCl for at least 6 hours, according to the technique of Harris et al. 2001 (Harris, Horwáth, & van Kessel, 2001) to remove inorganic carbon from the sediment. All subsamples were measured at the University of Washington Isolab on a Costech ECS 4010 Elemental Analyzer (EA), ThermoFinnigan Conflo III, ThermoFinnigan MAT253 IRMS for a continuous flow based measurement of the solid material $\delta^{13}C$ (VDPB) and concentration. Inorganic carbon concentration (SIC) and isotopic signature were determined by calculations of the difference between the total (STC) and organic measurements (SOC), according to Equations 4.1-4.3. EA measurements were determined against three standards: NIST 1547 and two in-house glutamic acid standards.

$$m_{SIC} + m_{SOC} = m_{STC} \tag{4.1}$$

$$\delta_{SIC} m_{SIC} + \delta_{SOC} m_{SOC} = \delta_{STC} m_{STC} \tag{4.2}$$

$$\delta_{SIC} = \frac{\delta_{STC} m_{STC} - \delta_{SOC} m_{SOC}}{m_{STC} - m_{SOC}} \tag{4.3}$$

4.2.6 Arsenic, Iron, and Manganese

During sampling, an aliquot of water was vacuum-filtered through a 0.2um PES filter, added to an acid-washed 15 mL Falcon centrifuge tube, and acidified to 1% acidity with ultra-trace metal nitric acid. Acidified samples were then measured for As, Fe, and Mn on an Elan DRC-e inductively coupled plasma mass spectrometer (ICP-MS). Samples were diluted to below 250 μg/L to achieve optimal measurement concentration and avoid matrix interferences caused by the NaCl salt in the initial solution. Internal standards, external standards, and blanks were run as quality control checks to ensure data quality.

4.3 Results

Prior to mixing materials together, carbon concentrations and isotopic signatures were determined for both sediment and water (Table 4.1). These values allow us to track carbon movement throughout the system. The conceptual model for our system is shown in Figure 4.1.

Table 4.1: Characterization of initial sample materials, prior to mixing in incubation experiments. DOC isotopic signature was not measured (nm), due to lack of sufficient concentration. Concentrations below detectable limits are noted as 'nd'.

Parameter/ Sample	Isotopic Signature (δ^{13}C VPDB)	Concentration	Phase
Glucose	-11.5896	nm	Solid
Sedimentary Organic Carbon (SOC)	-22.3385	0.11 %C	Solid
Sedimentary Total Carbon (STC)	-16.5949	0.13 %C	Solid
Sedimentary Inorganic Carbon (SIC)	+14.9949	0.02 %C	Solid
Dissolved Organic Carbon (DOC), NaCl Solution	nm	nd	Aqueous
Dissolved Inorganic Carbon (DIC), NaCl Solution	-11.3690	nd	Aqueous

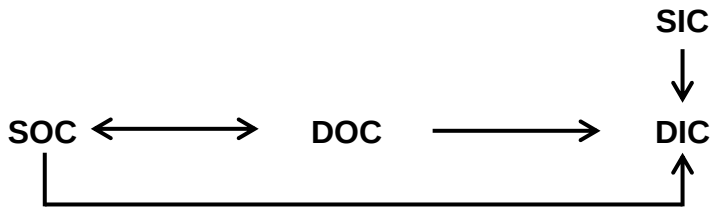

Figure 4.1: Conceptual model of carbon movement throughout our incubation microcosms. SOC: sedimentary organic carbon; DOC: dissolved organic carbon; DIC: dissolved inorganic carbon; SIC: sedimentary inorganic carbon

Concentrations of dissolved organic carbon over time in the incubation experiments (Figure 4.2a) started out around 480 mg C · kg^{-1} sediment in the high glucose samples, around 400-420 mg C · kg^{-1} sediment in the medium glucose samples, and ~270 mg C · kg^{-1} sediment (abiotic) and ~340 mg C · kg^{-1} sediment (biotic) in the low glucose samples (those with no glucose). Samples that were unamended with glucose contained only natural organic carbon, originating from the sediment. Previous laboratory incubations of sediment from Bangladesh showed a large pool of bioavailable organic carbon in sediment porewater (Neumann et al.,

2014). Over time, concentrations decreased down to ~30-60 mg C · kg^{-1} sediment in all the biotic samples. In contrast, DOC concentrations in the abiotic samples stayed relatively constant. The high glucose biotic samples (those that were spiked with 100 mg/L C with glucose), decreased in concentration almost immediately, with a decrease of ~42 mg C · kg^{-1} sediment between day 7 and day 28, reaching a low of ~30 mg C · kg^{-1} sediment at day 156. The medium glucose samples (those that were spiked with 50 mg/L C with glucose), remained relatively stable in concentration until dropping significantly between day 28 and day 100, dropping from 484 to 283 mg C · kg^{-1} sediment, reaching a final concentration of ~30 mg C · kg^{-1} sediment by day 156, mimicking the behavior of the high glucose samples. The low glucose samples (those that were not spiked with glucose), remained relatively stable in regards to DOC concentrations for the longest period of time, not dropping in concentration until they dropped from 358 to 76 mg C · kg^{-1} sediment between days 100 and 156 and reached a final concentration of 63 mg C · kg^{-1} sediment at day 226.

These concentration data help support the hypothesis that priming occurred, as spiking with glucose sped up the degradation processes occurring in the microcosms by 50 days. Further, the samples spiked with glucose were able to achieve slightly lower final concentrations, with the highly spiked samples achieving a final concentration of 38.8 mg C · kg^{-1} sediment (38.5 - 40.1 mg C · kg^{-1} sediment) vs. a final concentration of 63.5 mg C · kg^{-1} sediment (56.6 - 63.7 mg C · kg^{-1} sediment) in the unamended samples. These final concentrations hint at the ability of the glucose to prime the microbial community to access or utilize organic carbon otherwise recalcitrant.

Concentrations of dissolved inorganic carbon (DIC) behaved in a nearly opposite manner to the DOC, as would be expected (Figure 4.2b). Over time, the abiotic samples maintained

consistent DIC concentrations, while the biotic samples increased in concentration. The high glucose samples reached the highest concentration, around 550 mg C · kg^{-1} sediment vs. the unamended samples that reached approximately 430 mg C · kg^{-1} sediment.

Comparing the first and last timepoint, the change in mass of DOC was 277 mg C · kg^{-1} sediment for the unamended samples and was 437 mg C · kg^{-1} sediment for the high spiked samples. For these same samples, the difference between those timepoints in mass of DIC was larger at 353 mg C · kg^{-1} sediment and 502 mg C · kg^{-1} sediment, respectively. These discrepancies indicate that an additional carbon pool was responsible for the excess DIC formed, either SIC or SOC. Our measurements showed that SIC concentrations were too low to accurately calculate. Thus, the additional DIC was likely from SOC. The measured changes in SOC over the experiment (Figure 4.2c) were inconclusive in supporting this conclusion. SOC concentrations decreased in the incubations, but did so in both abiotic and biotic samples, indicating an abiotic reaction, such as equilibrium partitioning, was responsible for the decrease.

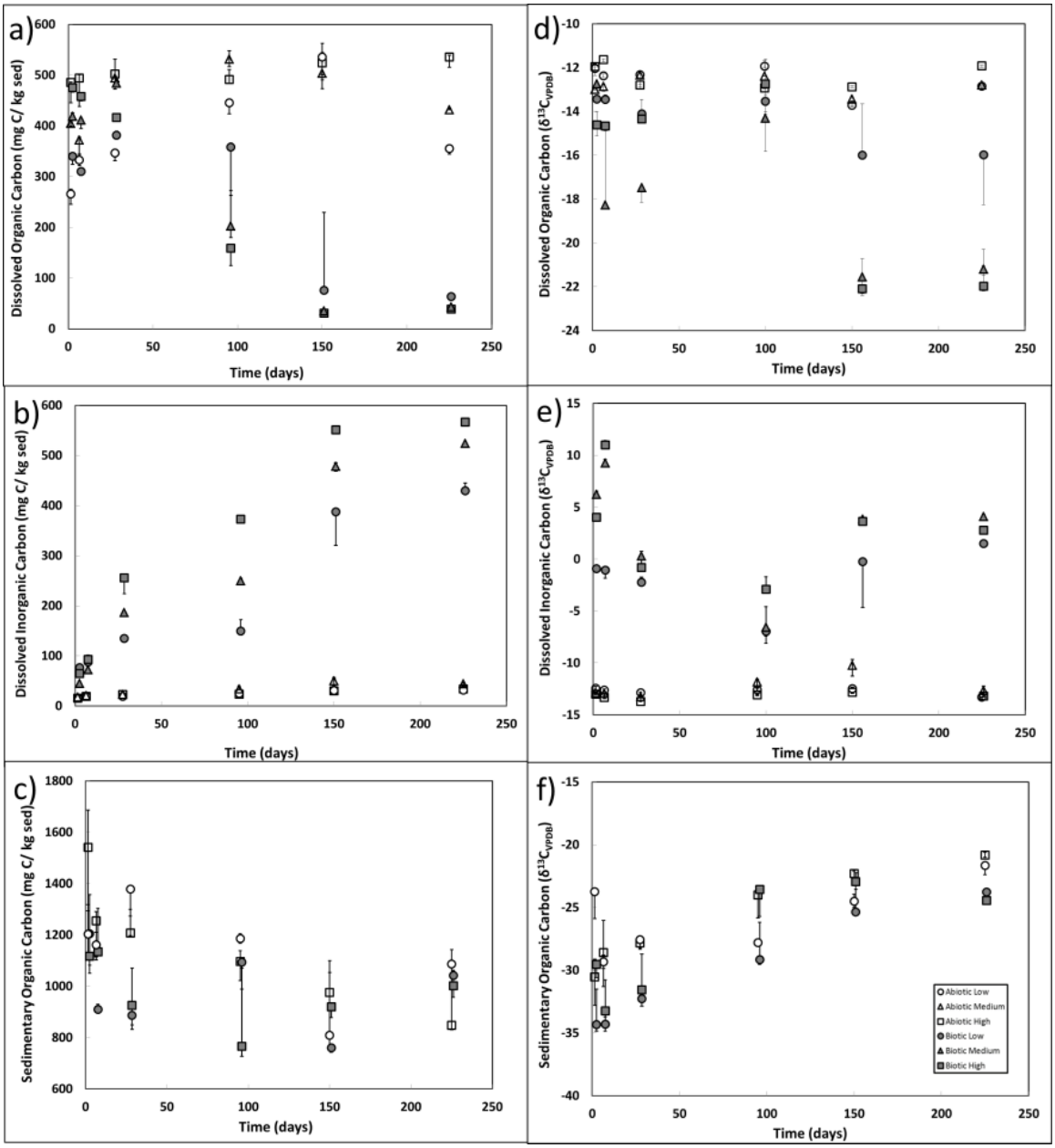

Figure 4.2 - Concentrations and isotopic signatures of carbon over time in the incubation experiments. Gray, filled-in symbols are biotic, while open symbols are abiotic. Square symbols represent those samples initially spiked with 100 ppm C glucose; triangle symbols represent those samples initially spiked with 50 ppm C glucose; circles are those samples that were unamended with glucose. Median values of experimental replicates are plotted, with error bars representing the upper and lower quartile of the experiment replicates. Note that samples spiked with 50 ppm C glucose were not analyzed for sedimentatry organic carbon concentration or isotopes (panels c and f).

Analysis of the isotopes of carbon in the incubation vials indicate an influence of an enriched carbon isotope on the overall composition of the DIC (Figure 4.2e). The DIC isotope data appear to indicate two phases of DIC formation, one between day 0 and day 100, where the isotopes in the biotic samples were depleted. For depletion to occur, the DIC had to evolve from either the glucose or the SOC, not merely dissolution of the SIC, as the SIC isotopes are a heavily enriched value of +14.9949 (see Table 4.1). However, after that timepoint, the DIC grows more enriched, pointing to an influence of an enriched carbon compound, such as SIC. The SOC isotopic composition (Figure 4.2f) also became more enriched over time, but this occurred in both the biotic and abiotic samples. These observations together point to a larger influence of SIC than originally hypothesized or observed via mass observations alone; despite low concentrations, the heavily enriched nature of the SIC implies that a very small amount of SIC could influence the isotopic signature in a large manner. The enriched SOC may have been formed as equilibrium partitioning reactions occurred, favoring the movement of depleted carbon into the aqueous phase. There are multiple reactions that are occurring that can influence the partitioning behavior of the SOC, such as those that change the pH or mineralize DOC from SOC partitioning into DIC, requiring further partitioning to create an equilibrium. The similar pattern between the abiotic and biotic samples suggests that pH-altering reactions, which can also influence SIC mobilization, are the most likely scenario occurring.

It is worth noting however, that the pH data (Figure 4.4c) are in line with the DIC isotope data, with its two phases of behavior. The pH of the biotic samples, especially the spiked samples, increased until day 150, at which point it started decreasing again. This is counter to the relatively consistent decrease in pH over the full time period in the abiotic samples, suggesting that the SOC composition change in the abiotic samples may be solely related to pH, while the

biotic samples behavior is more complex and multi-faceted. DOC isotope data (Figure 4.2d) also align with the two-phase behavior in composition change. In the first phase, DOC isotopes get heavier, and then become lighter in the second phase. Since SOC is lighter than the DOC isotopes in the first phase, the DOC isotopes are likely getting heavier due to conversion of DOC into DIC, with lighter isotopes being preferentially used. During the second phase, the DOC isotopes getting heavier either indicates conversion of SOC into DOC or a decrease in the amount of DOC being converted to DIC via microbial respiration.

To better assess the importance of some of these carbon pools and transformation pathways in our experimental systems, we tracked changes in ^{12}C and ^{13}C composition over time and compared the measurements to calculations based on our simplified model (see Figure 4.3). The simplified model assumes SIC input is negligible, an assumption made due to the small values of measured SIC. Additionally, we have eliminated the direct SOC-to-DIC pathway. Equations 4.4-4.9 demonstrate the approach to calculating DIC ^{12}C and ^{13}C and comparing it to the measured values. Results from each timestep are shown in Table 4.2. Comparing the calculated values for DIC to the directly measured values clearly indicates that the simplified model we presented is inadequate at capturing the full system. This likely indicates that the SIC plays a larger role than we were able to capture.

Figure 4.3: Simplified conceptual model of carbon movement throughout our incubation microcosms. SOC: sedimentary organic carbon; DOC: dissolved organic carbon; DIC: dissolved inorganic carbon.

$$\delta^{13}C_{sample} = \left[\frac{\left(\frac{^{13}C}{^{12}C}\right)_{sample}}{\left(\frac{^{13}C}{^{12}C}\right)_{VPDB}} - 1\right] \times 1000 \tag{4.4}$$

$$\Delta^{12}C_{SOC} \cong \Delta m_{SOC} \tag{4.5}$$

$$\Delta^{13}C_{SOC,TP1-2} = {}^{13}C_{SOC,TP2} - {}^{13}C_{SOC,TP1} \tag{4.6}$$

$${}^{13}C_{SOC,TP1} = \left({}^{12}C_{SOC,TP1}\right)\left(\frac{\delta^{13}C_{SOC,TP1}}{1000} + 1\right)\left(\frac{^{13}C}{^{12}C}\right)_{VPDB} \tag{4.7}$$

$$\Delta^{13}C_{DIC,TP1-2} = -\Delta^{13}C_{SOC,TP1-2} - \Delta^{13}C_{DOC,TP1-2} \tag{4.8}$$

$$\Delta^{12}C_{DIC,TP1-2} = -\Delta^{12}C_{SOC,TP1-2} - \Delta^{12}C_{DOC,TP1-2} \tag{4.9}$$

Table 4.2: Results of isotope calculations for each timestep of Low and High experiments.

		$\Delta^{12}C$			$\Delta^{13}C$			$\Delta^{12}C$	$\Delta^{13}C$	$\Delta^{12}C$	$\Delta^{13}C$
		SOC	DIC	DOC	SOC	DIC	DOC	DIC Calculated (-SOC-DOC)'		Measured DIC - Calculated DIC	
Biotic Low	Δ TP1-TP2	-296.0000	0.1237	-29.7540	9.8631	11.0297	-0.3299	325.7540	-9.5332	-314.7243	9.6569
	Δ TP2-TP3	-22.9100	0.5237	71.5512	-0.2286	46.8150	0.7904	-48.6412	-0.5618	95.4562	1.0855
	Δ TP3-TP4	207.3100	0.1577	-23.5586	2.2929	14.7743	-0.2587	-183.7514	-2.0343	198.5258	2.1920
	Δ TP4-TP5	-333.4300	2.6854	-282.0986	-3.6053	238.0325	-3.1291	615.5286	6.7345	-377.4961	-4.0490
	Δ TP5-TP6	282.7300	0.4831	-12.8427	3.1151	42.2544	-0.1420	-269.8873	-2.9731	312.1417	3.4561
Biotic High	Δ TP1-TP2	17.2000	0.3225	-17.2723	12.3224	27.9422	-0.1915	0.0723	-12.1309	27.8699	12.4535
	Δ TP2-TP3	-209.4300	1.8140	-52.4852	-2.2576	162.6657	-0.5797	261.9152	2.8373	-99.2494	-1.0233
	Δ TP3-TP4	-159.3300	1.3101	-246.6854	-1.6651	117.4663	-2.7294	406.0154	4.3944	-288.5491	-3.0843
	Δ TP4-TP5	154.0700	2.0363	-128.1617	1.6967	178.1214	-1.4251	-25.9083	-0.2717	204.0297	2.3079
	Δ TP5-TP6	81.5900	0.1715	7.7092	0.8791	15.6999	0.0848	-89.2992	-0.9639	104.9991	1.1354
Abiotic Low	Δ TP1-TP2	-41.7000	0.0396	67.1505	-0.5305	3.5680	0.7442	-25.4505	-0.2138	29.0185	0.2533
	Δ TP2-TP3	216.7000	-0.0013	14.0753	2.3911	-0.1164	0.1564	-230.7753	-2.5475	230.6589	2.5462
	Δ TP3-TP4	-192.8500	0.0694	98.7006	-2.1107	6.2480	1.0974	94.1494	1.0133	-87.9015	-0.9439
	Δ TP4-TP5	-376.7000	0.0633	90.3671	-4.0853	5.7004	0.9925	286.3329	3.0928	-280.6325	-3.0295
	Δ TP5-TP6	277.3500	0.0063	-180.4845	3.0751	0.5901	-1.9967	-96.8655	-1.0783	97.4556	1.0846
Abiotic High	Δ TP1-TP2	-287.3000	0.0412	8.7333	13.6916	3.7249	0.0987	278.5667	-13.7903	-274.8419	13.8315
	Δ TP2-TP3	-47.4000	0.0383	8.1524	-0.5069	3.4635	0.0840	39.2476	0.4229	-35.7841	-0.3846
	Δ TP3-TP4	-111.0000	0.0136	-11.0908	-1.1657	1.2109	-0.1237	122.0908	1.2894	-120.8798	-1.2758
	Δ TP4-TP5	-119.8200	0.0715	33.0485	-1.2953	6.4360	0.3668	86.7715	0.9284	-80.3355	-0.8570
	Δ TP5-TP6	-128.8400	0.0450	11.4720	-1.4015	4.0732	0.1330	117.3680	1.2684	-113.2948	-1.2234

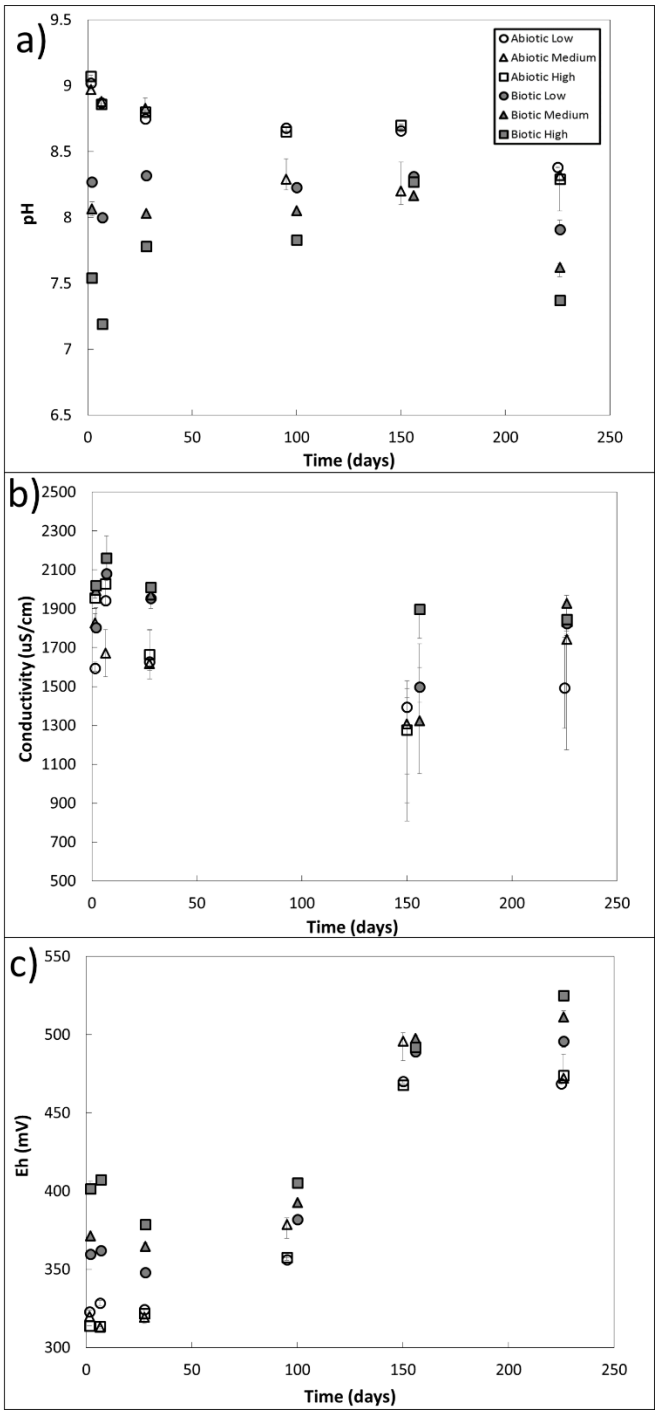

Figure 4.4 – Electrochemical readings of incubation experiments over time. Gray, filled-in symbols are biotic, while open symbols are abiotic. Square symbols represent those samples initially spiked with 100 ppm C glucose; triangle symbols represent those samples initially spiked with 50 ppm C glucose; circles are those samples that were unamended with glucose. Median values of experimental replicates are plotted, with error bars representing the upper and lower quartile of the experiment replicates.

In addition to carbon, concentrations of arsenic, iron, and manganese were monitored over time in these experiments. Despite the degradation of large amounts of organic carbon in the incubation bottles, we did not see any evidence of microbially-driven arsenic release into the waters. Arsenic concentrations, shown in Figure 4.5c, increased slightly between the first timepoint and day 100, then remained fairly constant or slightly decreased. Both the abiotic and biotic samples exhibited these trends, suggesting that any reactions occurring with regards to arsenic are not microbially-driven and thus not fueled by the addition of glucose to some of the vials.

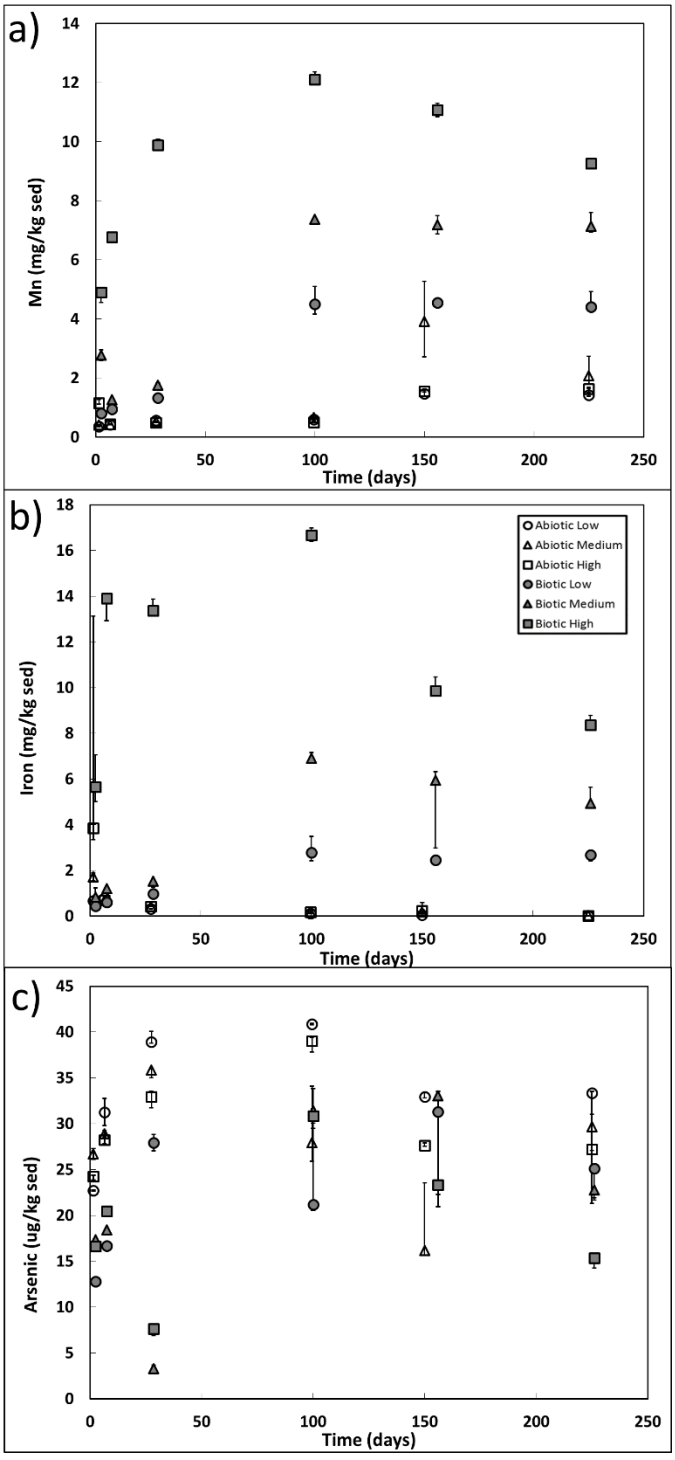

Figure 4.5 – Concentrations of manganese, iron, and arsenic in the incubation experiments over time. Gray, filled-in symbols are biotic, while open symbols are abiotic. Square symbols represent those samples initially spiked with 100 ppm C glucose; triangle symbols represent those samples initially spiked with 50 ppm C glucose; circles are those samples that were unamended with glucose. Median values of experimental replicates are plotted, with error bars representing the upper and lower quartile of the experiment replicates.

Conductivity measurements (Figure 4.4b) offer no insight into the lack of mobilization of arsenic off the aquifer sediment. Over time in the experiments, there is a decrease in conductivity, but it occurs in both the abiotic and biotic samples and shows no patterns along the low, medium, and high glucose samples.

The arsenic concentration results in our experiments show little impact of microbial influence on mobilization. In contrast, both the manganese (Figure 4.5a) and iron (Figure 4.5b) results indicate an impact of glucose amendment on the release of those metals, with clear distinctions between the abiotic samples and the biotic samples. Mobilized manganese concentrations quickly increase and reach their maximum in the samples that were amended with 100 ppm C glucose, while the samples amended with less glucose (50 ppm C glucose) or no glucose increased in [Mn] at day 100, plateauing. The high glucose samples had the highest final [Mn] of approximately 10 mg/kg sediment, with the medium glucose samples having the next highest, ~7 mg/kg sediment, and the unamended samples achieving a final concentration of ~4 mg/kg sediment.

Iron concentrations in the incubation vials behaved in a similar fashion to the manganese concentrations. Concentrations in the biotic, high glucose samples increased almost immediately and reached a maximum of ~16 mg / kg sediment, decreasing again to reach a final concentration of ~8 mg / kg sediment. The medium glucose and no glucose biotic samples remained low until day 100, where the medium glucose samples achieved an [Fe] of approximately 6 mg/kg sediment, and the unamended samples had [Fe] of ~2 mg/kg. Both the medium glucose and unamended samples remained constant from day 100 through the end of the experiment. These manganese and iron data considered together support the hypothesis that a pulse of highly

bioavailable organic carbon into an environmental system can impact the reactions that occur, by speeding up the process.

Arsenic mobilization may not have been impacted in the same manner, simply because there were more energetically-favorable electron acceptors available (Mn and Fe). Until the oxidation-reduction potential (Eh) of the system were decreased, the arsenic would not itself be reduced. Additionally, these data indicate that despite the reduction and release of iron into the aqueous phase, arsenic was not also released. Thus, either arsenic is not stabilized in this sediment via iron, or the phases that were reduced were not those associated with arsenic. Previous laboratory incubations of this same sediment (Gillispie et al., 2016) demonstrated that until manganese oxides were reduced, iron oxides wouldn't be reduced. Further, until these were fully reduced, arsenic mobilization wouldn't occur. In those experiments, the amount of carbon initially added was much higher than in our experiments (~7200 mg C/ kg sediment vs. 270 mg C/ kg sediment in our "high"), which may likely explain the difference in mobilization behavior from our experiments. Based on the solid phase concentrations measured on sediment collected from the same field site (Gillespie et al., 2016), the amount of carbon supplied by glucose alone should have sufficiently fueled manganese reduction (~20 mmol carbon/kg sediment to reduce ~10 mmol Mn/kg sediment). However, to fuel reductive dissolution of all the iron, ~1200 mmol C/ kg sediment would be needed, conservatively assuming the sediment iron concentration is ~300 mmol/kg.

In addition to iron and manganese dissolution, we saw evidence of mineral precipitation later in the experiment. After day 100, dissolved concentrations begin to decrease. This behavior has been observed before in batch experiments of anoxic aquifer sediment and water (Radloff et al., 2007). In that study, the authors hypothesized that saturation limits had been reached in the

water, and iron-sulfides and P-sulfides had started to form. Other studies have yielded similar results (Tufano & Fendorf, 2008), with arsenic and iron being released into the mobile phase following experiment initiation, then precipitation onto existing minerals or formation of new minerals resulting in decreasing dissolved concentrations. While we saw this behavior at around 100 days, these previous studies observed decreasing dissolved concentrations at day ~250 and ~30, respectively.

4.4 Discussion

Overall, the results of our experiment failed to show strong, conclusive evidence in support of microbial priming effects. The experiment showed that an influx of highly bioavailable organic carbon may speed up the rate of organic carbon degradation, however given enough time, an environmental system seems likely to stabilize, with no additional carbon being utilized that wouldn't otherwise be (i.e., no destabilization of sedimentary organic carbon fueled by the original priming pulse. While the final concentrations of DOC did show a difference between the glucose-amended and unamended samples, this difference (24.7 *(16.5-25.2)* mg C · kg^{-1} sediment) was not large and was not replicated in the SOC data.

Beyond priming a system to destabilize older SOC, priming can also alter the microbial community, as the glucose appeals to different microbes than those that may have a preference for different forms of carbon. A previous short-term (one-week) incubation study (Derrien et al., 2014) that assessed the impact of adding glucose to a soil on SOC mineralization, found that in that short time period, four stages of carbon mineralization occurred, with different microbial communities working in sequence to first mineralize the labile input, then the older, recalcitrant SOC. The two phase behavior that we observed in our experiment may reflect this same type of

priming effect, as the high-glucose-amended samples exhibited this the most drastically, in pH, DOC & DIC isotopes, and metal concentrations. Specifically, the two-phase behavior of the DOC isotopes strongly supports this type of priming effect, as SOC mineralization becomes a larger influence in the second phase.

It is possible that our experimental design inherently failed to induce a distinct priming effect by only introducing one labile sugar into the system. An incubation study conducted on forest soils in Germany found that priming effects were significantly amplified when two sugars were added to a microcosm, vs. only one (Hamer & Marschner, 2005). The addition of multiple sugars bolsters the growth of multiple microbial communities, increasing the ability of these communities to mineralize SOC.

These results also failed to show that a fresh input of organic matter will fuel extensive arsenic mobilization in aquifer sediments. Reductive dissolution of manganese and iron oxides did occur, and was clearly impacted by the glucose additions, as the highly-amended mobilized more than the unamended. However, these data taken in conjunction with the organic carbon data do not conclusively show that the differences in mobilization are due to anything other than the availability of more organic carbon available from the glucose to fuel the reactions, rather than the glucose destabilizing SOC which then also fuels these reductive reactions. Furthermore, the increase in aqueous iron and manganese did not correlate with an increase in mobilized arsenic, which also suggests that if arsenic is associated with iron or manganese minerals, it is perhaps associated with forms that were not targeted by the microbial reactions induced in these experiments. Most likely, the initial sediment chemistry prevented arsenic mobilization, by containing concentrations of Mn oxides that were too high. Previous incubations of the Cambodian aquifer sediment (Gillispie et al., 2016) showed a strong correlation between

reduction of manganese oxides and arsenic. However, both the manganese and iron oxides had to be significantly reduced before arsenic mobilization began, as the energetically-preferential reduction of these minerals may have inhibited arsenic mobilization. The two-phase behavior we observed most likely indicates precipitation of iron that was reductively dissolved into new minerals, or onto existing minerals as saturation limits were met. Given time, our incubations may have released arsenic, as concentrations of manganese and iron oxides were depleted.

4.5 References

Ahad, J. M. E., & Pakdel, H. (2013). Direct Evaluation of in Situ Biodegradation in Athabasca Oil Sands Tailings Ponds Using Natural Abundance Radiocarbon. *Environmental Science & Technology*, *47*(18), 10214–10222. https://doi.org/10.1021/es402302z

Atekwana, E. A., & Krishnamurthy, R. V. (1998). Seasonal variations of dissolved inorganic carbon and δ13C of surface waters: application of a modified gas evolution technique. *Journal of Hydrology*, *205*(3–4), 265–278. https://doi.org/10.1016/S0022-1694(98)00080-8

Derrien, D., Plain, C., Courty, P.-E., Gelhaye, L., Moerdijk-Poortvliet, T. C. W., Thomas, F., … Epron, D. (2014). Does the addition of labile substrate destabilise old soil organic matter? *Soil Biology and Biochemistry*, *76*, 149–160. https://doi.org/10.1016/j.soilbio.2014.04.030

Eusterhues, K., Rumpel, C., Kleber, M., & Kögel-Knabner, I. (2003). Stabilisation of soil organic matter by interactions with minerals as revealed by mineral dissolution and oxidative degradation. *Organic Geochemistry*, *34*(12), 1591–1600. https://doi.org/10.1016/j.orggeochem.2003.08.007

Fontaine, S., Mariotti, A., & Abbadie, L. (2003). The priming effect of organic matter: a question of microbial competition? *Soil Biology and Biochemistry*, *35*(6), 837–843. https://doi.org/10.1016/S0038-0717(03)00123-8

Gillispie, E. C., Andujar, E., & Polizzotto, M. L. (2016). Chemical controls on abiotic and biotic release of geogenic arsenic from Pleistocene aquifer sediments to groundwater. *Environmental Science: Processes & Impacts*. https://doi.org/10.1039/C6EM00359A

Gontikaki, E., Thornton, B., Huvenne, V. A. I., & Witte, U. (2013). Negative Priming Effect on Organic Matter Mineralisation in NE Atlantic Slope Sediments. *PLOS ONE*, *8*(6), e67722. https://doi.org/10.1371/journal.pone.0067722

Hamer, U., & Marschner, B. (2005). Priming effects in soils after combined and repeated substrate additions. *Geoderma*, *128*(1–2), 38–51. https://doi.org/10.1016/j.geoderma.2004.12.014

Hannides, A. K., & Aller, R. C. (2016). Priming effect of benthic gastropod mucus on sedimentary organic matter remineralization. *Limnology and Oceanography*, *61*(5), 1640–1650. https://doi.org/10.1002/lno.10325

Harris, D., Horwáth, W. R., & van Kessel, C. (2001). Acid fumigation of soils to remove carbonates prior to total organic carbon or CARBON-13 isotopic analysis. *Soil Science Society of America Journal*, *65*(6), 1853. https://doi.org/10.2136/sssaj2001.1853

Kuzyakov, Y. (2010). Priming effects: Interactions between living and dead organic matter. *Soil Biology and Biochemistry*, *42*(9), 1363–1371. https://doi.org/10.1016/j.soilbio.2010.04.003

Kuzyakov, Y., Friedel, J. K., & Stahr, K. (2000). Review of mechanisms and quantification of priming effects. *Soil Biology and Biochemistry*, *32*(11–12), 1485–1498. https://doi.org/10.1016/S0038-0717(00)00084-5

Li, Z.-P., Tao, M.-X., Li, L.-W., Wang, Z.-D., Du, L., & Zhang, M.-F. (2007). Determination of Isotope Composition of Dissolved Inorganic Carbon by Gas Chromatography-Conventional Isotope-ratio Mass Spectrometry. *Chinese Journal of Analytical Chemistry*, *35*(10), 1455–1458. https://doi.org/10.1016/S1872-2040(07)60089-9

Mikutta, R., Kleber, M., Torn, M. S., & Jahn, R. (2006). Stabilization of Soil Organic Matter: Association with Minerals or Chemical Recalcitrance? *Biogeochemistry*, *77*(1), 25–56. https://doi.org/10.1007/s10533-005-0712-6

Neumann, R. B., Pracht, L. E., Polizzotto, M. L., Badruzzaman, A. B. M., & Ali, M. A. (2014). Biodegradable Organic Carbon in Sediments of an Arsenic-Contaminated Aquifer in Bangladesh. *Environmental Science & Technology Letters*, *1*(4), 221–225. https://doi.org/10.1021/ez5000644

Radloff, K. A., Cheng, Z., Rahman, M. W., Ahmed, K. M., Mailloux, B. J., Juhl, A. R., … Van Geen, A. (2007). Mobilization of arsenic during one-year incubations of grey aquifer sands from Araihazar, Bangladesh. *Environmental Science & Technology*, *41*(10), 3639–3645.

St-Jean, G. (2003). Automated quantitative and isotopic (13C) analysis of dissolved inorganic carbon and dissolved organic carbon in continuous-flow using a total organic carbon analyser. *Rapid Communications in Mass Spectrometry: RCM*, *17*(5), 419–428. https://doi.org/10.1002/rcm.926

Tufano, K. J., & Fendorf, S. (2008). Confounding Impacts of Iron Reduction on Arsenic Retention. *Environmental Science & Technology*, *42*(13), 4777–4783. https://doi.org/10.1021/es702625e

UNICEF. (2009). *Arsenic in Cambodia*. UNICEF. Retrieved from http://www.unicef.org/cambodia/As_Mitigation_in_Cambodia_2009.pdf

van Geen, A., Bostick, B. C., Thi Kim Trang, P., Lan, V. M., Mai, N.-N., Manh, P. D., … Berg, M. (2013). Retardation of arsenic transport through a Pleistocene aquifer. *Nature*, *501*(7466), 204–207. https://doi.org/10.1038/nature12444

van Nugteren, P., Moodley, L., Brummer, G.-J., Heip, C. H. R., Herman, P. M. J., & Middelburg, J. J. (2009). Seafloor ecosystem functioning:: the importance of organic matter priming. *Marine Biology*, *156*(11), 2277–2287.

5. Conclusions

The far-reaching and extremely toxic nature of arsenic contamination demands that we continue to strive to better understand how arsenic is released into the environment and methods that can reduce human and environmental exposure. This study analyzed the sequestration mechanism of an *in situ* treatment system and examined mobilization mechanisms and factors that could influence mobilization of arsenic in contaminated aquifers.

The analysis of two implemented *in situ* treatment systems that utilize induced sulfate reduction (ISR) as a means to form sulfide and iron minerals in the subsurface yielded information that can be used to inform future engineering application decisions. Our work found that PRBs that use ZVI in conjunction with sulfate and carbon materials are more effective in arsenic removal, likely due to the formation of more stable minerals, such as iron-sulfides and iron oxyhydroxides. In addition to sorbing to the surface of these minerals, arsenic was potentially incorporated into the mineral matrix, which also lends stability to the treatment. In contrast, the data suggest that arsenic stabilization in the non-ZVI system was primarily controlled by arsenic-sulfide associations.

In pursuit of elucidating the reactions or cause of arsenic mobilization off aquifer sediment into groundwater supplies, the laboratory experiment conducted with aquifer materials from Bangladesh closely analyzed the organic carbon available to subsurface from aquifer recharge waters and aquifer sediment. Ultra-high resolution mass spectrometry (FT-ICR-MS) revealed a large, heterogeneous pool of organic compounds in the sediment porewater. Like other subsurface studies using FT-ICR-MS, many of the compounds in the sediment porewater we analyzed contained organosulfur compounds. Compared to the sediment porewater, the recharge waters that we studied had stark differences in lability, specifically when comparing percent of total compounds with H-to-C ratios greater than 1.5, a common lability index.

However, the sedimentary organic carbon had such greater amounts of total organic carbon, that it still had more total compounds that we could classify as “labile” than the recharge waters. Again, the recharge water organic carbon also contained many organosulfur compounds. This commonality of organosulfur in our study and in others, leads us to suggest that S-containing compounds might be a fingerprint carbon evolving from organic-rich, anaerobic subsurface environments.

Over time, as microbial activity consumed carbon, the remaining compounds became enriched in sulfur and phosphorus. Additionally, the lability indices were ineffective in effectively explaining the microbial degradation. These results suggest that our current understanding of microbial organic carbon mineralization is incomplete and needs to be further examined.

The discovery of such a sizable, diverse pool of organic carbon in sediment porewater of an arsenic-contaminated aquifer in Bangladesh led to the analysis of an arsenic-contaminated aquifer in Cambodia, with sediment more vulnerable to arsenic mobilization via reduction dissolution of iron (oxy)hydroxides fueled by organic carbon. We hypothesized that microbial priming could make this large organic pool available to microbes and fuel subsurface reactions, including reductive dissolution. Our laboratory incubation experiments of Cambodian aquifer sediment failed to show strong, conclusive evidence in support of microbial priming effects, but did show that an influx of highly bioavailable organic carbon may speed up the rate of organic carbon degradation.

Despite bioavailable carbon being available to microbes and degraded over time, arsenic mobilization was limited, most likely due to large concentrations of manganese and iron oxides that needed to first be reduced before dissolved arsenic would increase. We did observe a

bimodal behavior in the metals, that could reflect alterations to the microbial community, where multiple communities were developed that worked in sequence. More likely is that this behavior reflects mineral precipitation begin to occur as iron is reduced and begins to saturate the solution. The results of this study do not raise immediate concern for future contamination of currently clean aquifers, as a carbon influx neither released substantial amounts of sediment carbon nor mobilized arsenic. However, further work that is not limited by the enclosed, static nature of incubation experiments should be conducted; if water is not allowed to remain still long enough to become iron-saturated, further reduction may occur and allow for arsenic mobilization.

Appendix A: Supporting Information for Chapter 3

Appendix.1: Calculation of organic carbon in sediment

Sediment Porewater Organic Carbon (DOC) = 0.33 ± 0.06 mg OC g-1 sediment

Sediment Organic Matter (LOI) = 6.5 ± 1.5 mg/g

Using van Bemmelan factor(United States Department of Agriculture, Natural Resources Conservation Service, 2011) (58% OM = OC) to estimate sediment OC:

6.5 mg/g * 0.58 = 3.77 mg OC/g sed

DOC in sediment porewater as percent of sediment OC:

0.33/3.77 * 100 = 8.75 %

Error for the above calculation:

Err,gy= 0.06/3.77=0.0159

Err,gt=0.33/(3.77^2)*(0.58*1.5)=0.0202

Err = sqrt[(0.06/3.77)^2+(0.33/(3.77^2)*(0.58*1.5))^2]

= 0.0257 mg OC/g sed

0.0257/3.77*100=0.68 %

DOC in sediment porewater represented 8.8 ± 0.7 % of OC in sediment.

Appendix.2: FT-ICR-MS Analysis Methodology

Frozen incubation samples mailed to EMSL for FT-ICR-MS analysis were diluted 1:2 (v/v) with LC-MS grade methanol less than 30 minutes before analysis to minimize esterification. Ion accumulation time was optimized for all samples. A standard Bruker ESI source was used to generate negatively charged molecular ions. Samples were introduced to the ESI source equipped with a fused silica tube (200 μm i.d) through a syringe pump at a flow rate of 3.0 μL/min. Experimental conditions were as follows: needle volt-age, +4.4 kV; Q1 set to 150 m/z; and the heated resistively coated glass capillary operated at 180 °C. One hundred forty four individual scans were averaged for each sample and internally calibrated using OM homologous series separated by 14 Da (–CH2 groups). The mass measurement accuracy was typically within 1 ppm for singly charged ions across a broad m/z range (i.e. 200, <m/z <1200). DataAnalysis software (BrukerDaltonik version 4.2) was used to convert raw spectra to a list of m/z values applying FTMS peak picker with S/N threshold set to 7 and absolute intensity threshold to the default value of 100. Chemical formulae were assigned using an in-house built software following the Compound Identification Algorithm (CIA), described by Kujawinski and Behn(Kujawinski & Behn, 2006) and modified by Minor et al.(Minor, Steinbring, Longnecker, & Kujawinski, 2012) Chemical formulae were assigned based on the following criteria: S/N >7, and mass measurement error <1 ppm, taking into consideration the presence of C, H, O, N, S and P and excluding other elements.

Figure Appendix.1. Aromaticity Index of Native Incubation Materials

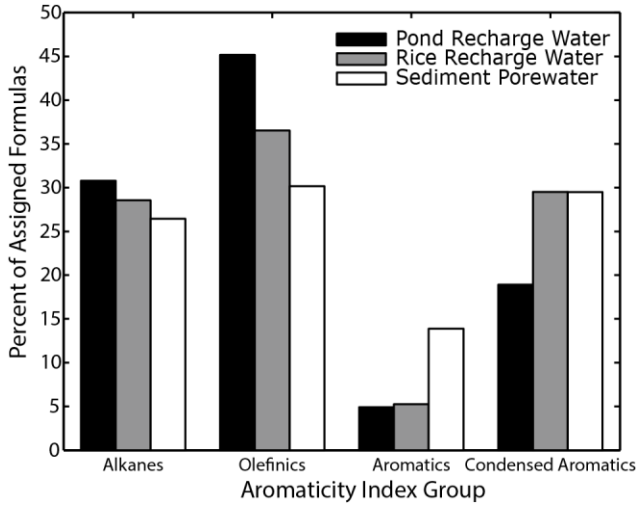

Figure Appendix.1. Classification via aromaticity index (AI) of organic matter present in native incubation materials: pond recharge water, rice field recharge water and sediment porewater.

Figure Appendix.2. Relative Mass Distributions for Native Incubation Materials

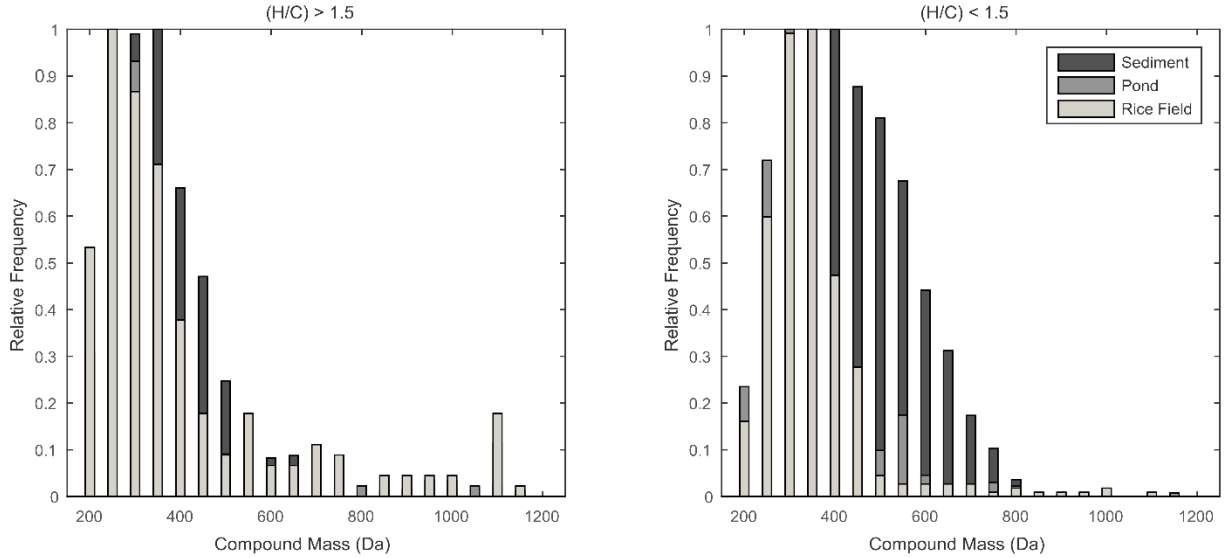

Figure Appendix.2. Relative frequency of compounds in the native incubation materials with a given compound mass. Each bar represents the relative frequency of compounds present in the sample within a 50 Da range.

Figure Appendix.3. van Krevelen Diagrams for Biotic Rice Field Incubation at Days 1.5 and 85

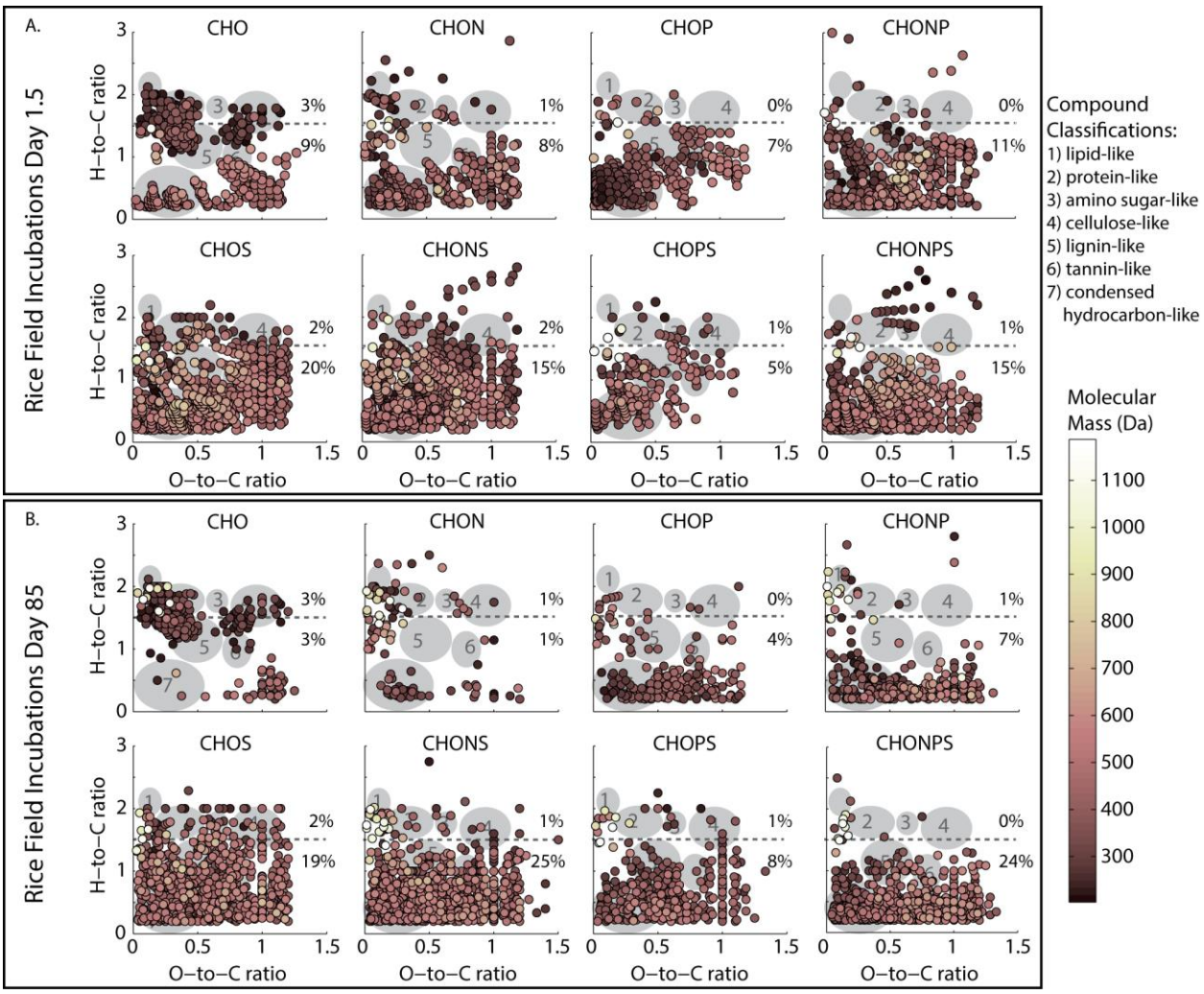

Figure Appendix.3. van Krevelen diagrams for each heteroatom group in the biotic rice field incubation. (A) Day 1.5 of incubation. (B) Day 85 of incubation. Data point color reflects the molecular mass of the organic compound according to the color bar. Grey shaded areas mark the H-to-C and O-to-C ratios of model chemical classes, as indicated in the legend. The percent of compounds present in each heteroatom group with H-to-C ratios above and below 1.5 is noted on each diagram above and below the dashed line, respectively.

Figure Appendix.4. van Krevelen Diagrams for Biotic Pond Incubation at Days 1.5 and 85

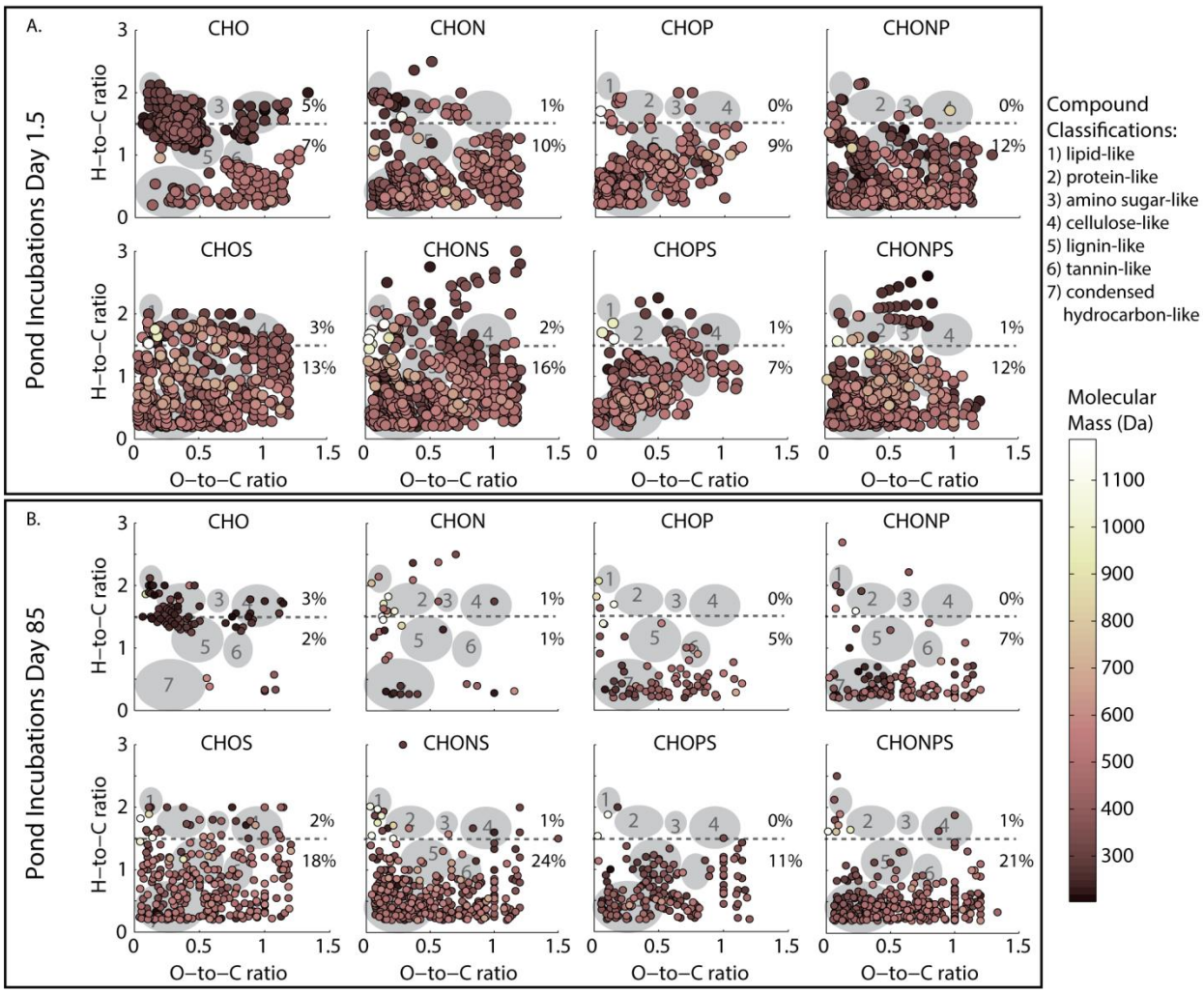

Figure Appendix.4. van Krevelen diagrams for each heteroatom group in the biotic pond incubation. (A) Day 1.5 of incubation. (B) Day 85 of incubation. Data point color reflects the molecular mass of the organic compound according to the color bar. Shaded grey areas mark the H-to-C and O-to-C ratios of model compounds, as indicated in the legend. The percent of compounds present in each heteroatom group with H-to-C ratios above and below 1.5 is noted on each diagram above and below the dashed line, respectively.

Figure Appendix.5: Elemental Ratios for Abiotic Rice Field Incubation

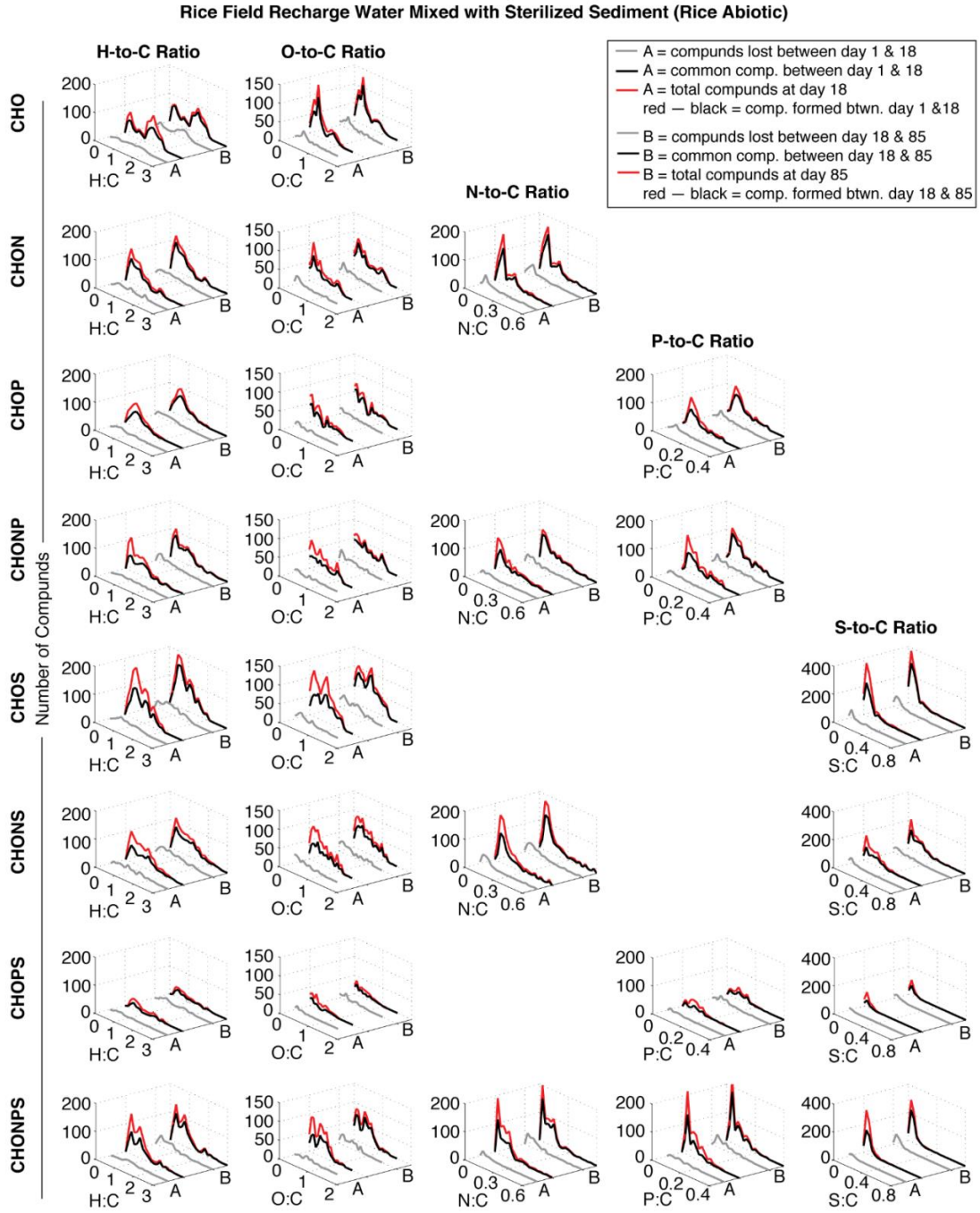

Figure Appendix.5. Evolution of H-to-C, O-to-C, N-to-C, P-to-C, and S-to-C ratios over time in the abiotic rice field incubations for each heteroatom group. Grey lines reflect the number of compounds lost between day 1.5 and 18 (labeled A) and between day 18 and 85 (labeled B), black lines reflect the number of compounds common between the noted timepoints, and red lines reflect the total number of compounds at the latest of the noted timepoints (i.e., day 18 for line A and day 85 for line B).

Figure Appendix.6: Elemental Ratios for Biotic Pond Incubation

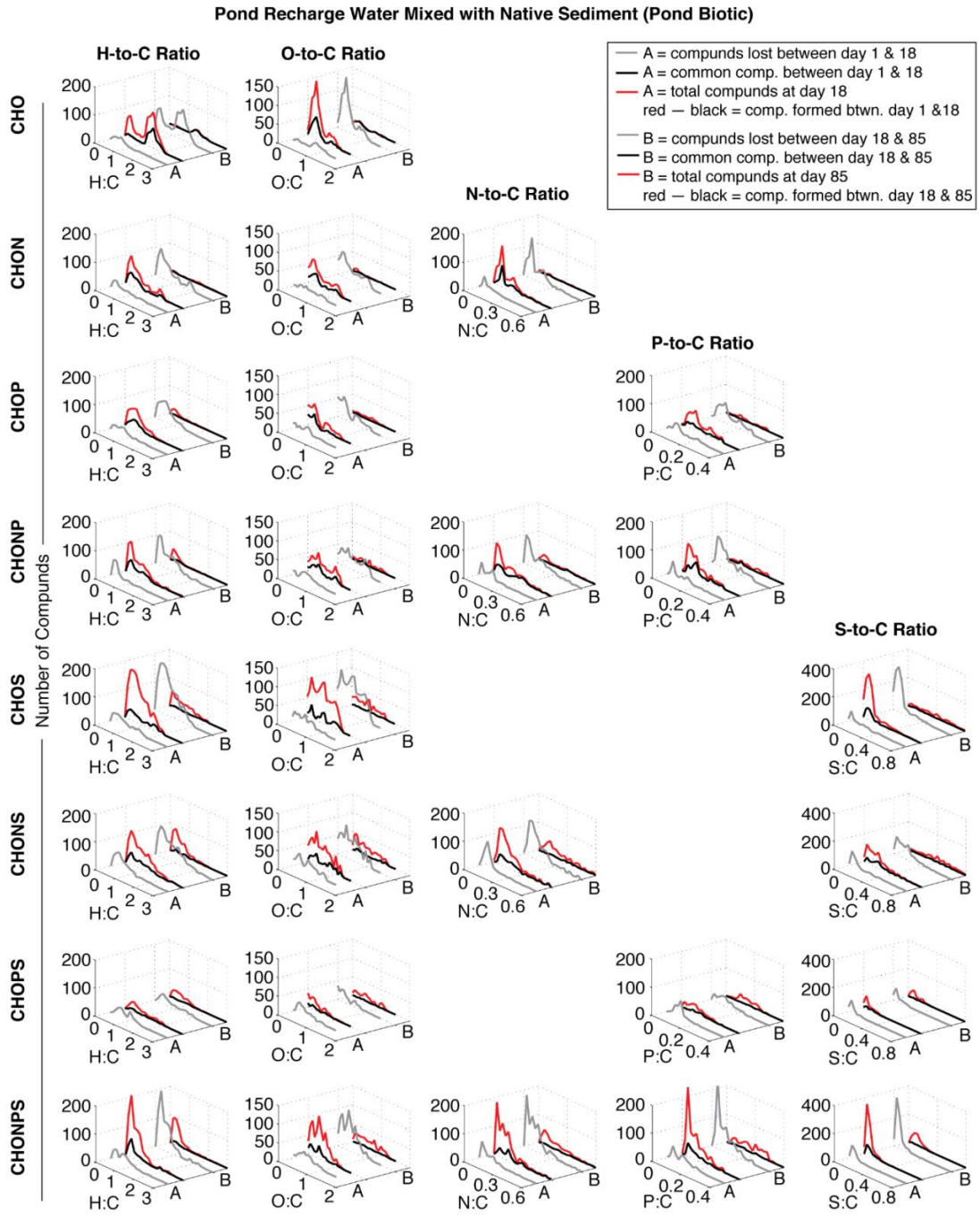

Figure Appendix.6. Evolution of H-to-C, O-to-C, N-to-C, P-to-C and S-to-C ratios over time in the biotic pond incubations for each heteroatom group. Grey lines reflect the number of compounds lost between day 1.5 and 18 (labeled A) and between day 18 and 85 (labeled B), black lines reflect the number of compounds common between the noted timepoints, and red lines reflect the total number of compounds present at the latest of the noted timepoints (i.e., day 18 for line A and day 85 for line B).

Figure Appendix.7: Elemental Ratios for Abiotic Pond Incubation

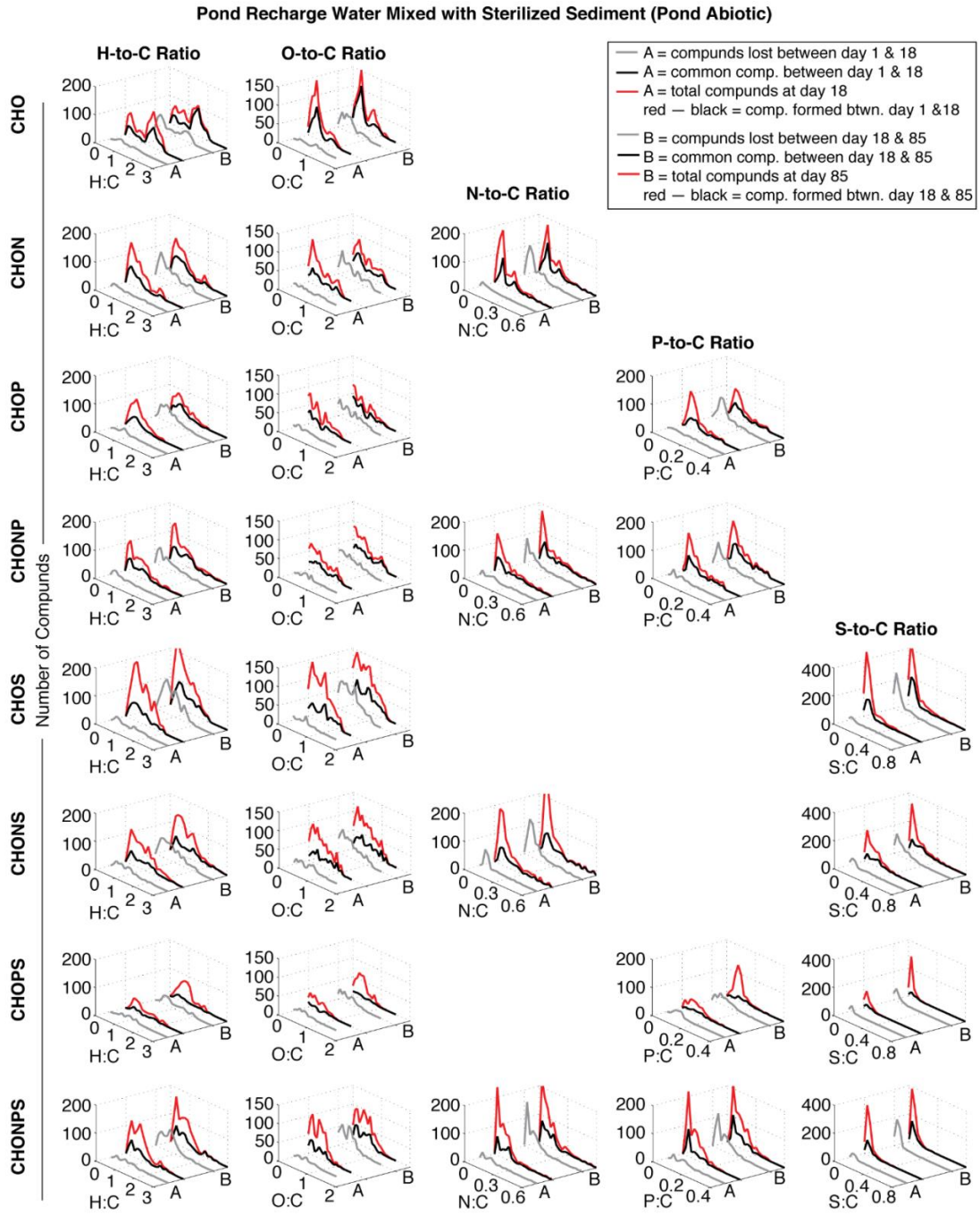

Figure Appendix.7 Evolution of H-to-C, O-to-C, N-to-C, P-to-C and S-to-C ratios over time in the abiotic pond incubations for each heteroatom group. Grey lines reflect the number of compounds lost between day 1.5 and 18 (labeled A) and between day 18 and 85 (labeled B), black lines reflect the number of compounds common between the noted timepoints, and red lines reflect the total number of compounds present at the latest of the noted timepoints (i.e., day 18 for line A and day 85 for line B).

Figure Appendix.8: Mass Distributions for Abiotic Incubations at Day 1.5 and Day 18

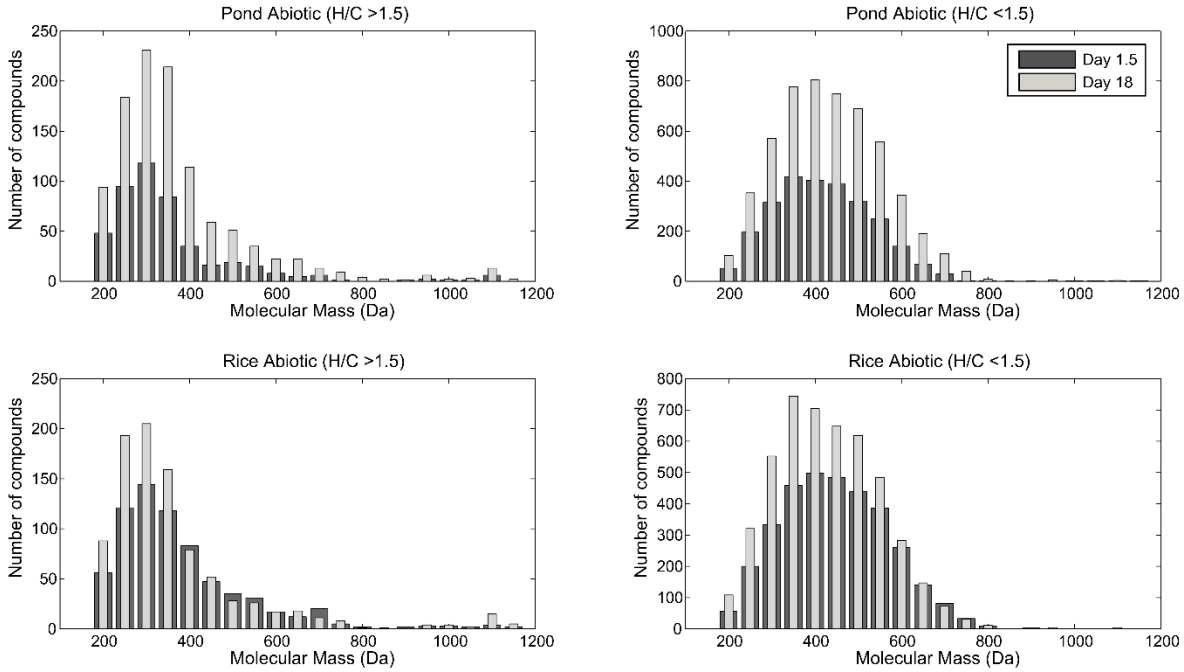

Figure Appendix.8. Number of compounds in each of the abiotic incubations with a given compound mass at day 1.5 (dark grey bars) and day 18 (light grey bars). Each bar represents the number of compounds present for the sample within a 50 Da range.

Figure Appendix.9: Mass Distributions for Biotic Incubations at Day 1.5 and Day 18

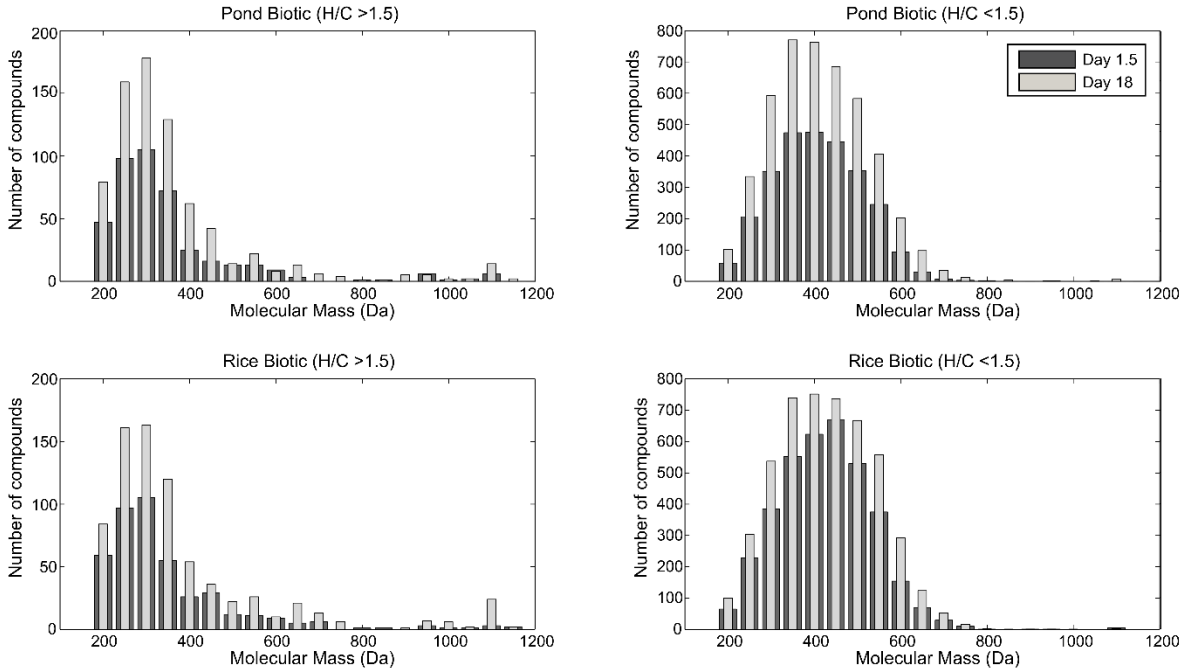

Figure Appendix.9. Number of compounds in each of the biotic incubations with a given compound mass at day 1.5 (dark grey bars) and day 18 (light grey bars). Each bar represents the number of compounds present for the sample within a 50 Da range.

Figure Appendix.10: Mass Distributions for Abiotic Incubations at Day 18 and Day 85

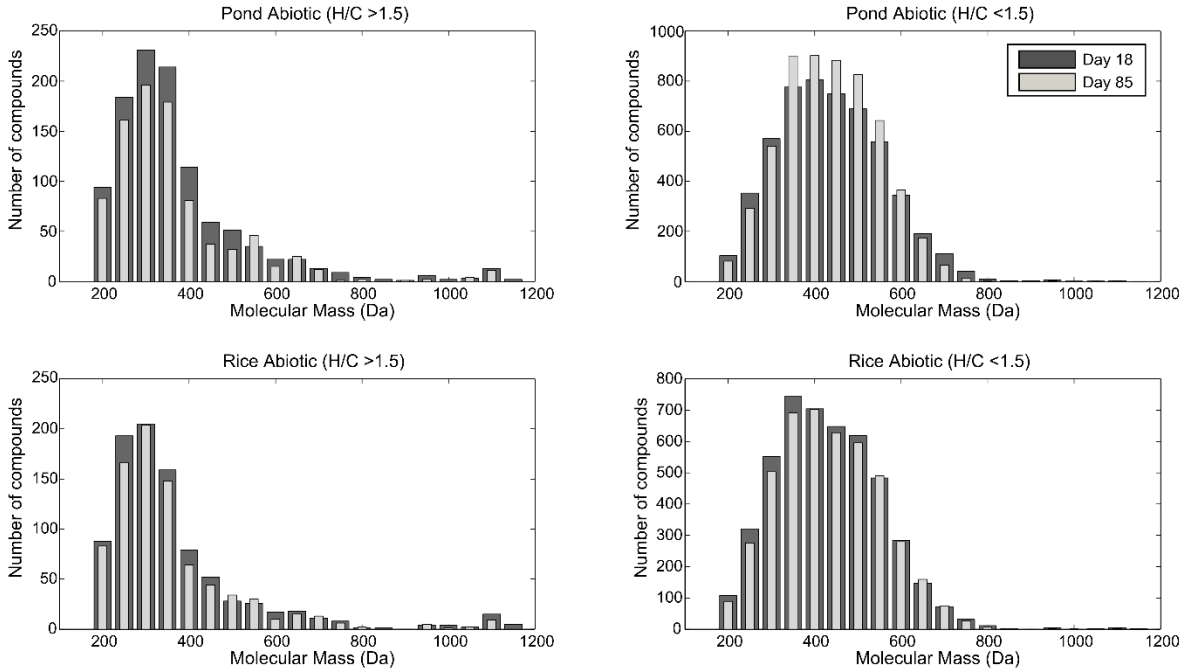

Figure Appendix.10: Number of compounds in each of the abiotic incubations with a given compound mass at day 18 (dark grey bars) and day 85 (light grey bars). Each bar represents the number of compounds present for the sample within a 50 Da range.

Figure Appendix.11: Mass Distributions for Biotic Incubations at Day 18 and Day 85

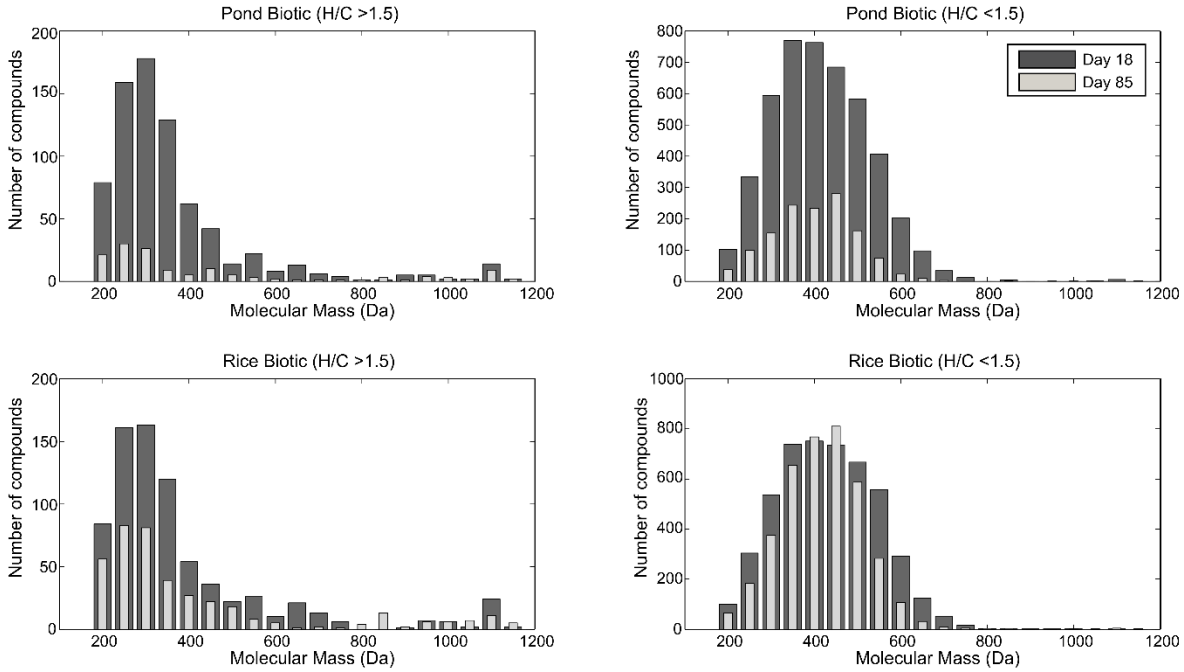

Figure Appendix.11: Number of compounds in each of the biotic incubations with a given compound mass at day 18 (dark grey bars) and day 85 (light grey bars). Each bar represents the number of compounds present for the sample within a 50 Da range.

Appendix.3: References

Kujawinski, E. B., & Behn, M. D. (2006). Automated analysis of electrospray ionization fourier transform ion cyclotron resonance mass spectra of natural organic matter. *Analytical Chemistry*, *78*(13), 4363–4373. https://doi.org/10.1021/ac0600306

Minor, E. C., Steinbring, C. J., Longnecker, K., & Kujawinski, E. B. (2012). Characterization of dissolved organic matter in Lake Superior and its watershed using ultrahigh resolution mass spectrometry. *Organic Geochemistry*, *43*, 1–11. https://doi.org/10.1016/j.orggeochem.2011.11.007

United States Department of Agriculture, Natural Resources Conservation Service. (2011). *Soil Survey Laboratory Information Manual* (Soil Survey Investigations No. 45, Version 2.0). National Soil Survey Center, Lincoln, Nebraska.

VITA

Lara Elizabeth Pracht

Born on June 23rd, 1987 in Garden City, KS (USA)

Citizen of the United States of America

2006-2010 Studies in Civil Engineering, University of Kansas

2010-2016 PhD studies in Environmental Engineering, University of Washington